Master's Thesis

for the acquisition of the academic degree
Master of Science in Mathematics

On Optimal Transport for Seismic Inverse Problems

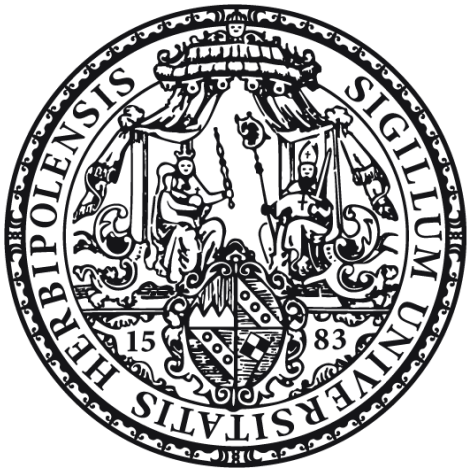

Julius-Maximilians-Universität Würzburg
Faculty of Mathematics and Computer Science
Chair of Mathematical Fluid Mechanics

Submitted by
Melissa Lange

Supervised by
Professor Dr. Christian Klingenberg

Würzburg, February 3, 2025

Acknowledgements

I would like to express my sincere gratitude to Professor Dr. Christian Klingenberg for his supervision of my master's thesis. I am deeply thankful for the opportunity to work on such an interesting topic and to further develop my knowledge in the field of inverse problems and PDEs. I enjoyed our discussions on the subject of this thesis and have learned a lot during my time in his work group. I am also thankful for facilitating my contact with Yunan Yang from Cornell University.

I am grateful to Lutz for his keen interest in my topic as well as for our discussions on Python and for reviewing my thesis. Thanks a lot for your time and always being there for me. I love having you with me on my way.

I am also thankful to Janina. Thank you for your help with proofreading this thesis, our discussion on swarm-based optimisation methods and for being my friend.

Finally, I would like to cordially thank my parents and grandparents. I am grateful not only for your financial support during my studies, but also for your constant and lovely encouragement in everything I do.

Abstract

Seismic imaging aims to create images of Earth's interior by solving an inverse problem. One technique to address this problem is full waveform inversion, which uses surface measurements to infer subsurface properties. In this approach, seismic waves generated by surface vibrations propagate through Earth's layers. As they pass through different layers, the waves refract, reflect, and convert, with the reflected waves returning to the surface to be recorded by receivers. These measurements are then used to reconstruct subsurface images. The key of this inverse problem is estimating the velocity field of Earth's layers, as seismic wave velocity varies across different materials. In this thesis, the acoustic wave equation is used to model the forward problem, with the aim of reconstructing the velocity coefficient of this equation. Full waveform inversion is formulated as an optimisation problem, where the velocity parameter of the wave equation is adjusted to ensure that the simulated waves match the measured data. Therefore, a misfit function must be defined. The L^2-norm is commonly used to quantify this mismatch between the measurements and the simulated data, but it often leads to trapping in local minima. In this thesis, we use the Wasserstein metric from optimal transport theory as misfit function.

In Section 1, we provide the necessary background on inverse problems and present a fundamental technique from seismic geophysics used to create seismic images, namely reverse time migration. In Section 2, the solution of the forward problem is described using finite differences and reverse time migration is presented within the context of inverse problems. From there, full waveform inversion is derived in Section 3 and the choice of misfit function is discussed. In Section 4, relevant results from optimal transport theory are given and the Wasserstein metric is considered in the context of seismic imaging. Moreover, data normalisation is discussed, which is necessary when applying optimal transport. Numerical results are presented in Section 5. Finally, Section 6 discusses the results, and the Python code can be found in the appendix.

Contents

1 Introduction

The study of earthquakes is a long-standing yet still highly relevant and significant field. Earthquakes create seismic waves that can be measured even hundreds of kilometres away from the eruption site. These waves contain information about the media they propagate through, offering valuable insights into Earth's subsurface. To this end, the study of seismic waves does not only increase the understanding of earthquakes but is also an important tool for finding new water reservoirs and raw minerals. To gain knowledge on Earth's interior, geophysicists set up small explosions to simulate earthquakes. To this end, they set up vibrations that serve as the source of seismic waves, allowing the waves to propagate through Earth. While propagating through Earth's subsurface, the waves encounter several heterogeneities, different earth layers of various materials, where they refract, convert and reflect [Rob10]. The reflected waves travel back to the surface, where they are eventually recorded by receivers. From these recordings, images of Earth's interior structure can be reconstructed. The reconstruction of detailed images of Earth's interior is the aim of seismic imaging and there are a several techniques to achieve that. The key point behind many of these techniques is that the velocity of seismic waves changes when propagating from one layer of Earth into another.

Seismic waves propagate at a characteristic *acoustic velocity*, which depends on the medium they are travelling through. In order to create an image of the subsurface, we need to estimate the velocity field of Earth's layers through which the waves propagate [Rob10]. From a mathematical point a suitable model that describes the wave propagation has to be found. In the context of this thesis, we approximate the wave propagation by the *acoustic wave equation*

$$\begin{cases} m(x)\frac{\partial^2 u(x,t)}{\partial t^2} - \Delta u(x,t) = s(x,t), \\ u(x,0) = 0, \\ \frac{\partial u}{\partial t}(x,0) = 0. \end{cases} \quad [1]$$

There, $u(x,t)$ describes the wave at location x and time t, the coefficient $m(x)$ is the velocity coefficient. The latter captures information on the acoustic velocity at location x. In this thesis, we focus on the imaging technique of full waveform inversion (FWI). In FWI, we aim to reconstruct the layers of the subsurface by using the data measured by the receivers. To this end, we solve the inverse problem of finding the waves' velocity coefficient by using the measurements made by the receivers. FWI consists of the following steps:

1. Guessing the velocity coefficient and solving the model equation to obtain the corresponding synthetic data $u(x,t)$,
2. Calculating the misfit between the measured and synthetic data,
3. Minimising the misfit by iteratively adjusting the velocity coefficient via a gradient-based method.

To accomplish the second step, we have to find a suitable metric that measures this misfit. A common choice of misfit function often found in literature is the L^2-norm of the difference between the two data sets. The application of the L^2-norm in the context of FWI was discussed in [Bun+95; Tar05; VO09] for instance. However, to overcome certain issues arising with the L^2-norm, we use the Wasserstein distance instead, which is known

from optimal transport theory. The idea of applying optimal transport to seismic signals was proposed in [EF14] and further developed in [Yan+16; Yan+17a; Yan+17b].

1.1 Inverse Problems

Sometimes one wishes to deduce a non–observable quantity x from an observable quantity y. This is a situation where one solves an inverse problem. In general, the quantities x and y do not need to be related to each other. However, in applications, most often x is referred to as the cause for the effect y. There are many fields of applications where inverse problems arise. In the following, we put our definition of inverse problems in a more formal framework.

Definition 1.1 (Inverse problem, [Stu10])**.** *Let $\mathcal{G}$ be the mathematical model describing a phenomenon and let y be the measurements made by observing this phenomenon. The inverse problem is then to find the input x of the model, such that it fits the observations made. Formally, we solve*

$$\mathcal{G}(x) = y \tag{2}$$

for $x \in X$, given $y \in Y$, where X and Y are Banach spaces and $\mathcal{G} : X \to Y$ is a mapping. We call $\mathcal{G}$ the modelling operator.

Remark 1.2. *One might ask, if in analogy to inverse problems, there are also corresponding forward problems. Assume we are given a model $\mathcal{G}$ and call y the observations and x the input as in definition* [1.1]*. Then, the forward problem asks to find y for given x. That is, we search for the effects given the causes. Therefore, we can specify our naming of $\mathcal{G}$ and call it the forward modelling operator.*

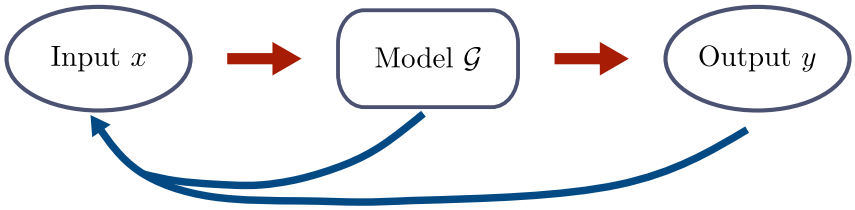

Figure 1: Scheme of the forward problem (red arrows) and the corresponding inverse problem (blue arrows)

It is typical of inverse problems, that they are ill–posed. A mathematical problem is called ill–posed, if it is not well–posed. Thus, if at least one of the properties in definition [1.3] does not hold.

Definition 1.3 (Well-posedness, [Stu10])**.** *An inverse problem is called well-posed, if it fulfils the following three properties.*

1. *There exists a solution x,*
2. *The solution is unique,*
3. *The solution depends continuously on the input data y.*

There are many ways to solve inverse problems and handle the ill–posedness. One of them is the *Least–Squares approach* (LS). A similar approach is the *Bayesian framework*. There, the aim is to find the most likely input x to fit the data y. While the Bayesian approach is probabilistic, the Least–Squares approach is deterministic. Further background information on these techniques can be found in [Ric20] and [Stu10]. The *Least–Squares approach* will be described in the sequel of this section and this approach provides the basis for the methods considered in the subsequent sections.

Definition 1.4 (Linear problem, [Ric20])**.** *Let x, y live in vector spaces $X \in \mathbb{R}^m$ and $Y \in \mathbb{R}^n$ and let $m, n \in \mathbb{N}$. In case of a linear forward problem, we write*

$$Ax = y, \tag{3}$$

where the matrix $A \in \mathbb{R}^{n \times m}$ characterises the linear forward modelling operator.

Remark 1.5.

1. *Note that the forward problem asks to solve $Ax = y$ for y, while the corresponding inverse problem asks to find x for given y. Symbolically, in the inverse problem, we want to solve $A^{-1}y = x$ for x. This formulation makes clear, why we call the problem an inverse problem.*

2. *Note that the inverse of A might not exist.*

Remark 1.6. *It is well known from linear algebra, that in the case of $A \in \mathbb{R}^{n \times m}$ being a matrix, the existence and the uniqueness of* [1.4] *are equivalent to $m = n$ and A being regular, which implies that $A^{-1} \in \mathbb{R}^{n \times m}$ exists and A is a continuous linear mapping from X to Y [Fis13]. If X and Y are infinite-dimensional, this reasoning does not work anymore [Kel76].*

As we stated in definition [1.3], the inverse problem might have no (unique) solution or the solution may depend continuously on the observations. This can be due to noisy measurement data or an inappropriate choice of the model. In fact, dealing with noisy data is one of the main challenges when solving inverse problems. Before we discuss these challenges, we summarise the meaning of the three properties in definition [1.3] in terms of equation [1.4].

Corollary 1.7 (On well-posedness)**.** *If A is a linear mapping as defined in* [1.4]*, the three requirements for well-posedness correspond to the following three properties respectively.*

1. *$y \in range(A) \coloneqq \{Ax \in Y \mid x \in X\}$,*

2. *A is injective on X, i.e. $x_2 \neq x_1$ implies $Ax_2 \neq y$,*

3. *A^{-1} is continuous.*

If the first property is violated, then $y \notin range(A)$. In that case, there might be x, which minimises the *residual*

$$r(x) \coloneqq y - Ax. \tag{4}$$

To solve the minimisation problem, we recall the definition of a norm.

Definition 1.8 (Normed space on $\mathbb{R}$, [Ste23]). *Let X be a vector space over $\mathbb{R}$. A mapping*

$$\|\cdot\| : X \to [0, \infty)$$

is called norm on X, if for all $x \in X$ holds:

1. $\|\lambda x\| = |\lambda| \|x\|$ *for all* $\lambda \in \mathbb{K}$,
2. $\|x + y\| \leq \|x\| + \|y\|$ *for all* $y \in X$,
3. $\|x\| = 0$ *if and only if* $x = 0 \in X$.

Definition 1.9 (p-norms, [Ste23]).

- *Let $X = \mathbb{R}^N$. The $p-$norm is defined as*

$$\|x\|_p = \left(\sum_{i=1}^{N} |x_i|^p \right)^{1/p} \quad \text{for } p \in [1, \infty).$$

- *Let $X = L^p(\Omega)$, i.e. the space of real-valued p–fold integrable functions on $\Omega \subset \mathbb{R}^d$. The $p-$norm or L^p-norm is defined as*

$$\|u\|_p = \left(\int_\Omega |u(x)|^p dx \right)^{1/p} \quad \text{for } p \in [1, \infty).$$

To solve the minimisation problem 4, a common choice is the 2-norm, which we will also use here. Then, the minimisation problem reads

$$\min_{x \in X} \|y - Ax\|_2, \tag{5}$$

which is the *Least-Squares* approach [Kel76][Ric20].

Remark 1.10. *Since we consider X and Y in equation* [1.4] *as vector spaces, the $2-$norm is given by*

$$\|x\|_2 = \sqrt{\sum_{i=1}^{N} |x_i|^2}.$$

Remark 1.11. *We make use of the second part of definition 1.9, where $X = L^p$, in the further course of this thesis.*

To solve the linear Least-Squares problem 23, we rewrite equation [4]. Since x, y live in real vector spaces, it follows that

$$\begin{aligned} f(x) \coloneqq \|r(x)\|_2^2 &= \langle r(x), r(x) \rangle = r(x)^T r(x) \\ &= \langle y - Ax, y - Ax \rangle \\ &= x^T A^T A x - 2x^T A^T y + y^T y. \end{aligned}$$

To minimise for x, we need to calculate the gradient in x direction and solve for $\nabla f(x) = 0$. This yields the *normal equations*, with which x can be calculated [Ric20].

Remark 1.12. *The general version of A^T is referred to as the adjoint of A, denoted by A^*. Since we consider the special case of real vector spaces (and not complex vector spaces), the adjoint A^* is equivalent to the transpose of A and therefore we write A^T instead of A^*.*

Proposition 1.13 (Normal equations, [Ric20])**.** *The minimiser x can be obtained by $x = (A^TA)^{-1}A^Ty$.*

Proof. First, we calculate the gradient of $f(x)$.

$$\begin{aligned}\nabla f(x) &= \nabla x^TA^TAx - \nabla 2x^TA^Ty + \nabla y^Ty \\ &= \nabla x^TA^TAx - 2A^Ty.\end{aligned}$$

To calculate the gradient of the first term, consider a_{ij} as the entry of the symmetric matrix A^TA in column i and row j. Then, x^TA^TAx can be rewritten as

$$\begin{pmatrix}x_1 & \dots & x_n\end{pmatrix}\begin{pmatrix}a_{11}x_1 & \dots & a_{1n}x_n \\ \vdots & \ddots & \vdots \\ a_{nn}x_1 & \dots & a_{nn}x_n\end{pmatrix} = \sum_i a_{ii}x_i^2 + \sum_{i\neq j} 2a_{ij}x_ix_j. \qquad [6]$$

The derivative of [6] with respect to x_k now reads

$$\nabla\left(\sum_i a_{ii}x_i^2 + \sum_{i\neq j} 2a_{ij}x_ix_j\right) = 2a_{kk}x_k + \sum_{k\neq j} x_j.$$

The result above is exactly the k^{th} component of $2A^TAx$. Thus, the gradient of $f(x)$ in x direction is given by

$$\nabla f(x) = 2A^TAx - 2A^Ty.$$

Secondly, a necessary condition for a minimiser x^* is that $\nabla f(x^*) = 0$. Thus,

$$\nabla f(x) = 0 \qquad [7]$$
$$\Leftrightarrow A^TAx = A^Tb, \qquad [8]$$

where [8] represents the normal equations. □

Remark 1.14. *Note that the matrix A^TA is quadratic and of dimension n. A is invertible if and only if it has full rank. In that case, the linear Least-Squares problem admits a unique solution [Fis13].*

Remark 1.15. *The normal equations are also solvable if A is singular. Then, the residual is also unique, while the solution x is not [Ric15].*

Remark 1.16. *Note that A^TA can be very difficult to invert and may cause high computational complexity.*

Remark 1.17. *Assuming A^TA is invertible, we can calculate the minimiser by $x = (A^TA)^{-1}A^Ty$.*

When A^TA is not invertible, one can define the pseudoinverse, also known as Moore-Penrose inverse. This serves as a generalisation for the inverse. Since we do not need this concept for the thesis, we mention it only for the sake of completeness and refer to [Ric20] and [Kel76] for more literature on this topic.

Remark 1.18. *So far we have only considered the case where $Ax = y$ has no solution. If, on the other hand, $\ker(A) \neq \{0\}$, there exist infinitely many solutions. In this case, we choose the minimal norm solution, that is the solution x of the Least-Squares problem with minimal norm $\|x\|_X$ [Kel76].*

We now state a relationship between the solvability of $Ax = y$ and the adjoint operator A^T. This relationship is given by the *Fredholm–Alternative theorem.*

Theorem 1.19 (Fredholm–Alternative theorem, [Kut20][Her24])**.** *Given $A \in \mathbb{R}^{m\times n}, y \in \mathbb{R}^m$ and $x \in \mathbb{R}^n$.*
***First alternative**: $Ax = y$ admits solution x if and only if $\langle y, v\rangle = 0$ for all v satisfying $A^Tv = 0$.*
***Second alternative**: A solution x for $Ax = y$ exists and is unique if and only if $x = 0$ is the only solution of $Ax = 0$.*

Proof of Theorem 1.19, [Her24]. We start by proving the first alternative. Let $A^Tv = 0$ and $Ax_0 = y$.

$$\langle y, v\rangle = \langle Ax_0, v\rangle = \langle x_0, A^Tv\rangle = 0.$$

Then we have shown that if $Ax = y$ has a solution x, $\langle y, v\rangle = 0$ for all v satisfying $A^Tv = 0$.
For the other implication, assume that $\langle y, v\rangle = 0$ for all v such that $A^Tv = 0$. We can write y as a decomposed sum of a part that lives in the range of A and a part of the space orthogonal to the range of A. We write $y = y_R + y_O$. Then

$$\langle b_O, Ax\rangle = \langle A^Ty, x\rangle = 0$$

for all x. Since $\langle y, v\rangle = 0$ for all $v \in \ker(A^T)$, it follows that

$$\langle y, v\rangle = 0 = \langle b, b_O\rangle.$$

Our decomposition yields

$$0 = \langle b, b_O\rangle = \langle b_R + b_O, b_O\rangle = \langle b, b_O\rangle.$$

Since $b_R \in range(A)$, this gives $b_O = 0$. We conclude, that $Ax = b$ has a solution x.
We continue by proving the second alternative. Assume $Ax = 0$ for $x \neq 0$ and $Ax_0 = y$. Then $A(x_0 + \alpha x) = y$ for all $\alpha \in \mathbb{R}$. Then the solution is not unique. Conversely, if there are two different solutions x_1 and x_2, which satisfy $Ax_1 = y$ respectively $Ax_2 = y$, then one has a nontrival solution $x = x_1 - x_2$, such that $Ax = A(x_1 - x_2) = 0$. □

The following corollary summarises this result by using the definition of the adjoint of A.

Corollary 1.20. *Let $Ax = y$ and $A^Tv = 0$ for $v \in \ker(A)$. Note that since X, Y are*

vector spaces, we can multiply $Ax = b$ from the right using the dot product.

$$\begin{aligned} & Ax = y \\ \Leftrightarrow\ & Ax \cdot v = y \cdot v \\ \Leftrightarrow\ & Ax \cdot v = x \cdot A^T v \\ \Leftrightarrow\ & b \cdot v = 0, \end{aligned}$$

which implies $v \in range(A)$ [Kut20].

Our results do not only hold for x, y living in vector spaces, but also for X, Y being function spaces. For that purpose, we consider a linear differential operator L with $L(m)u = f$, which we shortly denote as $Lu = f$. Here, m is a coefficient and L, f and u are prescribed continuously on some interval and might also incorporate initial and boundary conditions.

In function spaces, the first Fredholm alternative states that $Lu = s$ admits a solution if and only if there exists v such that $L^T v = 0$. Analogously to the case for vector spaces, we formulate the following corollary for function spaces.

Corollary 1.21. *Let $Lu = s$ and $L^T v = 0$ for $v \in \ker(L)$. Thus,*

$$\begin{aligned} & Lu = s \\ \Leftrightarrow\ & \langle v, Lu \rangle = \langle v, s \rangle \\ \Leftrightarrow\ & \langle L^T v, u \rangle = \langle v, s \rangle \\ \Leftrightarrow\ & \langle v, s \rangle = 0, \end{aligned}$$

which implies $s \in range(L)$ [Kut20].

Many boundary value problems are non–linear. They arise in various fields like quantum mechanics or elasticity theory. However, if we are able to find an appropriate linear formulation of the problem, we can use the above results to solve it.

In this chapter we have established the necessary basic understanding of inverse problems. We have not yet considered the seismic inverse problem and therefore not yet discussed the choice of the model operator. These questions are addressed in section 2. Beforehand, we build the fundamentals for seismic imaging.

1.2 Seismic Geophysics

In this section, some fundamentals of seismic imaging are given. With this knowledge at hand, we will be able to develop corresponding imaging techniques such as reverse time migration (section 2.3). And as we will see, reverse time migration (RTM) can be formulated in the fashion of a *linear Least-Squares* problem. Finally we will be able to fully understand the concept of full waveform inversion, the main technique of this thesis.

In seismic imaging, one cares about *reflection images*. In a geophysical setup, vibrations imitate the source of seismic waves. These waves then propagate into Earth's subsurface, and while travelling through Earth, they encounter heterogeneities, the different materials layered under Earth's surface. Passing a heterogeneity, the waves refract, reflect or convert [Rob10]. The reflected waves travel back to Earth's surface, where receivers measure and record the amplitude of the seismic waves. The recorded data at a single receiver is called seismic trace, while the entire data set consists of the time history

measured at all receivers. The goal of seismic imaging is to create an image of these heterogeneities from all the recordings (see Figure [2]).

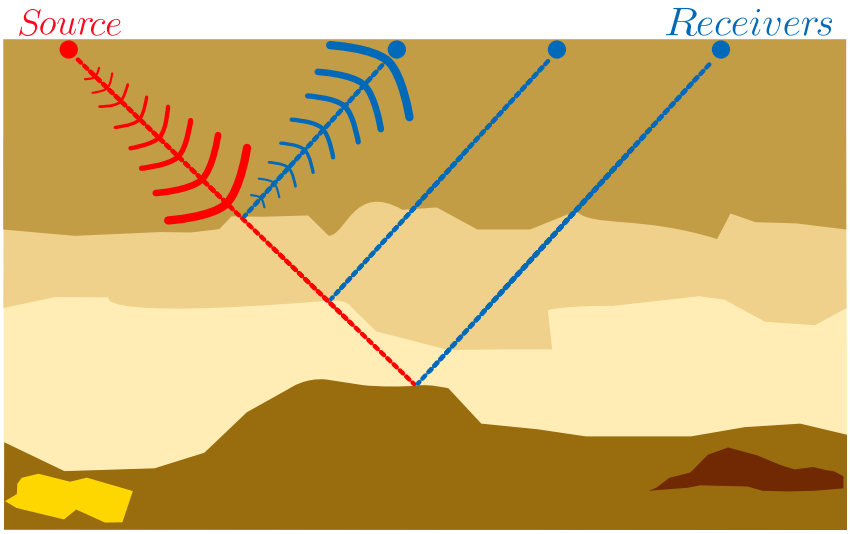

Figure 2: A seismic wave (red) is reflected (blue) at the first boundary layer, propagates further into the second and third layers, where it is reflected again at each boundary. The reflected waves are measured by receivers (three blue solid circles)

There are two main classes of seismic waves, named according to their arrival times at the receivers: primary waves (P-waves), which arrive first and secondary waves (S-waves), which are the second type of seismic wave to be measured by the receivers. The P–waves travel with 2 km/s to 8 km/s and are thus faster than S–waves, which merely reach velocities up to 4.5 km/s. Furthermore, P–waves are longitudinal waves, i.e. they oscillate in the direction of their propagation. During their travel through interfaces, some of the P–wave's energy is transformed into *S–waves*. S–waves are transversal, meaning they oscillate transverse to the direction of propagation. In addition to the P-waves and S–waves, there are also surface waves, which arise from the superposition of the P–waves and the S–waves. However, as their name suggests, they are characterised by the fact that they run on the surface and their amplitudes decrease heavily with depth. Thus, the latter do not have such a huge impact on seismic imaging. In fact, the waves that seismic reflection imaging deals with is mainly about *P–waves* [Rob10]. Therefore, seismic reflection imaging is sometimes referred to as *P–wave seismic imaging*.

Consequently, for this thesis, we neglect the existence of S–waves and focus on the propagation of P–waves. Hence, we focus on the class of pressure and sound waves. Furthermore, we neglect the elasticity of the media the waves travel trough. An approximative model which describes the propagation of P–waves is given by the (*acoustic*) *wave equation* 9.

$$\begin{cases} m(x)\frac{\partial^2 u(x,t)}{\partial t^2} - \Delta u(x,t) = s(x,t), \\ u(x,0) = 0, \\ \frac{\partial u}{\partial t}(x,0) = 0. \end{cases} \quad [9]$$

The coefficient $m(x)$ in the wave equation is defined as $m(x) = \frac{1}{c(x)^2}$, where $c(x)$ is the

velocity of the wave [Rob10][TW98][Yan+16].[1]. The wave equation will be addressed in detail in Section 2. With the wave equation at hand, we can understand the reflection process more precisely. We can already state that reflection occurs any time when the propagating wave encounters a change in the *acoustic impedance*. The acoustic impedance Z is a property of any medium, it is defined as

$$Z = \rho \cdot c, \tag{10}$$

where ρ is the density of the medium and c the propagation velocity [Rob10]. As stated in equation [10], the acoustic impedance depends proportionally on the propagation velocity c. Assuming we know the wave's velocity c at a specific location x, we can deduce information on the density of the medium at x, especially on the density difference between different locations. Therefore, it is poslensible to distinguish different Earth layers and possibly obtain information on their nature and material properties. From there, geophysicists can eventually find mineral deposits for instance [Rob10].

[1] In seismology, the definition of $m(x)$ is often referred to as *squared slowness* [Rob10].

2 Solving the Inverse Problem in the Setting of Seismic Geophysics

To define the inverse problem, we need to choose a model and observed data. As stated in Section 1.2, we choose the *wave equation* for modelling the wave propagation:

$$\begin{cases} m(x)\frac{\partial^2 u(x,t)}{\partial t^2} - \Delta u(x,t) = s(x,t), \\ u(x,0) = 0, \\ \frac{\partial u}{\partial t}(x,0) = 0 \end{cases}$$

and define $m(x) = \frac{1}{c(x)^2}$, where $c(x)$ is the wave's velocity at location x, $u(x,t)$ is the propagated wave at time t and location x and $s(x,t)$ is the source. In [GKnd] it was shown that the Ricker function not only provides good empirical results for modelling wave propagation, but it was also theoretically proven that the Ricker function is a reasonable source term to the wave equation for this purpose. Therefore, we stick to the Ricker wave as source term for our model equation. The Ricker wave is defined as the negative, normalised second derivative of a Gaussian function. It describes how the amplitude of a seismic signal changes within time t.

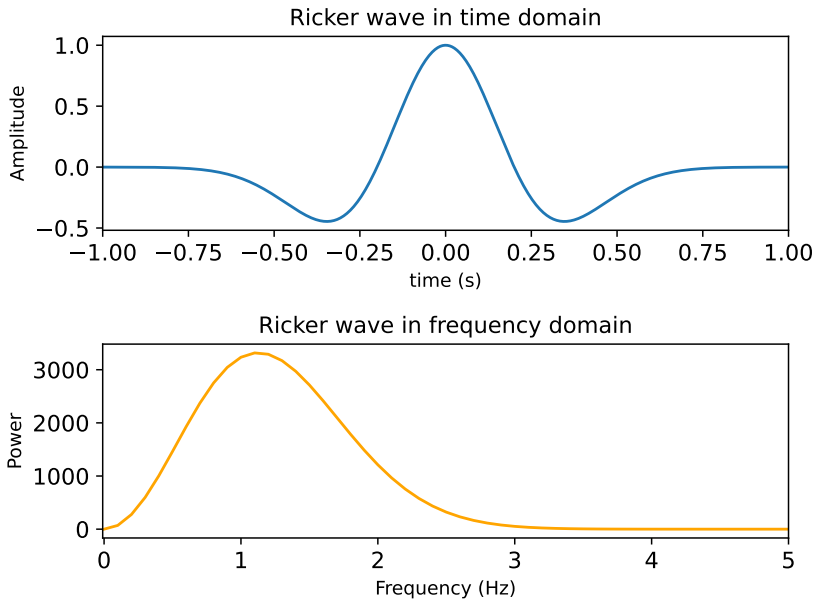

Figure 3: Ricker wave in time and frequency domain respectively

Definition 2.1. *(Ricker wave, [GKnd]) The function*

$$\psi(t) = \frac{2}{\sqrt{3\sigma}\pi^{\frac{1}{4}}}\left(1 - \left(\frac{t}{\sigma}\right)^2\right) e^{-\frac{t^2}{2\sigma^2}}$$

is called Ricker wave. The parameter σ describes the duration of the Ricker wave.

Definition 2.2. *(Power spectrum, [GKnd]) The power spectrum of the Ricker wave is*

defined as

$$S(\omega) = K \cdot \omega^2 \cdot \exp(-c\omega^2),$$

where ω is the frequency of the signal.

2.1 Solving the Forward Problem Analytically

We solve the wave equation using the method of *Separation of Variables* (cf. [TW98], chapter 5). The idea is to express $u(x,t)$ as a product of two functions: one depending only on x and the other one only on t. Thus, we seek functions $F(x)$ and $G(t)$ such that

$$u(x,t) = F(x)G(t). \tag{11}$$

As a first step, we differentiate $u(x,t)$ twice with respect to t and twice with respect to x:

$$u_{tt} = F(x)G''(t), \quad u_{xx} = F''(x)G(t).$$

Inserting this into the wave equation gives

$$\begin{aligned} F(x)G''(t) &= c^2 F''(x)G(t) \\ \Leftrightarrow \frac{F(x)}{F''(x)} &= c^2 \frac{G(t)}{G''(t)} \end{aligned}$$

Since the left–hand side depends only on t and the right-hand side only on x, both expressions are independent of x and t. Thus, we can separate the variables as follows:

$$\frac{G''(t)}{G(t)} = c^2 \frac{F''(x)}{F(x)} = -\kappa, \tag{12}$$

for a constant $\kappa \in \mathbb{R}$. This gives two ordinary differential equations (ODE), one for $F(x)$

$$-F''(x) = \kappa F(x), \quad F(0) = F(L) = 0, \tag{13}$$

and one for $G(t)$

$$-G''(t) = \kappa G(t). \tag{14}$$

The calculation of the corresponding eigenvalues of [13] and [14] is due to the following lemma.

Lemma 2.3. *(Eigenvalues of boundary value problems, [TW98]) We denote the general continuous eigenvalue problem corresponding to* [9] *by*

$$Lu = \lambda u$$

for a suitable nonzero twice differentiable function u. The corresponding eigenvalues and eigenfunctions are given by

$$\lambda_k = (k\pi)^2, \quad \textit{for } k \in \{1, 2, 3, \dots\}$$

and

$$u_k(x) = \sin(k\pi x), \quad \textit{for } k \in \{1, 2, 3, \dots\}$$

respectively.

Proof. To find the eigenvalues and eigenfunctions, we make use of the positive definiteness of L, which is proven in Lemma 2.4 in [TW98]. Also note that the eigenfunction must not be zero. Combining both properties, we conclude that $\lambda > 0$. Hence, we define

$$\kappa = \sqrt{\lambda}.$$

Therefore, we have to solve the second-order linear differential equation

$$u''(x) + \kappa^2 u(x) = 0.$$

It is well known that the solutions to the above equation is given by

$$u(x) = c_1 \cos(\kappa x) + c_2 \sin(\kappa x)$$

for constants c_1 and c_2. Using the boundary condition $u(0) = 0$, we obtain $c_1 = 0$. For the second boundary condition, $u(L) = 0$, we obtain $c_2 \sin(\kappa) = 0$. And thus

$$\kappa = \kappa_k = k\pi \quad \text{for } k \in \{1, 2, 3, \dots\}.$$

Hence, for $k \in \{1, 2, 3, \dots\}$ the eigenvalues are given by

$$\lambda_k = (k\pi)^2$$

and the corresponding eigenfunctions by

$$u_k(x) = \sin(k\pi x).$$

□

We continue with solving [13] and [14]. We consider the ODE for $F(x)$ first. Therefore, we solve the boundary value problem:

$$F''(x) + \kappa F(x) = 0, \quad F(0) = F(L) = 0 \qquad [15]$$
$$\Leftrightarrow -F''(x) = \kappa F(x), \quad F(0) = F(L) = 0. \qquad [16]$$

By Lemma 2.3 we know that the eigenvalues λ_k are given by

$$\lambda_k = k\pi \quad \text{for } k \in \{1, 2, 3, \dots\},$$

and the corresponding eigenfunctions are

$$F_k(x) = \sin(k\pi x).$$

Next, we consider $G(t)$. Therefore we solve the ODE:

$$G_k''(t) + \lambda_k G_k(t) = 0, \qquad [17]$$

which has the general solution:

$$G_k(t) = \alpha_k \cos(k\pi t) + \beta_k \sin(k\pi t),$$

where α_k and β_k are constants determined by the initial conditions. By combining the solutions for $F(x)$ and $G(t)$, we obtain the general solution for $u(x,t)$

$$u_k(x,t) = \sin(k\pi x)\left(\alpha_k \cos(k\pi t) + \beta_k \sin(k\pi t)\right).$$

This satisfies the boundary conditions $u(0,t) = u(L,t) = 0$. Since the wave equation is linear, the superposition principle holds [TW98]. That is, if $u_1(x,t)$ and $u_2(x,t)$ are solutions to the homogenous wave equation, then every linear combination of these solutions is a solution as well. Therefore, the general solution can be written as a sum over all k:

$$u(x,t) = \sum_{k=1}^{\infty} \sin(k\pi x)\left(\alpha_k \cos(k\pi t) + \beta_k \sin(k\pi t)\right), \qquad [18]$$

with initial conditions given by

$$u(x,0) = \sum_{k=1}^{\infty} \alpha_k \sin(k\pi x), \quad u_t(x,0) = \sum_{k=1}^{\infty} \beta_k k\pi \sin(k\pi x). \qquad [19]$$

To simplify the result, recall the following trigonometric identity (see [GS01], chapter 7.9, for a proof of 20):

$$\sin(\psi)\sin(\phi) = \frac{1}{2}\left[\cos(\psi - \phi) - \cos(\psi + \phi)\right]. \qquad [20]$$

Hence, the final solution can be written as

$$u(x,t) = \sum_{n=1}^{\infty} \left[\sin\left(\frac{n\pi}{L}(x+ct)\right) + \sin\left(\frac{n\pi}{L}(x-ct)\right)\right]. \qquad [21]$$

The first summand $\sin\left(\frac{n\pi}{L}(x+ct)\right)$ is a wave travelling to the left and the second summand $\sin\left(\frac{n\pi}{L}(x-ct)\right)$ is a wave travelling to the right with both the same shapes, which is why the wave equation is also called two–way wave equation [TW98].

2.2 Solving the Forward Problem Numerically

The finite difference method (FD) is a numerical technique used to approximate solutions of ordinary and partial differential equations. This is done by replacing derivatives with difference quotients calculated on a discrete grid. By discretising time and space into uniformly distributed points, the continuous problem is transformed into a discrete problem that can be solved iteratively. Finite difference methods are commonly used to solve equations such as the wave equation as they are easy to implement. Further, they often exhibit good numerical stability and convergence, especially when combined with the Courant-Friedrichs-Lewy (CFL) condition [TW98].

To apply the finite difference method, we define a discrete grid on both the spatial and

time domain. The grid defines the discrete points at which the values of the wave function $u(x,t)$ are approximated. In a spatially one-dimensional problem, the spatial domain is divided into a final number of Sections of length Δx and the time axis is divided into a final number of steps of size Δt. Each node in the grid represents a combination of a spatial and a temporal point, and the finite difference scheme approximates the derivatives at these points. The sequel of this Section on Finite Differences is based on chapter 5.3 in [TW98].

Let the spatial grid spacing be given by $\Delta x = 1/(n+1)$, where $n \in \mathbb{N}$. Then, the associated grid points are $x_j = j\Delta x$ for $j \in \{0, 1, 2, 3, \ldots, n+1\}$. The time points are given by $t_m = m\Delta t$ for $m \in \mathbb{N}_0$ with the time step $\Delta t > 0$.

We write $u_j^m = u(x_j, t_m)$ for the approximation of $u(x,t)$. In the following the finite differences are amplified by means of the derivative with respect to t. The finite differences regarding the spatial direction are build analogously. In a general analytical way, we write

$$\frac{df}{dt} = \lim_{\Delta t \to 0} \frac{f(t+\Delta t) - f(t)}{\Delta t}$$

for the derivative of f with respect to t. With the numerical scheme, we approximate the derivative by

$$\frac{df}{dt} \approx \frac{f(t+\Delta t) - f(t)}{\Delta t}.$$

To be precise, we approximate the derivative by *Taylor expansion*. By doing so, we obtain the *forward difference scheme*:

$$\frac{df}{dt} = \lim_{\Delta t \to 0} \frac{f(t+\Delta t) - f(t)}{\Delta t} \approx \frac{df}{dt} + \frac{d^2 f}{dt^2}\frac{\Delta t}{2!} + \frac{d^3 f}{dt^3}\frac{\Delta t^2}{3!} + \cdots.$$

Analogously, we can define the *backward difference scheme*:

$$\frac{df}{dt} = \lim_{\Delta t \to 0} \frac{f(t) - f(t-\Delta t)}{\Delta t} \approx \frac{df}{dt} - \frac{d^2 f}{dt^2}\frac{\Delta t}{2!} + \frac{d^3 f}{dt^3}\frac{\Delta t^2}{3!} - \cdots.$$

Note that the leading error terms are of order $\mathcal{O}(\Delta t)$. To reduce the order of the error term, we define the *central difference*:

$$\frac{df}{dt} \approx \frac{f(t+\Delta t) - f(t-\Delta t)}{2\Delta t} = \frac{df}{dt} + \frac{d^3 f}{dt^3}\frac{\Delta t^2}{3!} + \frac{d^5 f}{dt^5}\frac{\Delta t^4}{5!} + \cdots.$$

Now, the leading error term is of order $\mathcal{O}(\Delta t^2)$. Analogously to the derivatives of first order, we can define differences for the second derivatives:

$$\frac{d^2 f}{dt^2} = \lim_{\Delta t \to 0} \frac{f'(t+\Delta t) - f'(t)}{\Delta t}.$$

Then, the second central difference in time becomes

$$\frac{d^2 f}{dt^2} \approx \frac{f(t-\Delta t) - 2f(t) + f(t-\Delta t)}{\Delta t^2} + \mathcal{O}(\Delta t^2).$$

Analogously, the second central difference in space becomes

$$\frac{d^2 f}{dx^2} \approx \frac{f(x-\Delta x) - 2f(x) + f(t-\Delta x)}{\Delta x^2} + \mathcal{O}(\Delta x^2).$$

See Figure 4 for an illustration of the corresponding stencil. When applying the above results to the wave equation, we obtain the following iterative formula for the finite difference scheme:

$$\frac{u_j^{m-1} - 2u_j^m + U_j^{m+1}}{\Delta t^2} + \mathcal{O}(\Delta t^2) = c^2 \frac{u_{j+1}^m - 2u_j^m + U_{j-1}^m}{\Delta x^2} + \mathcal{O}(\Delta x^2).$$

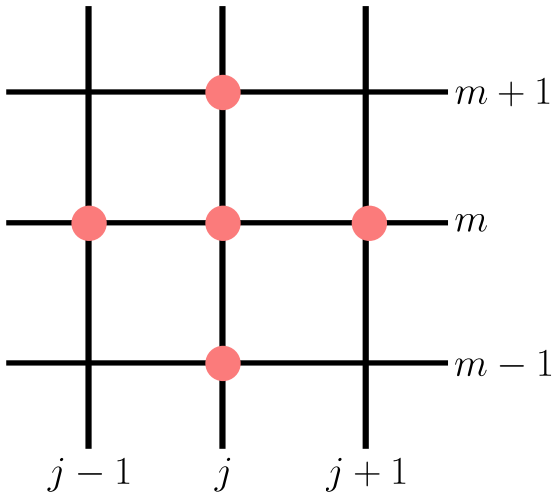

Figure 4: Five-point-stencil with equidistant grid points

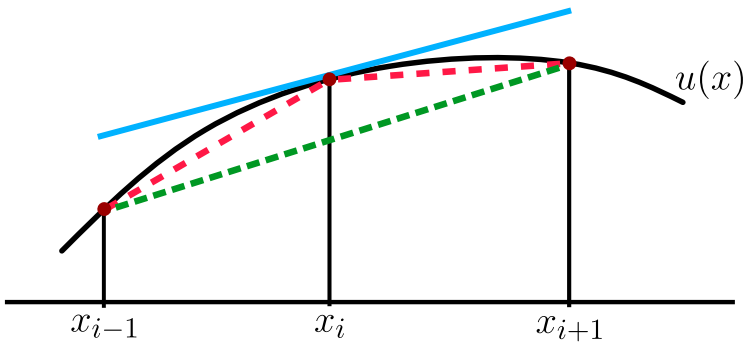

Figure 5: Backward difference (left red dashed line), forward difference (right red dashed line), central difference (green dashed line) and tangent (blue line)

The discrete solution also satisfies the boundary conditions, i.e.

$$u_0^m = u_{n+1}^m = 0 \text{ for } m \geq 0.$$

When $\{u_j^m\}_{j=1}^n$ and $\{u_j^m\}_{j=1}^n$ are known, the solutions $\{u_j^m+1\}_{j=1}^n$ can be computed directly with the finite difference scheme. To run the scheme, we need to define starting values

for the first two time steps u_j^0 and u_j^1. By the initial condition, we choose $u_j^0 = f(x_j)$ for $j = 1, 2, ..., n$. Next we derive an approximation for v_j^1. To this end, we use a Taylor expansion with respect to t:

$$u(x, \Delta t) = u(x, 0) + (\Delta t)u_t(x, 0) + \frac{(\Delta t)^2}{2!}u_{tt}(x, 0) + \mathcal{O}((\Delta t)^3)$$

Since $u_{tt}(x, 0) = u_{xx}(x, 0) = f''(x)$, we conclude that

$$u(x, \Delta t) = f(x) + (\Delta t)g(x) + \frac{(\Delta t)^2}{2!}f''(x) + \mathcal{O}((\Delta t)^3).$$

Therefore, we have obtained the following approximation u_j^1 for $u(x_j, \Delta t)$:

$$u_j^1 = v_j^0 + \Delta t g(x_j) + \frac{(\Delta t)^2}{2}\frac{v_{j-1}^0 - 2v_j^0 + f_{j+1}^0}{(\Delta x)^2}.$$

Alternatively, to express the finite difference scheme in a more compact form, we define the vector $u^m \in \mathbb{R}^n$ as $u^m = (u_1^m, u_2^m, \ldots, u_n^m)^T$, and $A \in \mathbb{R}^{n,n}$ as the tridiagonal matrix

$$A = \frac{1}{(\Delta x)^2}\begin{pmatrix} 2 & -1 & 0 & \ldots & 0 \\ -1 & 2 & -1 & \ldots & \vdots \\ 0 & -1 & \ddots & \ddots & 0 \\ \vdots & \ddots & \ddots & 2 & -1 \\ 0 & \ldots & 0 & -1 & 2 \end{pmatrix}.$$

Then, the finite difference scheme can be written as

$$u^{m+1} = (2I - (\Delta t)^2 A)u^m - u^{m-1} \quad \text{for } m \geq 1,$$

where the initial approximations u^0 and u^1 are determined by the given initial conditions. The time step size Δt is chosen to satisfy the CFL condition $\frac{\Delta t}{\Delta x} \leq 1$. If the mesh parameters satisfy this bound, the numerical solution behaves qualitatively as the exact analytical solution [TW98]. The information given in this section draws on [TW98]. The reader is referred to this reference and to [But16] for further reading on finite differences.

2.3 Reverse Time Migration

Since seismic imaging is mainly about reflections, our goal is to find those reflection points. Reverse time migration (RTM) is one technique to achieve that. The main point of RTM relies on the *imaging condition*. This goes back to 1971, when Claerbout stated his famous imaging principle [Cla71; Rob10]:

> *'Reflectors exist at points in the ground, where the first arrival of the downgoing wave is time coincident with an upgoing wave.'*

Let us define x_r as location, where a propagated wave is reflected. We refer to the reflected wave as *upgoing wave*, since it travels up to Earth's surface, and we refer to the incident wave before it reaches the reflection point as *downgoing wave* (see Figure 2; downgoing waves in red and upgoing in blue). When the reflected wave is measured by the receivers, we do not know the reflection point yet. The aim of RTM is to determine this reflection

point. By solving the wave equation for guessed $m(x)$, we know the wave's position at any certain point in the time interval. To determine the reflection coefficient, we solve two modelling tasks:

1. Forward modelling of the downgoing wave by solving the wave equation [9].
2. Backward modelling of the upgoing wave by solving the wave equation in reversed time.

Once the velocity coefficient is fixed, the workflow of the first step is clear by Section 2.1 and Section 2.2. To make a good guess for the velocity coefficient is quite unlikely without further ado. Therefore, helpful resources like borehole techniques need to apply beforehand [FN24]. The reader is pointed to [Rob10] and [BM21] for further reading on the geophysical techniques behind.

In the second step, to calculate the propagation of the upgoing wave field in reversed time, we use the measurements at the surface as new source term of the original wave equation [9]. The wave equation is then solved backwards in time, thus from the final recording time $t = T$ to $t = 0$.

Following Claerbout's imaging condition, we need to determine when the downgoing and upgoing waves are coincident in time and we eventually have found the reflection point. Recall that in the end we want to estimate reflection coefficients at every location in the subsurface. If the reflection coefficient at x_r is $r \in \mathbb{R}$, the amplitude of the reflected wave field is $r \cdot u(x,t)$. The existence of a reflector at x_r is indeed revealed by the similarity between the two wave fields. In general, the imaging condition is equal to the ratio of the amplitude of the reflected wave to the incident wave. Therefore, we could take the ratio of the two wave fields in the time interval in which the reflection occurs, or an average of this ratio for all times, but this is not defined once the downgoing wave is zero for some time in that interval. Therefore it is not common to calculate the ratio of the two fields, but to choose an alterative method to solve this: calculating the cross correlation coefficient between the upgoing and downgoing wave fields [Cla71][Rob10].

Definition 2.4. *(Cross–correlation coefficient, [Cla71][Rob10]) We call $R(x)$ calculated by*

$$R(x) = \sum_{shots} \int_0^T u(x,t) \cdot v(x,t)\, dt \qquad [22]$$

the cross–correlation coefficient at location x.

Corollary 2.5. *(RTM workflow, [Rob10])*

1. *Forward modelling of a wave field with a (good) velocity model to get u_{fwd} at successive time steps ηdt for $\eta \in \mathbb{N}$.*
2. *Backward propagation of the measured data d through the same value of $m(x)$ to get u_{bwd}.*
3. *Cross–correlation of the downgoing and upgoing wave fields with equation* [22].

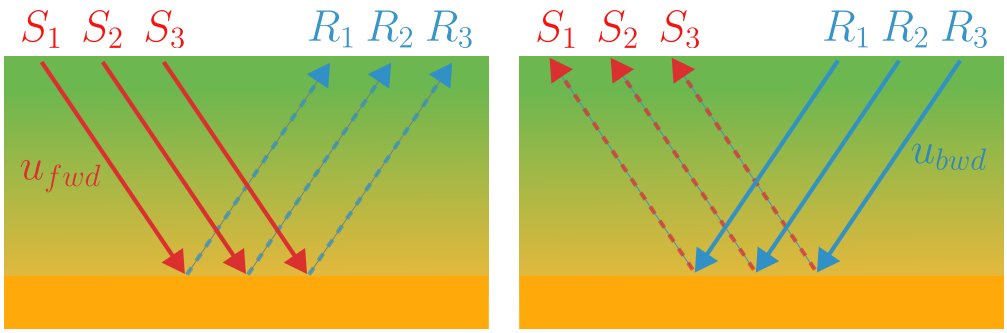

(a) Forward modelling (b) Backward modelling

Figure 6: Modelling workflow for RTM

The back propagation can equivalently be formulated by solving the adjoint wave equation in time reversed order. We will study the adjoint state method in Section 3.3 and derive the adjoint wave equation there. Also in Section 3, we will see that the adjoint wave equation is a useful tool for computing the gradient of the misfit function. Moreover, we link the notion of the adjoint wave equation to the adjoint operator that we mentioned in 1.1 in the context of the normal equations.

2.4 Least-Squares Reverse Time Migration

As described in Section 1.1, the Least-Squares problem is in general given by

$$\min_{x \in X} \|y - Ax\|_2. \tag{23}$$

There, A is the model, y represents the measurements taken and x is the input to the model. The problem is to find the most fitting x for given measurements y, that is, we wish to reconstruct the *true* data which generated the measurements. In the setting of this thesis we choose the scalar wave equation for modelling the wave propagation:

$$\begin{cases} m(x)\frac{\partial^2 u(x,t)}{\partial t^2} - \Delta u(x,t) = s(x,t), \\ u(x,0) = 0, \\ \frac{\partial u}{\partial t}(x,0) = 0. \end{cases} \tag{24}$$

We aim to find the wave that fits the measured signals. From now on, we refer to the observed data as d^{obs}. The inverse problem is to find the input $m(x)$ to the the forward model 24 that fits d^{obs}. The quantity which determines the solution u to the PDE is given by $m(x)$. Thus, we consider a *coefficient based inverse problem*. In analogy to d^{obs} we refer to $u(x,t)$ as synthetic data d^{syn}. Recall the measurements are taken at the *boundary* of the model space. To this end, we define a restriction operator R, to formally ensure u is evaluated at the boundary (cf. [Dem16], [Yan18]). So far, the problem we aim to solve reads

$$\min_m \frac{1}{2}\|Ru(m) - d^{obs}\|_2^2. \tag{25}$$

It is important to keep in mind, that u depends on m. Although the wave equation is linear, we have a non-linear mapping $\mathcal{F}(m)$ from model domain M to data domain that maps m to u. Therefore, to view the inverse problem 25 as a *linear* Least-Squares

problem, linearisation of the forward model is necessary. We call the linearised forward model $\mathcal{L}(m)$. In Section 2.4.1 we study a suitable linearisation for this forward map. The inverse problem is then to solve the following minimisation problem for m:

$$\min_m \frac{1}{2}\|\mathcal{L}(m) - d^{obs}\|_2^2. \tag{26}$$

2.4.1 A Linearisation for the Forward Map

We linearise the forward map $\mathcal{F}(m)$ to the first order, such that the linearisation is given by $\mathcal{L}(m) = \frac{\partial \mathcal{F}(m)}{\partial m}$. The well–known *Born approximation* is such a linearisation. Originally coming from quantum mechanics, it is a perturbation-theoretical approximation for scattering problems.[2] In seismology, it is common to consider a smooth background velocity and explain the scattered waves as reflections due to perturbations to this background velocity [HH80; Dem16].

That said, the perturbed $m(x)$ from [9] reads

$$m(x) = m_0(x) + \varepsilon m_1(x). \tag{27}$$

See Figure 7 and the blue lines in Figure 2 for illustrations of scattered waves. Since the choice of $m(x)$ determines the solution u of the wave equation [9], the wave field u also splits into two parts

$$u(x) = u_0(x) + u_s(x), \tag{28}$$

where u_s is the scattered wave field and u_0 solves the wave equation in the undisturbed wave equation with m_0, such that

$$m_0(x)\frac{\partial u_0}{\partial t^2} - \Delta u_0 = f(x,t) \tag{29}$$

with initial conditions as in [9]. The corresponding equation for the scattered wave u_{sc} can be determined as follows [Dem16]: By putting $u = u_0 + u_{sc}$ in [9] we obtain

$$m(x)\frac{\partial^2(u_0 + u_{sc})}{\partial t^2} - \Delta(u_0 + u_{sc}) = f(x,t) \tag{30}$$

$$\Leftrightarrow m(x)\frac{\partial^2 u_0}{\partial t^2} + m(x)\frac{\partial^2 u_{sc}}{\partial t^2} - \Delta u_0 - \Delta u_{sc} = f(x,t). \tag{31}$$

Subtracting [29] from [31] yields

$$\left(m(x)\frac{\partial^2 u_0}{\partial t^2} + m(x)\frac{\partial^2 u_{sc}}{\partial t^2} - \Delta u_0 - \Delta u_{sc}\right) - \left(m_0(x)\frac{\partial^2 u_0}{\partial t^2} - \Delta u_0\right) = 0 \tag{32}$$

$$\Leftrightarrow (m(x) - m_0(x))\frac{\partial^2 u_0}{\partial t^2} + m(x)\frac{\partial^2 u_{sc}}{\partial t^2} - \Delta u_{sc} = 0 \tag{33}$$

Since $m(x) = m_0(x) - \varepsilon m_1(x) \Leftrightarrow \varepsilon m_1(x) = m(x) - m_0(x)$, we plug this into [32]:

$$\varepsilon m_1(x)\frac{\partial^2 u_0}{\partial t^2} + m(x)\frac{\partial^2 u_{sc}}{\partial t^2} - \Delta u_{sc} = 0.$$

[2] It is named after Max Born who proposed this approximation during development of quantum theory.

As stated in [28], we assume that $u(x)$ describes the fully propagated wave in the sense that $u(x)$ consists of two parts: the incident wave $u_0(x)$ and the scattering u_{sc} [Dem16]. For the Born approximation, we suppose the scatterings are small, such that we can roughly estimate $u(x) \approx u_0(x)$. Therefore, we finally obtain the wave equation for the scattered wave u_{sc}:

$$m(x)\frac{\partial^2 u_{sc}}{\partial t^2} - \Delta u_{sc} = -\varepsilon m_1 \frac{\partial^2 u}{\partial t^2}. \tag{34}$$

We can rewrite u_{sc} in terms of a Green's function by

$$u_{sc}(x,t) = -\varepsilon \int_0^t \int_{\mathbb{R}^n} G(x,y;t-s) m_1(y) \frac{\partial^2 u}{\partial t^2}(y,s) dy ds. \tag{35}$$

Detailed literature on Green's functions can be found in [TW98] for instance. With [35] at hand, we find

$$u = u_0 - \varepsilon G m_1 \frac{\partial^2 u}{\partial t^2}$$

by plugging [35] into [28]. For the further derivation of the Born approximation, we rewrite the above equation to

$$u = u_0 - \varepsilon G m_1 \frac{\partial^2 u}{\partial t^2} \tag{36}$$

$$\Leftrightarrow u_0 = u + \varepsilon G m_1 \frac{\partial^2 u}{\partial t^2} \tag{37}$$

$$\Leftrightarrow u_0 = \left(I + \varepsilon G m_1 \frac{\partial^2 u}{\partial t^2} \right) u \tag{38}$$

$$\Leftrightarrow u = \left(I + \varepsilon G m_1 \frac{\partial^2 u}{\partial t^2} \right)^{-1} u_0, \tag{39}$$

where I is the identity operator. For simplification, we define

$$T \coloneqq \varepsilon G m_1 \frac{\partial^2 u}{\partial t^2}. \tag{40}$$

Therefore, [39] becomes

$$u = (I+T)^{-1} u_0.$$

This gives rise to the Neumann series, which is well known from operator theory [Dem16; Alt12].

Definition 2.6. *(Neumann series, [Alt12]) Let $(X, \|\cdot\|)$ be a normed space and $T : X \to X$ a continuous operator. This series $\sum_{n=0}^{\infty} T^n$ is called Neumann series.*

Lemma 2.7. *(On Neumann series, [Alt12]) If the Neumann series converges with respect to the operator norm, then $I - T$ is invertible and it holds*

$$(I-T)^{-1} = \sum_{k=0}^{\infty} T^k.$$

Remark 2.8. *A series converges with respect to the operator norm, if* $\|T\| < 1$ *[Alt12].*

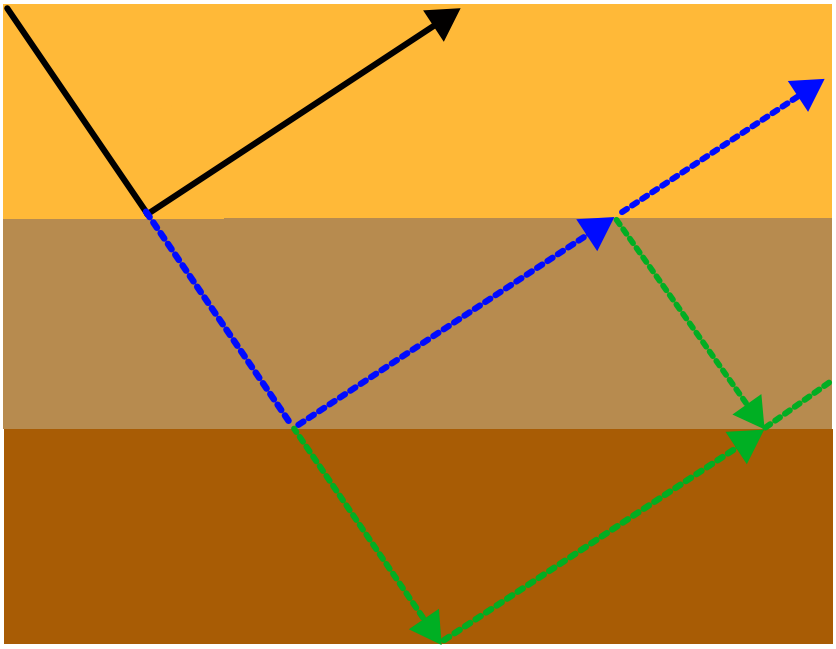

Figure 7: Single scattering (black) and multiple scatterings (blue and green)

Applying the Neumann series, we obtain by inserting 40 into definition 2.6

$$u = u_0 - \varepsilon \left(G m_1 \frac{\partial^2}{\partial t^2} \right) u_0 + \varepsilon G m_1 \frac{\partial d^2}{\partial t^2} \left(G m_1 \frac{\partial d^2}{\partial t^2} \right) + \ldots,$$

and summarise to

$$u = u_0 + \varepsilon u_1 + \varepsilon^2 u_2 + \ldots \varepsilon^n u_n. \qquad [41]$$

The series [41] is called *Born series*. A detailed proof of convergence of the Born series can be found in [Dem16] for instance. The basic idea relies on the assumption that the perturbation has a rather small influence on the wave propagation and thus multiple scatterings are not taken into account. This reasoning is also intuitive. If we measure the wave propagation at a fixed time t_f, it is more probable that the wave has been scattered only once by that time. The probability decreases further for a second scattering event, and even more so for subsequent scatterings. Thus, we approximate the Born series to the first order, which is the *Born approximation* [HH80; Dem16]:

$$u_{sc}(x) = \varepsilon u_1(x). \qquad [42]$$

From $u_1 = -G m_1 \frac{\partial^2 u_0}{\partial t^2}$ we can derive analogously to [34] the wave equation for $u_1(x)$:

$$m_0(x) \frac{\partial^2 u_1}{\partial t^2} - \Delta u_1 = -m_1(x) \frac{\partial^2 u_0}{\partial t^2}.$$

Thus, we can approximate u_s explicitly with εu_1. Therefore, we obtain a linear map

from m_1 to u_1:

$$\begin{cases} m_0(x)\frac{\partial^2 u_1(x,t)}{\partial t^2} - \Delta u_1(x,t) = -m_1 \frac{s(x,t)}{\partial^2 u_0(x,t)}, \\ u_1(x,0) = 0, \\ \frac{\partial u_1}{\partial t}(x,0) = 0. \end{cases} \quad [43]$$

Note that u_i for all $i \in \{1, 2, 3, \dots\}$ depends on m_1. To this end, the Born series can be seen as a Taylor series ([HH80; Dem16]) of the forward map $u = \mathcal{F}(m)$ in the sense of

$$u = u_0 + \varepsilon \frac{\partial \mathcal{F}}{\partial m}[m_0]m_1 + \frac{\varepsilon^2}{2}\left\langle \frac{\partial^2 \mathcal{F}}{\partial m^2}[m_0]m1, m1 \right\rangle + \cdots$$

or written compactly as

$$u = \sum_{n=0}^{\infty} \frac{\mathcal{F}^{(n)}(m_0)}{n!}(m(x) - m_0(x)).$$

The functional derivative $\frac{\partial \mathcal{F}}{\partial m} : m_1 \mapsto u_1$ is the linear approximation for the forward map $\mathcal{F}(m)$, which we denote by $\mathcal{L}$. With the linearised model at hand, we are able to solve the Least-Squares reverse time migration. This is addressed in the next section.

2.4.2 Solving the Least-Squares Reverse Time Migration Problem

In the previous section we chose m_0 as the background velocity. With m_0 known, we need to solve the wave equation to obtain the corresponding background wave field u_0. Afterwards, we need to solve equation [43], where we have to make a guess on the model perturbation εm_1 to simulate the scattered wave field εu_1. By solving this modelling task, we solve the forward problem.

Assuming the chosen background velocity m_0 was an accurate guess, the linearised map $\mathcal{L}$ maps the reflectivity m_r to the scattered wave field $d_r = \mathcal{F}(m) - \mathcal{F}(m_0)$, that is

$$\mathcal{L}m_r = d_r. \quad [44]$$

The inverse problem we aim to solve in the *Least-Squares reverse time migration problem* (LSRTM) is to solve equation [44] for m_r^*. In the Least-Squares approach, we find m_r^* by minimising the distance between the observed data d_r and the predicted scattered wave field m_r:

$$\min_m \|\mathcal{L}m_r - d_r\|_2^2.$$

The solution given by the normal equations is $m_r^* = (\mathcal{L}^T\mathcal{L})^{-1}\mathcal{L}^T d_r$, where $\mathcal{L}^T$ is the adjoint operator. It is well-known that solving the normal equations numerically, especially to invert $\mathcal{L}^T\mathcal{L}$, can be quite expensive and unstable [Ric20]. Therefore, the LSRTM problem is rather solved iteratively. In an iterative scheme like gradient descent $m(x)$ is updated successively until a certain tolerance is reached. Gradient descent is a local optimisation method, which can lead to the algorithm ending up in a local minimum [BTT11]. Global optimisation methods like swarm–based optimisation can avoid trapping into local minima [LTZ24b].

Although the accuracy of the images can be improved by the Least-Squares reverse time migration (compared to RTM), this method depends heavily on the choice of the background velocity. In practise, it is nearly impossible to make an exact guess for the background velocity. Furthermore, even small errors can make the forward and backward wave fields meet at a wrong location, which results in a wrong reflection point. Hence, we are not able to determine the true velocity coefficient $m(x)$. If we invert for the full $m(x)$ instead of guessing the background velocity m_0 first, we end up with a method called *full waveform inversion* [Rob10].

3 Full Waveform Inversion

The goal of full waveform inversion (FWI) is to reconstruct the velocity coefficient $m(x)$ in the wave equation [9], such that it fits the observed data. Once the true velocity coefficient is found, we gain information on the density of the corresponding media the waves have transmitted. By using many receivers and many sources, an image of the subsurface can eventually be reconstructed.

3.1 Overview

After one has chosen a proper model, full waveform inversion consists of three main iterative steps. See Figure 8 for an illustration of the scheme.

1. Solve the forward problem.
2. Compare solution of forward modelling and observed data.
3. Update the velocity coefficient and go back to the first step.

For $n \in \mathbb{N}$, let us denote by $d^{syn} \in \mathbb{R}^n$ the synthetic data, which are generated by a guess for $m(x)$. By $d^{obs} \in \mathbb{R}^n$, we denote data which was previously observed by the receivers. We now want to find the true $m(x)$, which describes the measurements correctly. To this end, we measure the distance $dist(d^{syn}(m), d^{obs})$ between the synthetic and the observed data and calculate

$$\underset{m}{\operatorname{argmin}}\, dist(d^{syn}(m), d^{obs}). \tag{45}$$

In this thesis, we choose to use gradient descent to update and therefore minimise the coefficient.

To measure the distance, we first need to define a misfit function. As in LSRTM, a common choice is to consider the L^2-norm of the distance between the synthetic and observed data. In time domain, the Least-Squares waveform misfit is defined as

$$dist(f, g) = \frac{1}{2} \sum_r \int |f(x_r, t; m) - g(x_r, t)|^2 dt, \tag{46}$$

where x_r are the receiver locations, $r \in \{1, 2, 3, \cdots, n\}$ [BOV09].

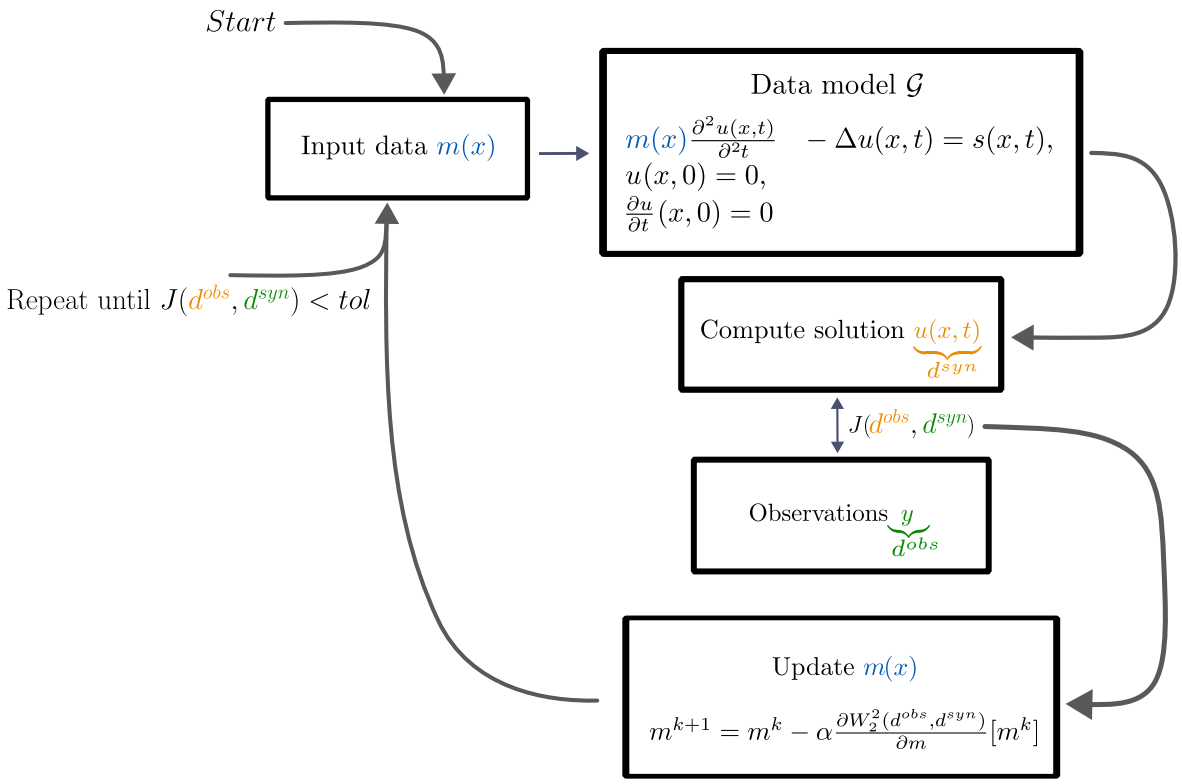

Figure 8: Scheme for FWI

3.2 Gradient Calculation

As we have seen in Section 1.1 and Section 1.2, we can find a solution for the inverse problem by using the adjoint of the model operator. What we aim for in FWI is the minimisation of the distance between the synthetic and the observed data. A common choice for the distance function is given by the L^2-norm. In Section 2.4.1 we have found a linearised forward model $\mathcal{L}(m)$. Thus, the inverse problem is to solve the following minimization for m:

$$J(m) = \frac{1}{2}\|\mathcal{L}(m) - d^{obs}\|_2^2. \qquad [47]$$

Our goal is now to minimise J with respect to m. We choose gradient descent as iterative optimisation scheme. The gradient descent scheme for [47] is given by

$$m^{k+1} = m^k - \alpha \frac{\partial J}{\partial m}[m^k], \qquad [48]$$

where α is for instance determined by a linesearch.

Proposition 3.1. *(On the adjoint operator, [Dem16]) Define the linearisation of $\mathcal{F}(m)$ as (cf. 2.4.2)*

$$\mathcal{L}(m) \coloneqq \frac{\partial \mathcal{F}}{m}[m].$$

Then $\frac{\partial J}{\partial m}[m] = \mathcal{L}^*(\mathcal{L}[m] - d)$.

Proof of Proposition 3.1, [Dem16].

$$\begin{aligned}\frac{\partial J}{\partial m}[m](h) &= \lim_{h\to 0}\frac{J(m+h)-J(m)}{h}\\ &= \lim_{h\to 0}\frac{\frac{1}{2}\|\mathcal{L}(m+h)-d\|-\frac{1}{2}\|\mathcal{L}(m)-d\|}{h}\end{aligned}$$

$$\begin{aligned}\|\mathcal{L}(m+h)-d\| &= \langle \mathcal{L}(m+h)-d, \mathcal{L}(m+h)-d\rangle\\ &= \langle \mathcal{L}(m-d), \mathcal{L}(m-d)\rangle + 2\langle \mathcal{L}h, \mathcal{L}[m]-d\rangle + \mathcal{O}(\|h\|^2)\end{aligned}$$

We calculate the distance $J[m+h]-J[m]$:

$$\begin{aligned}J[m+h]-J[m] &= \frac{1}{2}2\langle \mathcal{L}h, \mathcal{L}[m]-d\rangle + \mathcal{O}(\|h\|^2)\\ &= \langle h, \mathcal{L}^*(\mathcal{L}[m]-d)\rangle + \mathcal{O}(\|h\|^2),\end{aligned}$$

where the last equality follows by definition of the adjoint.

$$\frac{\partial J}{\partial m}[m] = \lim_{h\to 0}\left(\frac{\frac{1}{2}\|\mathcal{L}[m+h]-d\|-\frac{1}{2}\|\mathcal{L}[m]-d\|}{h}\right) = \mathcal{L}^*(\mathcal{L}[m]-d)$$

□

Similar to the inverse problem formulated in Section 1.1, we can solve the inverse problem by incorporating the adjoint of the model operator. Transposing[3] the operator $\mathcal{L} = \frac{\delta \mathcal{F}}{\delta m}$ is not an efficient way to compute the adjoint $\mathcal{L}^*$ [Dem16]. The next paragraph addresses the adjoint state method, which is an efficient way for computing the adjoint $\mathcal{L}^*$ [Cao+03; Dem16; Joh21; Ple06].

3.3 Adjoint State Method

Recall we want to find a suitable m, such that

$$J(m) = \frac{1}{2}\|\mathcal{L}(m)-d\|_2^2 \qquad [49]$$

is minimised. The first variation of 49 can by the chain rule be written as

$$\frac{\partial J}{\partial m} = \left\langle \frac{\partial J}{\partial u}, \frac{\partial u}{\partial m}\right\rangle. \qquad [50]$$

When computing [50] directly via the derivatives $\frac{\delta u}{\delta m}$, the wave equation needs to be solved for each value in $m(x)$. The goal of the adjoint state method is to provide a more efficient way to compute $\frac{\partial u}{\partial m}$. With the linearisation of the forward model we can write the wave equation as

$$\mathcal{L}(m)u = f, \qquad [51]$$

[3]Since seismic data consists of real numbers, transposing (instead of building the transpose and the complex conjugate) is sufficient in the context of this thesis.

to which we also refer as *state equation* [Ple06]. Differentiating with respect to m, we obtain by the chain rule

$$\frac{\partial \mathcal{L}}{\partial m} u + \mathcal{L} \frac{\partial u}{\partial m} = 0. \tag{52}$$

Next, we define the *adjoint state equation*

$$\frac{\partial J}{\partial u} = \mathcal{L}^* q, \tag{53}$$

where $\mathcal{L}^*$ is the adjoint operator and q the corresponding *adjoint field* [Ple06]. Therefore, we can see the left hand side, $\frac{\delta J}{\delta u}$, as the source term of the state equation 51. We substitute $\frac{\partial J}{\partial u}$ in [50] by $\mathcal{L}^* q$ and obtain

$$\frac{\partial J}{\partial m} \overset{(1)}{=} \left\langle \mathcal{L}^* q, \frac{\partial u}{\partial m} \right\rangle \overset{(2)}{=} \left\langle q, \mathcal{L} \frac{\partial u}{\partial m} \right\rangle \overset{(3)}{=} - \left\langle q, \frac{\partial \mathcal{L}}{\partial m} u \right\rangle,$$

where the second equality follows by definition of the adjoint and the third equality by transforming

$$\begin{aligned} \frac{\partial \mathcal{L}}{\partial m} u + \mathcal{L} \frac{\partial u}{\partial m} &= 0 \\ \Leftrightarrow \mathcal{L} \frac{\partial u}{\partial m} &= - \frac{\partial \mathcal{L}}{\partial m} u. \end{aligned}$$

The last term, after the third equality sign, is the *imaging condition* [Dem16], as we will prove in the sequel of this chapter. To this end, we compute the adjoint state equation, in particular the adjoint field, for the case of the wave equation [9].

Recall that we want to determine

$$\frac{\partial J}{\partial m}[m] = \mathcal{L}^* \left(\mathcal{L}(m) - d \right),$$

where

$$\mathcal{L} \colon m \mapsto d$$

is a mapping from model to data space, and

$$\mathcal{L}^* \colon d \mapsto m$$

is a mapping from data to model space. As we will see, the application of the adjoint is a simple form of imaging. If we make a good guess for m_0 and the experiment involves a sufficient[4] number of receivers, the first iteration of gradient descent

$$m^{(1)} = \alpha \mathcal{L}^* (d - \mathcal{L}(m_0))$$

often provides an image close to the true εm_1 [Dem16; Rob10]. Thus, $\mathcal{L}^*$ is not only called adjoint but also imaging operator. Indeed, the adjoint state method results in the imaging condition, as was outlined in Section 6 on reverse time migration.

[4]The number of receivers necessary is determined by the specific details of the experiment.

In general, by using the definition of the adjoint operator we can write

$$\langle d, \mathcal{L}m\rangle = \langle d, u\rangle \quad [54]$$
$$\Leftrightarrow \langle \mathcal{L}^* d, m\rangle = \langle d, u\rangle \quad [55]$$
$$\Leftrightarrow \langle d, \mathcal{L}m\rangle = \langle \mathcal{L}^* d, m\rangle. \quad [56]$$

We can further rewrite [54] to

$$\langle d, \mathcal{L}m\rangle = \sum_r \int_0^T d_r(t) u(x_r, t) dt \quad [57]$$

and we can also write

$$\langle \mathcal{L}^* d, m\rangle = \int_{\mathbb{R}^n} (\mathcal{L}^* d)(x) m(x) dx. \quad [58]$$

Since $\mathcal{L}$ is a differential operator, we need to integrate by parts in x to get from [57] to [58]. Therefore, the sum over the receivers in [57] needs to be transformed to an integral. To this end, we define for each measurement $d_r(t)$ a Dirac delta function located at x_r to take into account whether there are measurements made at x or not [Dem16].

Definition 3.2. *(Dirac delta function, [Rud13]) The Dirac delta function is defined on* $\mathbb{R}$ *as*

$$\delta(x) = \begin{cases} 0, & x \neq 0 \\ \infty, & x = 0, \end{cases}$$

such that

$$\int_{-\infty}^{\infty} \delta(x) = 1.$$

We call the new function $d_{new}(x, t)$ and define it formally as

$$d_{new}(x, t) = \sum_r d_r(t) \delta(x - x_r).$$

Then, equation [57] becomes

$$\langle d, \mathcal{L}m\rangle = \int_{\mathbb{R}^n} \int_0^T d_{ext}(x, t) u(x, t) dx dt. \quad [59]$$

As explained above (compare to equation [53]), we now use the *adjoint field* $q(x, t)$:

$$\left(m_0 \frac{\partial^2}{\partial t^2} - \Delta \right) q(x, t) = d_{ext}(x, t). \quad [60]$$

We consider the boundary conditions below. Our next step is to derive the adjoint state equation, which we briefly mentioned in Section 2.3. Recall that we want to find $\mathcal{L}^*$ such that

$$\langle d, \mathcal{L}m\rangle = \langle \mathcal{L}^* d, m\rangle.$$

To achieve this, we first substitute d_{ext} in equation [60] and then integrate by parts both in time and in space [Dem16]:

$$\begin{aligned}
\langle d, \mathcal{L}m\rangle &= \int_{\mathbb{R}^n}\int_0^T \left(m_0\frac{\partial^2}{\partial t^2} - \Delta\right) q(x,t)u(x,t)dxdt \\
&= \int_{\mathbb{R}^n}\left[m_0\frac{\partial d}{\partial dt}q(x,t)u(x,t)\right]_0^T - \int_{\mathbb{R}^n}\int_0^T m_0\frac{dq}{dt}\frac{d}{dt}u(x,t)dt \\
&\quad + \int_{\partial\mathbb{R}^n}\int_0^T \frac{dq}{dn}u(x,t)dS_x dt - \int_{\mathbb{R}^n}\int_0^T \Delta u(x,t)q(x,t)dxdt \\
&= \int_{\mathbb{R}^n}\left[m_0\frac{\partial d}{\partial dt}q(x,t)u(x,t)\right]_0^T - \int_{\mathbb{R}^n}\left[m_0 q(x,t)\frac{d}{dt}u(x,t)\right]_0^T + \int_{\mathbb{R}^n}\int_0^T m_0 q(x,t)\frac{d^2}{dt^2}u(x,t)dxdt \\
&\quad + \int_{\partial\mathbb{R}^n}\int_0^T u(x,t)\frac{dq}{dn}dS_x dt - \int_{\partial\mathbb{R}^n}\int_0^T q(x,t)\frac{du}{dn}dS_x + \int_{\mathbb{R}^n}\int_0^T q(x,t)\cdot(\Delta u(x,t))dx \\
&= \int_{\mathbb{R}^n}\left[m_0\frac{\partial d}{\partial dt}q(x,t)u(x,t)\right]_0^T - \int_{\mathbb{R}^n}\left[m_0 q(x,t)\frac{d}{dt}u(x,t)\right]_0^T \\
&\quad + \int_{\partial\mathbb{R}^n}\int_0^T u(x,t)\frac{dq}{dn}dS_x dt - \int_{\partial\mathbb{R}^n}\int_0^T q(x,t)\frac{du}{dn}dS_x \\
&\quad + \int_{\mathbb{R}^n}\int_0^T q(x,t)\cdot(-\Delta u(x,t)) + q(x,t)m_0\frac{d^2}{\partial dt^2}u(x,t)dx \\
&= \int_{\mathbb{R}^n}\int_0^T \left(m_0\frac{\partial^2}{\partial t^2} - \Delta\right) q(x,t)u(x,t)dxdt \\
&\quad + \int_{\mathbb{R}^n}\left[m_0\frac{\partial q}{\partial t}u\right]_0^T dx - \int_{\mathbb{R}^n}\left[m_0 q\frac{\partial u}{\partial t}\right]_0^T dx + \int_{\partial\mathbb{R}^n}\int_0^T \frac{dq}{dn}udS_x dt - \int_{\partial\mathbb{R}^n}\int_0^T q\frac{\partial u}{\partial n}dS_x dt.
\end{aligned}$$

We consider the wave equation with boundary conditions (cf. equation 9)

$$u(x,0) = 0 \quad \text{and} \quad \frac{\partial u}{\partial t}(x,0) = 0.$$

Hence the boundary terms become zero at $t = 0$. Since we are interested in the values of $q(x,t)$ for $t \in [0,T]$, we need to consider the other boundary conditions at $t = T$. Then, they become zero only if $q|_{t=T} = \frac{\partial q}{\partial t}|_{t=T} = 0$. Considering time values $0 \leq t \leq T$, we can think of the above conditions as *final* conditions [Dem16; Joh21; Ple06]. The data is sampled at the receivers at time $t = T$. Therefore, we can think of the adjoint equation [60] [60] as run backward in time from $t = T$ to $t = 0$.[5] Following [Dem16], we transform the adjoint state equation [60] to the imaging condition [61]:

$$\begin{aligned}
\langle d, \mathcal{L}m\rangle &= \int_{\mathbb{R}^n}\int_0^T q(x,t)\left(m_0\frac{\partial^2}{\partial t^2} - \Delta\right)u(x,t)dxdt \\
&= -\int_{\mathbb{R}^n}\int_0^T q(x,t)m(x)\frac{\partial^2 u_0}{\partial t^2}dxdt.
\end{aligned}$$

[5]Recall the backward propagation in RTM.

Since this equals $\langle m, \mathcal{L}^* d \rangle$, we obtain

$$(\mathcal{L}^* d)(x) = -\int_0^T q(x,t) \frac{\partial^2 u_0}{\partial t^2} dt \tag{61}$$

regardless of m. In equation [61], $q(x,t)$ is the solution to the adjoint wave field and $\frac{\partial^2 u_0}{\partial t^2}$ is the upgoing wave field in the context of RTM (cf. Section 2.3). Until now we have omitted the source term in the wave equation. When we consider the L^2-norm as misfit function $J[u] = \frac{1}{2}\|Ru - d\|_2^2$, the source term of the adjoint wave equation becomes

$$\frac{\partial J}{\partial u} = R^*(Ru - d).$$

Corollary 3.3. *When considering the L^2-norm as misfit function, the adjoint wave equation is of the form*

$$\begin{cases} m(x)\frac{\partial^2 q(x,t)}{\partial t^2} - \Delta q(x,t) = R^*(Ru - d), \\ q(x,T) = 0, \\ \frac{\partial q_t}{\partial t}(x,T) = 0. \end{cases} \tag{62}$$

Corollary 3.4. *Due to the adjoint state method, we have found a formal representation of $\frac{\partial J}{\partial m}$:*

$$\frac{\partial J}{\partial m} = -\int_0^T \frac{d^2 u(x,t)}{dt^2} v(x,t),$$

where v is the solution to the adjoint wave equation [62].

As we have seen above in the adjoint state equation [53], the derivative of the misfit function is exactly the source term of the adjoint wave equation. When a different objective function is employed, the only aspect that changes is the source term. The source term of the adjoint wave equation is also discussed in [FBI06].

In the context of LSRTM, it has already been shown that the initial guess is often not very accurate in practice, even when supplemented with additional information from borehole seismics [BM21]. Hence, the imaging condition usually does not yield a good image. Therefore, we use the concept of full waveform inversion, where we invert for the $m(x)$ that fits the measurements by minimising the distance between d^{obs} and d^{syn}. To address this optimisation problem, the next step involves employing a gradient-based method, such as gradient descent. For this purpose, it is necessary to define a misfit function. While the L^2-norm is commonly used, it has certain limitations that justify considering alternative norms. In the following subsection, we explore the applicability of several potential norms.

3.4 Choice of Misfit Function

The standard choice for the misfit function is the L^2-norm. However, given that the L^2-norm is just one among many other well-established norms and is known for its sensitivity to noise, the question arises as to whether it is truly the most suitable choice. In the following, we compare the L^2-norm, the L^1-norm and the *Huber loss*, the latter being widely used in machine learning. After discussing these norms, we introduce another

norm derived from the field of optimal transport – the Wasserstein metric – and evaluate its suitability as a misfit function for seismic imaging.

Before diving into a discussion on the above norms, let us first recall the definition of the Huber loss function.

Definition 3.5 (Huber loss, [Hub64]). *For* $\delta \in \mathbb{R}^+$

$$L_\delta(a) = \begin{cases} \frac{1}{2} r(x)^2 & \text{for } |r(x)| \leq \delta \\ \delta \cdot \left(|r(x)| - \frac{1}{2}\delta \right), & \text{otherwise.} \end{cases}$$

The factor $r(x)$ *often refers to the difference between the observed and synthetic (or predicted) values, i.e.* $r(x) = y - f(x)$.

It is widely known that the L^1-norm is less sensitive to noise than the L^2-norm [LLM16; Alp10; SSBD14]. However, a significant drawback of the L^1-norm is its lack of differentiability (see Figure 9), which makes it challenging to use effectively in optimisation problems. The Huber loss, on the other hand, is also less sensitive to noise compared to the L^2-norm. Yet, in order to maximise model accuracy, the parameter δ must also be optimised, which increases computational complexity.

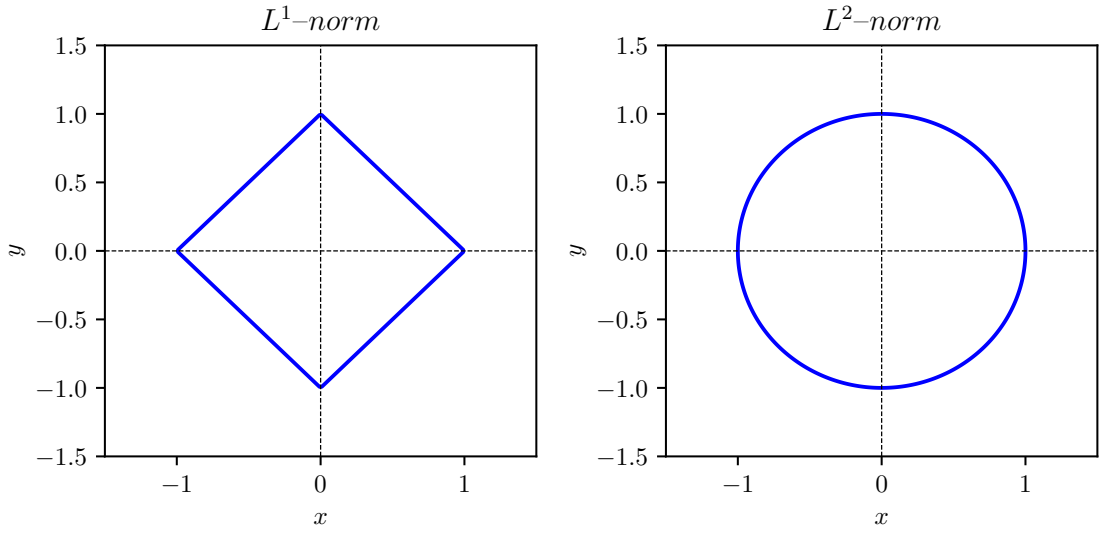

Figure 9: Unit sphere for L^1-norm and L^2-norm in $\mathbb{R}^2$

This reasoning contributes to the standard use of the L^2-norm as a misfit function. Next, we will be more precise and consider the L^2-norm in the context of full waveform inversion.

In FWI, we begin by estimating the velocity coefficient $m(x)$ and solving the wave equation based on this initial guess. Once the wave equation is solved, we obtain the synthetic data d^{syn}. We then compare d^{syn} to the observed data d^{obs}. When solving the wave equation for any $m(x)$ that does not fit the true data accurately, three scenarios can (probably simultaneously) occur to d^{syn}: time shifts relative to d^{obs}, partial amplitude changes, and dilations or contractions (see Figures 19, 20, 22) [Yan+17b]. These scenarios will be addressed in detail in Section 4.5.

A metric which deals with these issues should incorporate horizontal shifts rather than focusing solely on amplitude differences, as the L^2-norm does. One distance that fulfils our

wish for incorporating the horizontal shift between the signals, is the *Wasserstein distance* [EF14]. In Figures 10 and 11 the difference in the behaviour between Wasserstein distance W^2 and L^2 are illustrated.

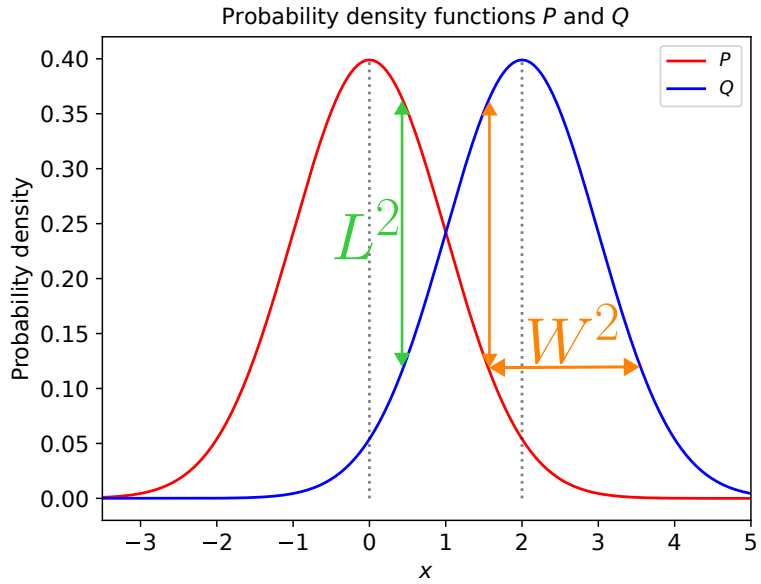

Figure 10: Two horizontally shifted, overlapping Gaussian probability density functions and $L^2(P, Q)$ and $W^2(P, Q)$ distances.

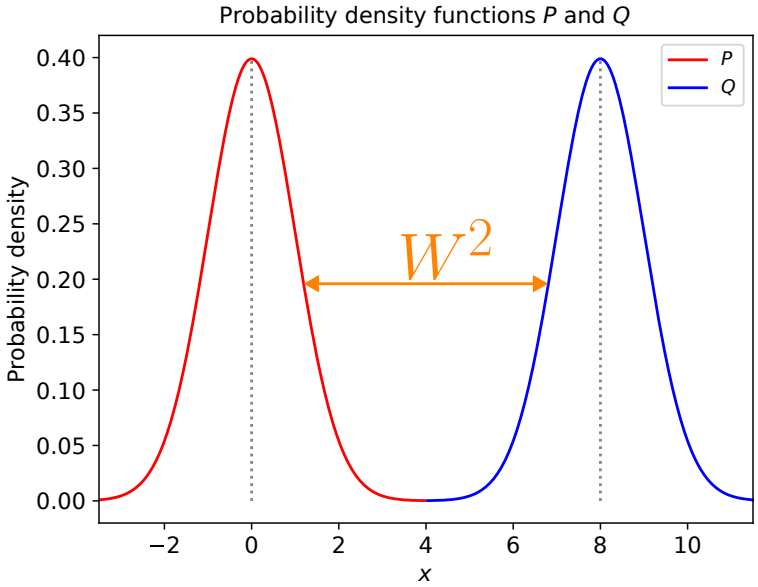

Figure 11: Two horizontally shifted but not overlapping Gaussian probability density functions and $W^2(P, Q)$ distance; $L^2(P, Q)$ can not measure any distance there.

The Wasserstein distance function originates from the field of optimal transport. In optimal transport, signals are treated as probability density functions, and the objective is

to determine the minimal cost required to transform one into the other [EF14][Vil03]. In Section 4 we give all necessary prerequisites from optimal transport theory and rigorously define the Wasserstein distance. As we will see, the Wasserstein metric is a natural way to compare the probability distributions of two random variables X and Y. At this point, we only *illustrate* the difference between common loss functions and the Wasserstein distance to show the reader the perspective of using the Wasserstein distance as a misfit function. Therefore, consider two probability density functions P and Q (see Figure 12).

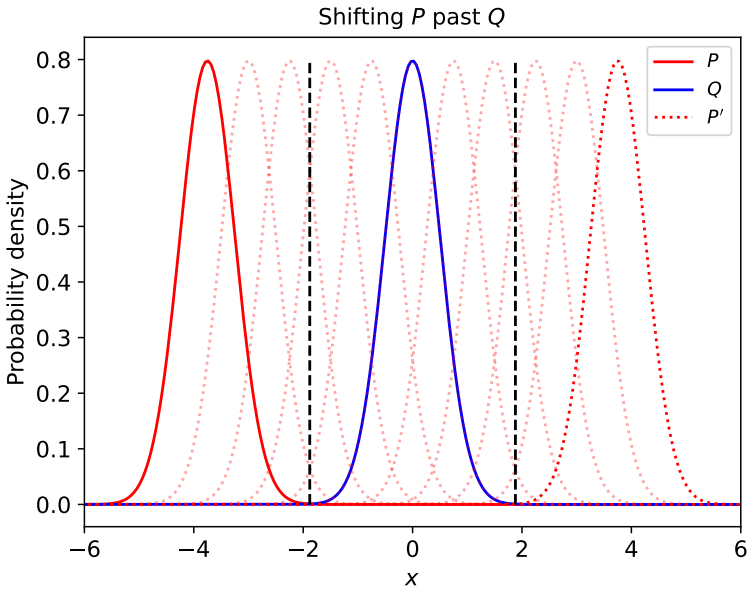

Figure 12: One signal shifted past the other (dotted red curves) and their overlapping points (dashed black lines).

We shift P towards and past Q (illustrated by the dotted red curves). The behaviour of the above norms with respect to shift values is shown in Figure 13. While L^1, L^2 and Huber loss in Figure 13 begin measuring the distance once the non zero values of the two densities start overlapping, the Wasserstein metric measures a distance greater than zero for the whole interval of shift values, even though P and Q are not overlapping. This illustrates the ability of the Wasserstein distance to measure horizontal shifts. In Section 4.2 we will formally consider the behaviour of the Wasserstein distance.

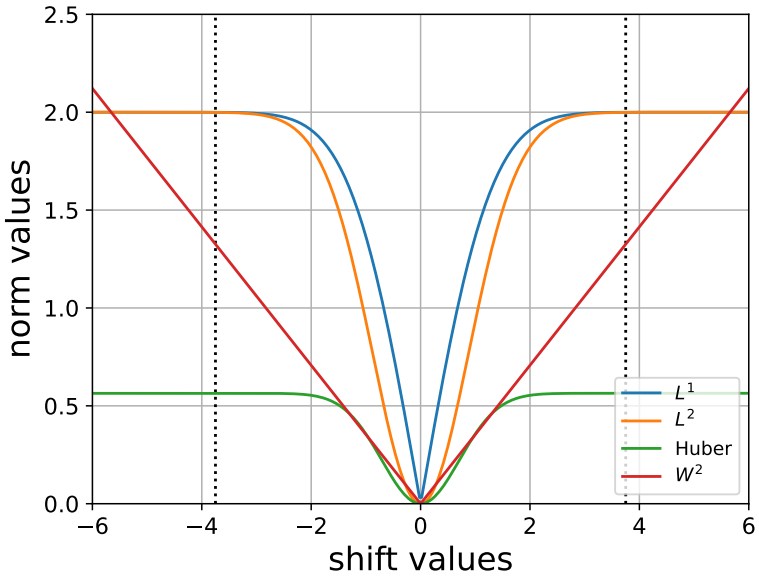

Figure 13: Several norms in comparison regarding their behaviour with respect to shift.

Furthermore, in the context of full waveform inversion, the L^2-norm faces a significant challenge known as cycle-skipping. The periodic propagation of seismic waves may cause this issue: if the observed and synthetic data are more than half a wavelength apart (see Figure 16), there is a phase mismatch between the observed an the synthetic data. Then, the gradient of the misfit function might go into the wrong direction, leading to convergence towards a local minimum [SJV22; Tar05; Yan18]. But even for smaller time shifts between the observed and synthetic data, the L^2-norm possibly produces local minima (see Figure 15).

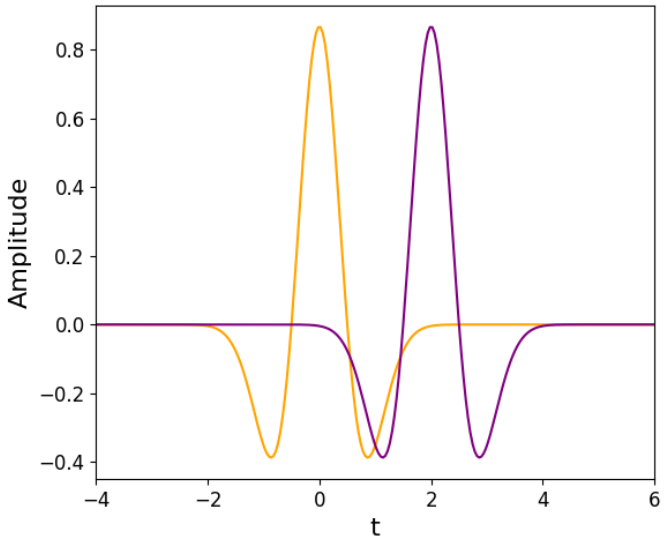

Figure 14: Two time-shifted Ricker waves

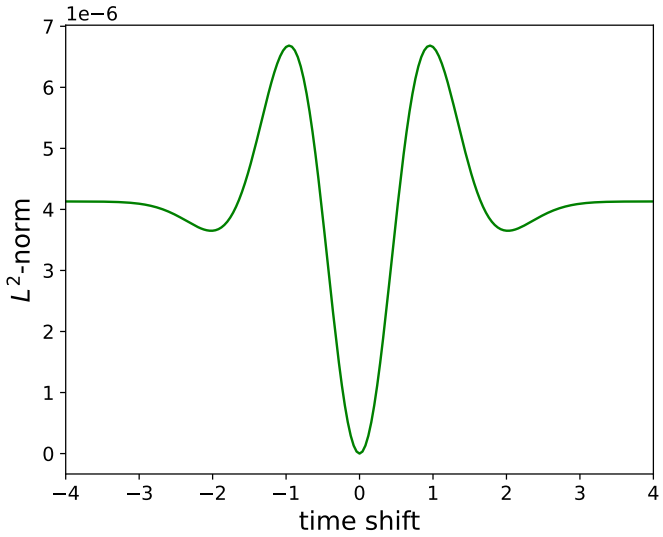

Figure 15: L^2-norm between two shifted Ricker waves from Figure 14 leading to local minima

The problem of cycle skipping is less pronounced at lower frequencies, where phase mismatches are less likely, as the wavelength increases inversely with frequency:

$$\lambda = \frac{c}{f}.$$

In the above equation, λ is the wavelength, c is the wave propagation velocity, and f is the frequency. Unfortunately, seismic FWI often involves high-frequency waveforms due to the nature of seismic data, increasing the risk of cycle-skipping [EF14; Yan+17b]. A practical approach to addressing this issue is to start with low-frequency waves in the initial velocity model. By progressively inverting from lower to higher frequencies, the risk of phase mismatches can be mitigated, thereby improving the robustness of the inversion process [EF14; Yan+17b]. Therefore, using the Wasserstein metric appears to be an effective tool for overcoming cycle-skipping

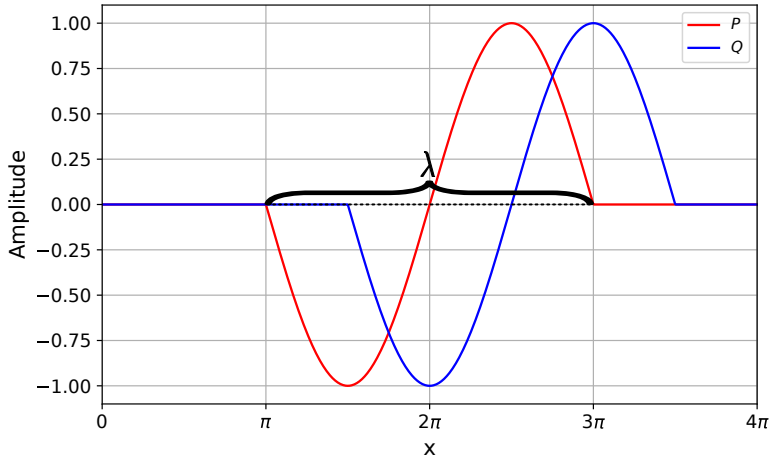

Figure 16: Q is shifted from P by $\frac{\pi}{2}$.

4 Optimal Transport

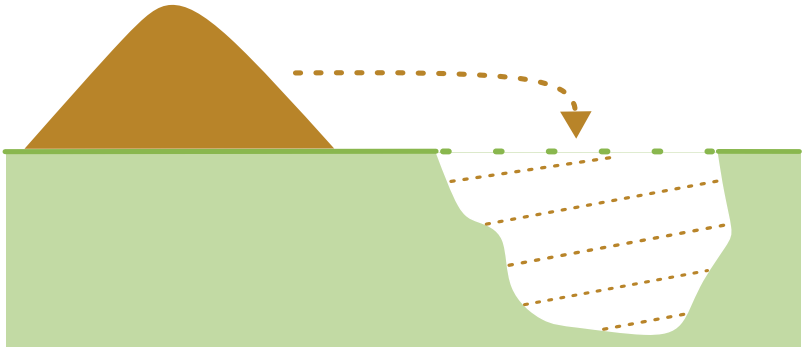

Figure 17: A mass transportation problem

Optimal transport dates back to the 18th century and was first described by Gaspard Monge, who found a solution to a mass transportation problem. To illustrate this problem, assume we have a pile of sand and wish to use the entire amount to fill a hole with the same volume (cf. Figure 15). In optimal transport, we model the pile and the hole by probability measures μ and ν defined on (not yet specified) measure spaces $\mathcal{X}$ and $\mathcal{Y}$ respectively. Let $\mathcal{A}$ be a measurable subset of $\mathcal{X}$ and $\mathcal{B}$ be a measurable subset of $\mathcal{Y}$. Then, $\mu(\mathcal{A})$ measures the amount of sand is located in $\mathcal{A}$. Analogously, $\nu(\mathcal{B})$ measures the amount of sand in $\mathcal{B}$. Moving the sand can be quite costly in effort, and we wish to fill the hole at minimal cost. To this end, we define a cost function $c(x, y)$ defined on $\mathcal{X}$ and $\mathcal{Y}$, which gives the effort of moving one unit of mass from a location x in the pile to a location y in the hole. In the sequel, we formally define the relevant terms from optimal transport and give main results.

4.1 Monge's and Kantorovich's formulation

Definition 4.1. *(Transport mapping) Consider two measurable spaces X and Y with non-negative Borel measures μ and ν respectively. Further, let*

$$T : \mathcal{X} \to \mathcal{Y}$$

be a measurable bijective mapping, which we call the transport mapping.

For rearranging one distribution into the other, we require two conditions: mass preservation and volume equality.

Definition 4.2. *(Mass preservation, [Vil03]) We want T to be a measure preserving map, thus*

$$\mu(T^{-1}(\mathcal{A})) = \nu(\mathcal{A}). \tag{63}$$

In shorter notation, it is common to write $T_{\#}\mu = \nu$, when equation [63] *holds.*

Definition 4.3. *(Volume equality, [Vil03]) It holds $\mu(\mathbb{R}^n) = \nu(\mathbb{R}^n)$.*

Definition 4.4. *(Cost function) We denote by*

$$c : \mathcal{X} \times \mathcal{Y} \to \mathbb{R}$$

the cost for the transport of mass between x and y.

Example 4.5. *The most common choice for the cost function $c(x, y)$ is the euclidean norm between x and y, thus $\|x - y\|^2$ as defined in definition 1.8.*

Remark 4.6. *The L^1-norm has also been used in literature, especially in the context of machine learning, see [ACB17; PC19] for instance. We will revisit the choice of the cost function in Section 4.3.*

Definition 4.7 (Monge's formulation (1781), [Vil03])**.** *Solve the optimisation problem*

$$\inf_{T_{\mu,\nu}\in\mathcal{M}} \mathscr{M} := \inf_{T_{\mu,\nu}\in\mathcal{M}} \left\{ \int_{\mathbb{R}^n} c(x, T(x))\ d\mu(x) \right\}$$

in compliance with volume equality and mass preservation.

Note that by definition of the transport mapping, each element of $\mathcal{X}$ is mapped to exactly one element in $\mathcal{Y}$. Therefore, mass splitting is not possible in Monge's formulation.

Example 4.8. *(Monge problem and mass splitting, [Tho18])*
Consider two discrete dirac measures

$$\begin{aligned} \mu &= \delta(x_1), \\ \nu &= \frac{1}{2}\delta(y_1) + \frac{1}{2}\delta(y_2), \end{aligned}$$

where $y_1 \neq y_2$. Then $\nu(y_1) = \frac{1}{2}$, but $\mu(T^{-1}(y_1)) \in \{0, 1\}$ depending on whether $x_1 \in T^{-1}(y_1)$.

Corollary 4.9. *The Monge problem does not always have a solution, since mass splitting is not possible.*

To allow mass splitting and therefore achieve solvability of the optimisation problem, Kantorovich formulated a relaxed version of the Monge problem. Instead of searching for a bijective transportation mapping, Kantorovich aimed for a transportation plan. In this transportation plan, we capture the transported mass in a probability measure π, which is measure-supported on the product space $\mathcal{X} \times \mathcal{Y}$. There, x can be transported to multiple points y_i, while in the Monge problem this was not possible. To match up with the requirements of the Monge problem, we want

$$\int_{\mathcal{X}} d\pi(x, y) = d\mu(x) \tag{64}$$

and

$$\int_{\mathcal{Y}} d\pi(x, y) = d\nu(x). \tag{65}$$

In other words, we want for $\mathcal{A} \subset \mathcal{X}$, that

$$\pi(A, \mathcal{Y}) = \mu(\mathcal{A}), \tag{66}$$

and for $\mathcal{B} \subset \mathcal{Y}$, that

$$\pi(\mathcal{Y}, B) = \nu(\mathcal{B}). \tag{67}$$

Definition 4.10. *(Marginals) We say that the measures π that satisfy* [66] *and* [67] *have marginals μ and ν respectively.*

Definition 4.11. *(Admissible transportation plans, [Vil03]) We denote the set of all admissible transportation plans π by*

$$\Pi(\mu,\nu) = \{\pi \in P(X \times Y) \mid [66] \text{ and } [67] \text{ hold for all } \mathcal{A} \text{ and } \mathcal{B}\}\,.$$

Definition 4.12 (Kantorovich's formulation (1939),[Vil03; Kan06])**.** *Solve the optimisation problem*

$$\inf_{\pi\in\Pi(\mu,\nu)} \mathscr{K} \coloneqq \inf_{\pi\in\Pi(\mu,\nu)} \left\{ \int_{\mathcal{X}\times\mathcal{Y}} c(x,T(x))d\pi(x,y) \right\}. \tag{68}$$

Corollary 4.13. *Since every transport mapping determines a transportation plan of the same cost, the Kantorovich problem is weaker than the Monge problem. Therefore, it holds*

$$\inf_{\pi\in\Pi(\mu,\nu)} \left\{ \int_{\mathcal{X}\times\mathcal{Y}} c(x,T(x))d\pi(x,y) \right\} \leq \inf \left\{ \int_{\mathbb{R}^n} c(x,T(x))\ d\mu(x) \right\}.$$

While for the Monge problem it is not guaranteed to find an optimal mapping, the Kantorovich problem is solvable for any continuous cost function with lower bound [Vil03]. In particular, the problem is solvable for cost functions of the form $|x-y|^p$, when μ and ν are absolutely continuous with respect to the Lebesgue measure. We specify this statement in the following theorem, which is a corollary of Brenier's Theorem [Bre91].

Theorem 4.14. *(Relation between the solvability of the Kantorovich and the Monge problem, [Kan06; Vil03]) Consider compactly supported probability measures μ and ν on $\mathbb{R}^n$, which are continuous with respect to the Lebesgue measure. Further consider $x(x,y) = \|x-y\|^2$ as cost function. Due to the strict convexity of the L^p-norm for $p>1$, there exists a unique solution to the Kantorovich problem, which is then also a solution to the Monge problem.*

Proof. See proof of theorem 2.12 (iii) in [Vil03].[6] □

We assume that the cost function $c(x,y)$ has lower bound and X, Y are bounded. Therefore the infimum in equation [68] is finite. Hence, to establish the existence of a minimum, we use a compactness argument. To this end, recall the well known Bolzano-Weierstrass theorem.

Theorem 4.15 (Bolzano-Weierstrass theorem, [Ste23])**.** *Let $f : U \to \mathbb{R}$ be continuous and let U be a compact set. Then, f achieves a minimum on U [Ste23] .*

Theorem 4.16 (Existence of a minimiser for the Kantorovich problem, [Vil03; Kan06])**.** *Assume $c(x,y)$ is bounded below and continuous. Then the Kantorovich problem admits a minimiser.*

Proof. Since the cost function $c(x,y)$ lives in $\mathbb{R}^n$, we can think of compact spaces in the sense of sequentially compact spaces and thus need to define a notion of convergence. Fix

[6] We give a proof for the case where $\mu, \nu \in \mathbb{R}$ in Section 4.3.

$U = \Pi(\mu, \nu)$. A sequence of measures γ_n converges to γ, i.e. $\gamma_n \to \gamma$, if

$$\int_{X\times Y} g(x,y)d\gamma_n(x,y) \to \int_{X\times Y} g(x,y)d\gamma \quad \forall g \in C^0(X \times Y).$$

To make use of the Bolzano-Weierstrass theorem, we need to verify these two conditions:

1. $\Pi(\mu, \nu)$ is compact,
2. $c(x, y)$ is convergent.

To check the first assumption, choose $\pi_n \in \Pi(\mu, \nu)$ and find a convergent subsequence π_{n_k}, which converges to $\pi \in \Pi(\mu, \nu)$. We need to check the marginals (cf. definition [4.10]). Choose $g(x) \in C^0(x)$.

$$\begin{aligned}\int_{X\times Y} g(x)d\pi(x,y) &= \lim_{\kappa\to\infty} \int_{X\times Y} g(x)d\pi_{n_k}(x,y) \\ &= \int_X g(x)d\mu(x),\end{aligned}$$

since $\Pi_{n_\mu} \in \Pi(\mu, \nu)$ and therefore the marginal over X is μ. Analogously, the marginal of Π over Y is ν. Thus, $\Pi(\mu, \nu)$ is compact. For the second assumption, we need to check if

$$f(\pi) = \int_{X\times Y} c(x,y)d\pi(x,y) \quad \text{for } \pi \in U.$$

Again, choose $\pi_n \in \Pi(\mu, \nu)$ such that $\pi_n \to \Pi(\mu, \nu)$. To prove continuity, we need to show

$$f(\pi_n) \to f(\pi).$$

$$f(\pi_n) = \int_{X\times Y} c(x,y)d\pi_n(x,y) \to \int_{X\times Y} c(x,y)d\pi(x,y) = f(\pi),$$

since $\pi_n \to \pi$ by assumption and further we assumed $c(x, y)$ to be continuous. Hence, f is continuous. By the Bolzano-Weierstrass theorem, the Kantorovich formulation admits a minimiser for a real-valued, continuous cost function over a compact set. □

Remark 4.17. *The minimiser is not necessarily unique.*

Remark 4.18. *We did not need to specify a metric for the cost function, as it is sufficient for the space to be metrisable. Furthermore, the solvability of the Kantorovich problem can be proven not only for continuous cost functions but also for lower semi-continuous cost functions, provided certain conditions are met. Specifically, when considering Polish spaces $\mathcal{X}$ and $\mathcal{Y}$, compactness follows from the Prokhorov theorem, ensuring the existence of optimal transportation plans. Since the conditions from Theorem* [4.16] *are sufficient for the purpose of this thesis, we stick to the results thereof. The reader is pointed to [Tho18] and [Kan06] for further reading on the solvability of the Kantorovich problem for lower semi-continuous cost functions and the relevant theory behind.*

4.2 The Wasserstein Distance

With the relaxed formulation by Kantorovich, a new distance function between probability densities on a given metric space was invented: the Wasserstein distance.

Definition 4.19 (Wasserstein distance (1969), [Kan06; Vil03])**.**

$$W_p(\mu,\nu) = \left(\inf_{T_{\mu,\nu}\in\mathcal{M}} \int_{\mathbb{R}^n} c(x, T_{\mu,\nu}(x))^p d\mu(x) \right)^{1/p}$$

for all $p \in [1,\infty)$ and where $\mathcal{M}$ is the set of all maps that rearrange the distribution μ into ν.

Definition 4.20. *(Wasserstein distance with cost function of L^p type)*

$$W_p(\mu,\nu) = \left(\inf_{T_{\mu,\nu}\in\mathcal{M}} \int_{\mathbb{R}^n} \|x - T_{\mu,\nu}(x)\|^p d\mu(x) \right)^{1/p}$$

for all $p \in [1,\infty)$. In analogy to $p-$norms we refer to these kind of Wasserstein distance as Wasserstein $p-$distance.

Remark 4.21. *In the sequel, we will often use the quadratic Wasserstein $2-$distance. It is defined with the L^2-norm as cost function:*

$$W_2^2(\mu,\nu) = \left(\inf_{T_{\mu,\nu}\in\mathcal{M}} \int_{\mathbb{R}^n} \|x - T_{\mu,\nu}(x)\|^2 d\mu(x) \right).$$

Also note the added upper index.

Theorem 4.22. *(Wasserstein distance is a metric, [Vil03]) For a symmetric and (non-strictly) positive cost function, the Wasserstein distance satisfies the definition of a metric. That is,*

- *Symmetry: $W_p(\mu,\nu) = W_p(\nu,\mu)$,*
- *Positivity: $W_p(\mu,\nu) \geq 0$ and $W_p(\mu,\nu) = 0 \Leftrightarrow f = g$,*
- *Triangle inequality: $W_p(\mu,\nu) \leq W_p(\mu,\sigma) + W_p(\sigma,g)$.*

Remark 4.23. *Note that the Wasserstein metric depends on the definition of $T_{\mu,\nu}(x)$. While $T_{\mu,\nu}(x)$ is a transport mapping in Monge's formulation, it is a transportation plan in Kantorovich's formulation. Theorem 4.22 can be proven in general when viewing $T_{\mu,\nu}$ as a transportation plan. As we will see, the Wasserstein distance also fulfils the properties of a metric in the Monge's case, when considering the p-norms as cost functions.*

To prove the triangle inequality in the Kantorovich case, we apply the well-known *gluing lemma* to probability spaces.

Lemma 4.24 (Gluing lemma, [Ste23])**.** *Let μ,ν,σ be three probability measures, supported on measure spaces $\mathcal{X},\mathcal{Y},\mathcal{Z}$ respectively. Further define two transportation plans $\pi_{12} \in \Pi(\mu,\nu)$ and $\pi_{23} \in \Pi_{(\nu,\sigma)}$. Then there exists a probability measure $\pi \in P(\mathcal{X}\times\mathcal{Y}\times\mathcal{Z})$ with marginals π_{12} on $\mathcal{X}\times\mathcal{Y}$ and π_{23} on $\mathcal{Y}\times\mathcal{Z}$.*

Another lemma we will use in the proof, is on the Minkowski inequality.

Lemma 4.25. *(Minkowski Inequality, [Ste23]) For $\mu \in L^p$ and $\nu \in L^p$ holds for all $p \in [1, \infty)$:*

$$\|\mu + \nu\|_{L^p} \leq \|\mu\|_{L^p} + \|\nu\|_{L^p}.$$

Proof of Theorem 4.22 for Kantorovich's formulation. For the proof we need to check the above three properties of a metric. We start by proving symmetry. Since the cost function is symmetric, the Wasserstein metric is as well. Positivity incorporates three conditions:

1. $W_p(\mu, \nu) \geq 0$,
2. $\mu = \nu \Rightarrow W_p(\mu, \nu) = 0$,
3. $W_p(\mu, \nu) = 0 \Rightarrow \mu = \nu$.

The first property follows by positivity of the cost function $c(x, y)$, the second one by the symmetry condition. For the third one, assume $W_p(\mu, \nu) = 0$.
Then, there exists a transportation plan $\pi \in \Pi(\mu, \nu)$, such that

$$\int_{\mathcal{X}\times\mathcal{Y}} |x - y|^p d\pi(x, y) = 0.$$

This means, π is supported on $\{(x, y) \in \mathcal{X} \times \mathcal{Y} \mid x = y\}$. Choose $\mathcal{A} \subseteq \mathcal{X}$.

$$\begin{aligned}
\mu(\mathcal{A}) &= \int_{\mathcal{A}} d\mu(x) = \int_{\mathcal{A}\times\mathcal{Y}} d\pi(x, y) \\
&= \int_{\mathcal{A}\times\mathcal{A}} d\pi(x, y) = \int_{\mathcal{X}\times\mathcal{A}} d\pi(x, y) \\
&= \nu(\mathcal{A})
\end{aligned}$$

Hence, $\mu = \nu$ and (3) holds.

Finally, we show the triangle inequality. To this end, assume $\mu, \nu, \sigma \in P(\mathcal{X})$ and let π_{12} and π_{23} as in Lemma [4.24] be optimal transportation plans. We choose $\mathcal{X}$ to be the support of μ, $\mathcal{Y}$ to be the support of ν and $\mathcal{Z}$ to be the support of σ. Analogously, let π_{13} be the marginal of π on $\mathcal{X} \times \mathcal{Z}$ and $\pi_{13} \in \Pi_{(\mu,\sigma)}$.

$$\begin{aligned}
W_2(\mu, \sigma) &\leq \left(\int_{\mathcal{X}\times\mathcal{Z}} d(x, z)^p d\pi_{13}(x, z) \right)^{1/p} && [69] \\
&= \left(\int_{\mathcal{X}\times\mathcal{Y}\times\mathcal{Z}} d(x, z)^p d\pi(x, y, z) \right)^{1/p} && [70] \\
&\leq \left(\int_{\mathcal{X}\times\mathcal{Y}\times\mathcal{Z}} (d(x, y) + d(y, z))^p d\pi(x, y, z) \right)^{1/p}, && [71]
\end{aligned}$$

whereat [69] we used the fact that $W_2^2(\mu, \nu)$ is not necessarily optimal. Since $\mathcal{Y}$ is independent of the above distance, we can rewrite [69] to [70]. In [71], we used the triangle

inequality. Next we obtain [73] by the Minkowski inequality:

$$\left(\int_{\mathcal{X}\times\mathcal{Y}\times\mathcal{Z}} (d(x,y)+d(y,z))^p d\pi(x,y,z)\right)^{1/p} \tag{72}$$

$$\leq \left(\int_{\mathcal{X}\times\mathcal{Y}\times\mathcal{Z}} d(x,y,z)^p d\pi(x,y,z)\right)^{1/p} + \left(\int_{\mathcal{X}\times\mathcal{Y}\times\mathcal{Z}} d(y,z)^p d\pi(x,y,z)\right)^{1/p} \tag{73}$$

$$= \left(\int_{\mathcal{X}\times\mathcal{Y}} d(x,y)^p d\pi(x,y)\right)^{1/p} + \left(\int_{\mathcal{Y}\times\mathcal{Z}} d(y,z)^p d\pi_{23}(y,z)\right)^{1/p} \tag{74}$$

$$= W_p(\mu,\nu) + W_p(\nu,\sigma), \tag{75}$$

which proves the claim. □

Corollary 4.26. *This holds in particular for cost functions of L^p type.*

Next, we prove that the Wasserstein $p-$distance defines a metric, when T is a transport mapping as in *Monge's formulation* and the cost function is of L^p type.

Theorem 4.27. *For an L_p type cost function, the Wasserstein distance fulfils the properties of a metric.*

Proof of Theorem 4.27. We start by proving symmetry. Since the cost function is symmetric, the Wasserstein metric is as well. Positivity incorporates three conditions:

1. $W_P(\mu,\nu) \geq 0$,
2. $\mu = \nu \Rightarrow W_p(\mu,\nu) = 0$,
3. $W_p(\mu,\nu) = 0 \Rightarrow \mu = \nu$.

The first property follows by positivity of the cost function $c(x,y)$, the second one by the symmetry condition. For the third one, assume $W_p(\mu,\nu) = 0$.
Then, there exists a transportation plan $\pi \in \Pi(f,g)$, such that

$$\int_{\mathcal{X}\times\mathcal{Y}} |x-y|^p d\pi(x,y) = 0.$$

This means, π is supported on $\{(x,y) \in \mathcal{X}\times\mathcal{Y} \mid x = y\}$. Choose $\mathcal{A} \subseteq \mathcal{X}$.

$$\begin{aligned}\mu(\mathcal{A}) &= \int_{\mathcal{A}} d\mu(x) = \int_{\mathcal{A}\times\mathcal{Y}} d\pi(x,y) \\ &= \int_{\mathcal{A}\times\mathcal{A}} d\pi(x,y) = \int_{\mathcal{X}\times\mathcal{A}} d\pi(x,y) \\ &= g(\mathcal{A})\end{aligned}$$

Hence, $\mu = \nu$ and (3) holds.

To proof the triangle inequality, define three mappings

$$\begin{aligned} T_1 &: \mu \to \sigma \\ T_2 &: \sigma \to \nu \\ T &: \mu \to \nu, \end{aligned}$$

where $T = T_2 \circ T_1$. Further, define $Id(x) = x$ for all $x \in \mathcal{X}$. Since $T : f \to g$ may not be optimal, we obtain

$$\begin{aligned} & W_p(\mu,\nu) \leq \left(\int |x - T(x)|^p d\mu \right)^{1/p} = \|Id(x) - T(x)\|_{L_p(\mu)} \\ \Leftrightarrow\ & W_p(\mu,\nu) \leq \|Id(x) - T_1(x)\| L_p(\mu) + \|T_1(x) - T(x)\|_{L_p(\mu)} \\ \Leftrightarrow\ & W_p(\mu,\nu) \leq \left(\int |x - T_1(x)|^p d\mu(x) \right)^{1/p} + \left(\int |T_1(x) - T_2(T_1(x))|^p d\mu \right)^{1/p} \\ \Leftrightarrow\ & W_p(\mu,\nu)_{\text{،}} \leq \left(\int |x - T_1(x)|^p d\mu(x) \right)^{1/p} + \left(\int |T_1(x) - T_2(T_1(x))|^p d\mu \right)^{1/p} \\ \Leftrightarrow\ & W_p(\mu,\nu) \leq W_p(\mu,\sigma) + \left(\int |y - T_2(y)|^p d\sigma \right)^{1/p} \\ \Leftrightarrow\ & W_p(\mu,\nu) \leq W_p(\mu,\sigma) + W_p(\sigma,\nu) \end{aligned}$$

Finally, we have shown the triangle inequality. □

In Section 3.4, we already illustrated the behaviour of Wasserstein distance in comparison to other commonly used misfit functions. In Figure 13, the behaviour of Wasserstein distance and other commonly used misfit functions as L^2-norm were plotted with respect to horizontal shifts. While the L^2-norm measures the vertical differences between the red and the blue curve, it is illustrated that the Wasserstein distance *additionally* captures the horizontal distance between the two curves. When the curves do not overlap, the L^2-norm is not able to compare the curves horizontally, while the Wasserstein distance indeed is. This idea was also summarised schematically in Figures 10 and 11.

The formal definition of the Wasserstein metric at hand, we are now able to prove our earlier observations. We formally capture the results in the following lemma.

Lemma 4.28. *(Behaviour of Wasserstein and L^2-distance) Let f and g be probability density functions and s their horizontal shift, such that $f(x) = g(x - s)$ as illustrated in Figures 10 and 11 from Section 3.4. For overlapping f and g, both L^2 and W^2 are of complexity $\mathcal{O}(s)$, while for non overlapping f and g, $L^2 \in \mathcal{O}(1)$ but $W^2 \in \mathcal{O}(s)$.*

Proof. We first consider the case, when the two density functions overlap as in Figure 10.

$$\begin{aligned} L_2(f,g) = \|f - g\|_{L^2} &= \left(\int (f-g)^2 dx \right)^{1/2} \\ &= \left(\int \mathcal{O}(s^2) \right)^{1/2} \\ &= \mathcal{O}(s) \end{aligned}$$

Note that f and g are shifted by $g(x) = f(x - s)$.

$$\begin{aligned} W_2(f,g) &= \left(\int [x - T(x)]^2 f(x) dx \right)^{1/2} \\ &= \left(\int s^2 f(x) dx \right)^{1/2} \\ &= \mathcal{O}(s) \end{aligned}$$

Hence, for overlapping density functions, both L^2 and W^2 increase linearly within the horizontal shift s.
Next, we consider the case, when f and g are not overlapping as in Figure 11.

$$\begin{aligned} L_2(f,g) &= \|f - g\|_{L_2} \\ &= \left(\int (f - g)^2 dx \right)^{1/2} \\ &= \left(\int 2f^2 dx \right)^{1/2} \\ &= \mathcal{O}(1) \\ W_2(f,g) &= \left(\int [x - T(x)]^2 f(x) dx \right)^{1/2} \\ &= \mathcal{O}(s) \end{aligned}$$

As we can see, the L^2 distance is bounded, when f and g do not overlap (cf. [EF14]). □

Corollary 4.29. *From Lemma 4.28 we conclude, that the Wasserstein distance is a suitable metric for incorporating horizontal shifts.*

At this point, we show another elementary result for the Wasserstein distance, which will be useful in Section 4.5.3.

Lemma 4.30. *The quadratic Wasserstein distance fulfils the convexity property:*

$$W_2^2(\alpha\mu_1 + (1-\alpha)\mu_2,\, \alpha\nu_1 + (1-\alpha)\nu_2) \leq \alpha W_2^2(\mu_1, \nu_1) + (1-\alpha) W_2^2(\mu_2, \nu_2).$$

Proof. We proof this lemma for Kantorovich's formulation. Define $\mu = \alpha\mu_1 + (1-\alpha)\mu_2$ and $\nu = \alpha\nu_1 + (1-\alpha)\nu_2$. Let $\pi_1 \#_{\mu_1} = \nu_1$ and $\pi_2 \#_{\mu_2} = \nu_2$ be optimal transportation plans. Define $\pi = \alpha\pi_1 + (1-\alpha)\pi_2$. Then we have to show that π is a feasible transportation plan. Thus we need to check the marginals. To this end, define $A \subset X$ and $B \subset Y$ as in definition 4.10.

$$\begin{aligned} \pi(A, Y) &= \alpha\pi_1(A, Y) + (1-\alpha)\pi_2(A, Y) \\ &= \alpha\mu_1(A) + (1-\alpha)\mu_2(A) \\ &= \mu(A) \end{aligned}$$

and

$$\begin{aligned}\pi(X,B) &= \alpha\pi_1(X,B) + (1-\alpha)\pi_2(X,B)\\ &= \alpha\nu_1(B) + (1-\alpha)\nu_2(B)\\ &= \nu(B).\end{aligned}$$

Therefore, we have

$$W_2^2(\mu,\nu) \leq \int_{X\times Y} (x-y)^2 d\pi(x,y) \quad [76]$$

$$= \alpha \int_{X\times Y} (x-y)^2 d\pi_1(x,y) + (1-\alpha)\int_{X\times Y} (x-y)^2 d\pi_2(x,y) \quad [77]$$

$$= \alpha W_2^2(\mu_1,\nu_1) + (1-\alpha)W_2^2(u_2,\nu_2), \quad [78]$$

where equation 77 holds since π_1 and π_2 are optimal. □

Remark 4.31. *In Sections 4.5.1,4.5.2 and 4.5.3 we show the convexity of the quadratic Wasserstein metric concerning shift, dilation, and partial amplitude changes.*

With the Wasserstein metric, we have defined a way to measure the distance between two probability densities. The Wasserstein metric utilises the transportation mapping in Monge's formulation and the transportation plan in Kantorovich's. In general, it is difficult and not always possible to find an explicit formulation for the transportation. However, in the one-dimensional case, i.e., for $x \in \mathbb{R}$, we can indeed derive an explicit formulation. To this end, we focus on the one-dimensional case in Section 4.3. In Section 4.6, we apply this explicit formulation in the context of full waveform inversion.

4.3 Optimal Transport in One Dimension

To find an approach to the one-dimensional optimal transport problem, we choose the L^2-norm as cost function.

Problem 4.32. *(Monge's formulation) Solve*

$$\min\left\{\int \|(x - T(x))\|^2 f(x)dx, \right. \quad [79]$$

such that

$$\int_{T^{-1}(\mathcal{A})} \mu(x)dx = \int_{\mathcal{A}} \nu(y)dy$$

for all $\mathcal{A} \subset \mathbb{R}$.

In the one-dimensional case we only have two possible directions on the coordinate axis, in which we can transport data. This gives rise to the idea, that the optimal transport mapping may be monotone. We proof this for general probability density functions in the following proposition.

Proposition 4.33 (Monotonicity of the one-dimensional optimal transport mapping, [Vil03])**.** *For a quadratic cost function the optimal map* $T(x)$ *is monotone.*

Proof of Proposition 4.33, [Vil03]. Let $x_1 \in I_1$ and $x_2 \in I_2$, where I_1 and I_2 are open intervals, and assume without loss of generality that $x_1 < x_2$. Let $\varepsilon > 0$ such that

$$\int_{I_1} \mu(x)dx = \varepsilon = \int_{I_2} \mu(x)dx \tag{80}$$

holds. Assume x_1 and x_2 are mapped by $T(x)$ to some y_1 and y_2, where $y_1 < y_2$. For $i \in \{0, 1, 2, \dots\}$ define

$$T(x_i) = y_i.$$

We define a second mapping $\tilde{T}(x)$

$$\tilde{T}(x) = \begin{cases} y_1, & \text{if } x = x_2 \\ y_2, & \text{if } x = x_1 \\ T(x), & \text{if } x \notin I_1 \cup I_2. \end{cases}$$

Suppose $T(x)$ is optimal. Then by definition of optimality

$$\begin{aligned}
& \frac{1}{2}\int_{I_1\cup I_2} |(x - T(x))|^2 \mu(x)dx \leq \frac{1}{2}\int_{I_1\cup I_2} |(x - \tilde{T}(x))|^2 \mu(x)dx \\
\Leftrightarrow \quad & \frac{1}{2}\int_{I_1} x^2\mu(x)dx + \frac{1}{2}\int_{I_1} T(x)^2\mu(x)dx - \int_{I_1} xT(x)\mu(x)dx \\
+ \quad & \frac{1}{2}\int_{I_2} x^2\mu(x)dx + \frac{1}{2}\int_{I_2} T(x)^2\mu(x)dx - \int_{I_2} xT(x)\mu(x)dx \\
\leq \quad & \frac{1}{2}\int_{I_1} x^2\mu(x)dx + \frac{1}{2}\int_{I_1} \tilde{T}(x)^2\mu(x)dx - \int_{I_1} x\tilde{T}(x)\mu(x)dx \\
+ \quad & \frac{1}{2}\int_{I_2} x^2\mu(x)dx + \frac{1}{2}\int_{I_2} \tilde{T}(x)^2\mu(x)dx - \int_{I_2} x\tilde{T}(x)\mu(x)dx
\end{aligned}$$

Using equation [80], dividing by ε and rewriting the above inequality such that the right hand side becomes zero, we obtain

$$\frac{1}{\varepsilon}\int_{I_1} x(\tilde{T}(x) - T(x))\mu(x)dx + \frac{1}{\varepsilon}\int_{I_2} x(\tilde{T}(x) - T(x))\mu(x)dx \leq 0. \tag{81}$$

Recall that we consider Monge's formulation for a quadratic cost under the constraint that

$$\int_{T^{-1}(\mathcal{A})} \mu(x)dx = \int_{\mathcal{A}} g(y)dy$$

for all $\mathcal{A} \subset \mathbb{R}$. To this end, we take $\varepsilon \to 0$. Assuming the limit exists, we obtain

$$\begin{aligned}
& \lim_{\varepsilon\to 0}\left(\frac{1}{\varepsilon}\int_{I_1} x(\tilde{T}(x) - T(x))\mu(x)dx + \frac{1}{\varepsilon}\int_{I_2} x(\tilde{T}(x) - T(x))\mu(x)dx\right) \\
= \quad & x_1(y_2 - y_1) + x_2(y_1 - y_2),
\end{aligned}$$

which in summary means that

$$x_1(y_2 - y_1) + x_2(y_1 - y_2) \leq 0.$$

Since x_i and y_i are real values, we can rewrite this equation to

$$\begin{aligned} & x_1y_2 - x_1y_1 + x_2y_1 - x_2y_2 \leq 0 \\ \Leftrightarrow \quad & y_2x_1 - y_1x_1 + y_1x_2 - y_2x_2 \leq 0 \\ \Leftrightarrow \quad & (y_2 - y_1)(x_2 - x_1) \geq 0, \end{aligned}$$

where both the first and the second factor is greater or equal to zero. Hence, the optimal transportation map is monotone. □

Remark 4.34. *Note that the above is true for a quadratic cost and does not hold for other cost functions in general [Vil03].*

Theorem 4.35 (Explicit formulation of the one-dimensional optimal transport mapping, [Vil03])**.** *In the one-dimensional case we can formulate an explicit expression for the optimal transport mapping.*

The optimal map is constructed via the cumulative distribution function of the given densities f and g for the synthetic and observed data respectively. Before we can proof the theorem by deriving the explicit formulation, we give some prerequisites from probability theory first.

Definition 4.36. *(Cumulative distribution function (I), [BT08]) In probability theory, the cumulative distribution function (CDF) of a real-valued random variable X, evaluated at x, is the probability that X will take a value less than or equal to x. Formally,*

$$F_X(x) = P(X \leq x).$$

Every probability distribution supported on the real numbers is uniquely identified by a right-continuous monotone non-decreasing function $F : \mathbb{R} \to [0, 1]$ which satisfies

$$\lim_{x \to -\infty} F(x) = 0$$

and

$$\lim_{x \to \infty} F(x) = 1.$$

Definition 4.37. *(Cumulative distribution function (II), [BT08]) For a given density $f(x)$, we define the corresponding cumulative distribution function as*

$$F(x) = \int_{-\infty}^{x} f(t)dt.$$

Definition 4.38 (Inverse of CDF, [BT08])**.** *If the CDF $F(x)$ is strictly increasing and continuous, the inverse distribution function (also called the quantile function) is defined as*

$$F^{-1}(p) = x, \quad p \in [0, 1],$$

where x is the unique value such that $F(x) = p$.

Definition 4.39 (Generalised inverse of CDF, [BT08])**.** *If a distribution does not have a unique inverse, we define the generalised inverse as*

$$F^{-1}(p) = \inf\{x \in \mathbb{R} \mid F(x) \geq p\}, \quad p \in [0, 1].$$

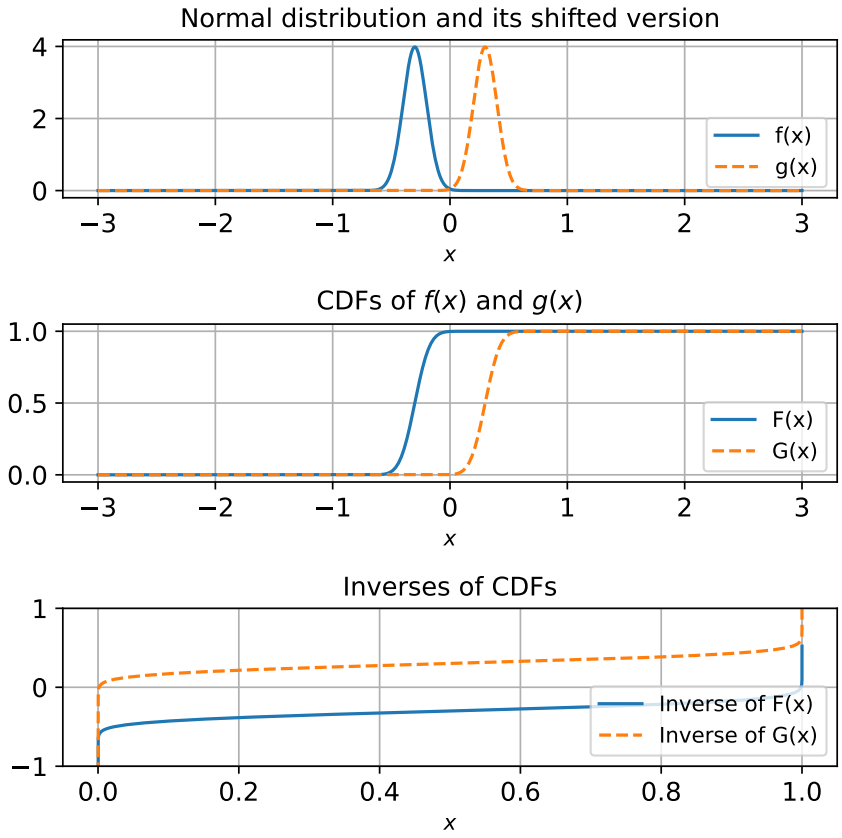

Figure 18: Normal distribution $f(x)$ and its shifted version $g(x)$, their CDFs and the respective inverses of the CDFs

Proof of Theorem 4.35. For given strictly positive densities $f(x)$ and $g(x)$, we define their respective cumulative distribution functions as

$$F(x) = \int_{-\infty}^{x} f(t)dt$$

and

$$G(y) = \int_{-\infty}^{y} f(t)dt.$$

Take a point x, which is mapped to $T(x) = y$ by the optimal transport mapping. We know by proposition 4.33 that this mapping is monotone. That is, for a fixed x we have

$$F(x) = \int_{-\infty}^{x} f(t)dt = G(y) = \int_{-\infty}^{y} f(t)dt.$$

In shorter notation we can write

$$F(x) = G(T(x)). \tag{82}$$

Thanks to definitions 4.37 and 4.38 we reformulate this equation to

$$T(x) = G^{-1}(F(x)). \tag{83}$$

Thus, with equation [83] we have found an explicit expression for the one-dimensional optimal transport map. □

Remark 4.40. *Note that we assumed f and g to be strictly positive, since otherwise we would not have been able to transform equation* [82] *into equation* [83].

Theorem 4.41. *(On the optimal transportation in the one-dimensional case, [San15; Vil03]) Let $\mu, \nu \in \mathbb{R}$ be probability density functions with cumulative distributions F and G respectively. Let $c(x, y) = \|x - y\|_{L^2}$. Further, let $\pi^\star$ be the measure on $\mathbb{R}^2$ with cumulative distribution function $H(x, y) = \min(F(x), G(y))$. Then,*

1. *$\pi^\star \in \Pi(\mu, \nu)$ and $\pi^\star$ is optimal for the Kantorovich problem with cost function $c(x, y)$.*
2. *The Wasserstein metric is given by $W_2^2(\mu, \nu) = \int_0^1 |F^{-1}(t) - G^{-1}(t)|^2 dt$.*

In the proof of the above theorem, we make use of the following lemma.

Lemma 4.42. *([San15]) Assume $x_1 < x_2$ for x_1, x_2, y_1, y_2. Furthermore, define a continuous and strictly convex cost function, such as $|x - y|_{L^2}$. When it holds*

$$\|x_1 - y_1\|_{L^2} + \|x_2 - y_2\|_{L^2} \leq \|x_1 - y_1\|_{L^2} + \|x_2 - y_1\|_{L^2} \tag{84}$$

for all tuple $(x_1, y_1), (x_2, y_2)$, then $y_1 \leq y_2$.

Proof of Lemma 4.42, [San15]. Assume $y_1 > y_2$. Then, equation 84 reads

$$\|x_1 - y_1\|_{L^2} + \|x_2 - y_2\|_{L^2} \leq \|y_2 - x_1\|_{L^2} + \|y_1 + x_2\|_{L^2}.$$

Moreover, $y_1 > y_1$ implies $y_2 - x < y - x$. Therefore, $y_2 - x_1$ and $y_1 + x_2$ live in $[y_2 - x_2, y - x]$. Define $\delta = \frac{x_2 - x_1}{(x_2 - y_2) - (x_1 - y_1)}$ living in $(0, 1)$, which can be seen by expanding the fraction. Then,

$$y_2 - x_1 = (1 - \delta)(y_2 - x_2) + \delta(y_1 - x_1), \quad y_1 + x_2 = \delta(y_2 - x_2) + (1 - \delta)y_1 - x_1.$$

Define $a = y - x$, $b = y_2 - x_2$ and $d = x_2 - x_1$. The strict convexity of the cost function yields

$$\begin{aligned} c(a) + c(b) &\leq c(b + d) + c(a - d) \\ &< (1 - \delta)c(b) + \delta c(a) + \delta c(b) + (1 - \delta)c(a) \\ &= c(a) + c(b), \end{aligned}$$

which is a contradiction. Therefore, $y_1 \leq y_2$. □

Proof of Theorem 4.41, [San15; Vil03]. By Theorem 4.16, there exists an optimal transportation plan $\pi \in \Pi(\mu, \nu)$. We first proof that $\pi = \pi^\star$. By proposition 4.33, we know that the optimal transport mapping in one dimension is monotone. This is equivalent to

$$\|x_1 - y_1\|_{L^2} + \|x_2 - y_2\|_{L^2} \leq \|x_1 - y_1\|_{L^2} + \|x_2 - y_1\|_{L^2}$$

for all tuples $(x_1, y_1), (x_2, y_2)$ in the support of $\pi^\star$. For these x_1, x_2, y_1, y_2 we additionally assume without loss of generality that $x_1 < x_2$.

Define $A = (-\infty, x] \times (y, \infty)$ and $B = (x, \infty) \times (-\infty, y]$. From Lemma 4.42 we know that for all tuple $(x_1, y_1), (x_2, y_2)$ in the support of $\pi^\star$ is holds $y_1 \leq y_2$. Therefore, we have for $(x_0, y_0) \in supp(\pi^\star)$:

$$supp(\pi^\star) \subset \{(x, y) : x \leq x_0, y \leq y_0\} \cup \{(x, y) : x \geq x_0, y \geq y_0\}.$$

Therefore, either $\pi^\star(A) \neq \emptyset$ or $\pi^\star(B) \neq \emptyset$. When using the definitions of A and B, we obtain

$$\begin{aligned}
&\pi(-\infty, x] \times (-\infty, y]) && [85]\\
&= \min\{\pi(-\infty, x] \times (-\infty, y]) \cup A, \pi(-\infty, x] \times (-\infty, y]) \cup B\} && [86]\\
&= \min\{\pi(-\infty, x] \times (-\infty, y]) \cup ((-\infty, x] \times (y, \infty)), && [87]\\
&\qquad \pi(-\infty, x] \times (-\infty, y]) \cup (x, \infty) \times (-\infty, y]\} && [88]\\
&= \min\{\pi((-\infty, x] \times \mathbb{R}), \pi(\mathbb{R} \times (-\infty, y])\} && [89]\\
&= \min\{F(x), G(y)\}, && [90]
\end{aligned}$$

where the last equality follows with definition 4.37. Thus, we have shown the first statement in Theorem 4.41.
For the second statement, recall definition 4.2. We analogously define the short notation

$$G^{-1}_{\#}\mathscr{L}_{[0,1]}((-\infty, x], (-\infty, y]) = \nu((-\infty, x], (-\infty, y]) \quad [91]$$

for a measure ν and the Lebesgue measure $\mathscr{L}_{[0,1]}$ defined on $[0, 1]$, when we mean the mass preservation

$$\nu(-\infty, x], (-\infty, y]) = \mathscr{L}_{[0,1]}(G^{-1}(-\infty, x], (-\infty, y])).$$

We want to proof that

$$\int_{\mathbb{R}\times\mathbb{R}} \|x - y\|_{L^2} d\pi^\star(x, y) = \int_0^1 \|F^{-1}(t) - G^{-1}(t)\|_{L^2} dt.$$

Therefore, we need to verify

$$\pi^\star = (F^{-1}, G^{-1})_{\#}\mathscr{L}_{[0,1]},$$

since then we will finally obtain

$$\begin{aligned}
\int_{\mathbb{R}\times\mathbb{R}} \|x - y\|_{L^2} d\pi^\star(x, y) &= \int_{\mathbb{R}\times\mathbb{R}} \|x - y\|_{L^2} d((F^{-1}, G^{-1})_{\#}\mathscr{L}_{[0,1]})(x, y)\\
&= \int_0^1 \|F^{-1}(t) - G^{-1}(t)\|_{L^2} dt.
\end{aligned}$$

Next, let us reformulate $\pi^\star = (F^{-1}, G^{-1})_\# \mathscr{L}_{[0,1]}$:

$$\begin{aligned}(F^{-1}, G^{-1})_\# \mathscr{L}_{[0,1]}((-\infty, x] \times (-\infty, y]) &\overset{[91]}{=} \mathscr{L}_{[0,1]}(F^{-1}, G^{-1})^{-1}((\infty, x] \times (-\infty, y])) \\ &= \mathscr{L}_{[0,1]}(\{t : F^{-1}(t) \leq x \wedge G^{-1}(t) \leq y\}) \\ &\overset{[4.39]}{=} \mathscr{L}_{[0,1]}(\{t : F(t) \geq t \wedge G(y) \geq t\}) \\ &= \min\{F(x), G(y)\} \\ &\overset{[85]}{=} \pi^\star((-\infty, x] \times (-\infty, y]))\end{aligned}$$

Hence, we have shown that $\pi^\star$ is the optimal solution to the Kantorovich problem and the Wasserstein metric can be rewritten as

$$\int_{\mathbb{R}\times\mathbb{R}} \|x - y\|_{L^2} d\pi^\star(x, y) = \int_{\mathbb{R}\times\mathbb{R}} \|x - y\|_{L^2} d((F^{-1}, G^{-1})_\# \mathscr{L}_{[0,1]})(x, y) \quad [92]$$

$$\overset{(*)}{=} \int_0^1 \|F^{-1}(t) - G^{-1}(t)\|_{L^2} dt, \quad [93]$$

where the second equality (*) in the above equations is obtained by substituting $F(x) = G(y) = t$ for $t \in \mathbb{R}$. □

Corollary 4.43. *The first statement of Theorem 4.41 implies that for an L^2 cost function the solution to the Kantorovich problem is unique.*

Corollary 4.44 (of Theorem 4.41 and Theorem 4.35)**.**
Let μ and ν be two positive probability densities. When we do not allow mass splitting, then

$$\inf_{\pi \in \Pi(\mu,\nu)} \mathscr{K} = \inf_{T_\# \mu = \nu} \mathscr{M}.$$

Therefore, the optimal solution to the Kantorovich problem is also a solution to the Monge problem.

Proof of Corollary 4.44. In Theorem 4.35, we have shown that for strictly positive densities μ and ν, the optimal transportation to the *Monge* problem is given by

$$T(x) = G^{-1}(F(x)).$$

From corollary 4.13, we know that the Kantorovich problem is weaker than the Monge problem and therefore, every solution to the Monge problem is also a solution to the Kantorovich problem. In 4.41 (ii), we have found an expression for the Kantorovich problem with the L^2 cost function. Thus, we have for densities $f, g > 0$:

$$\begin{aligned}\inf_{\pi \in \Pi(\mu,\nu)} \mathscr{K}(\pi) &= \int_0^1 \|(F^{-1}(t) - G^{-1}(t))\|_{L^2} dt \\ &= \int_{\mathbb{R}} \|x - G^{-1}(F(x))\|_{L^2} d\mu(x) \\ &\geq \inf_{T_{\mu,\nu} \in \mathcal{M}} \mathscr{M}.\end{aligned}$$

Since $\inf_{T_{\mu,\nu}\in\mathcal{M}} \geq \min_{\pi\in\Pi(\mu,\nu)} K$, is holds

$$\inf_{\pi\in\Pi(\mu,\nu)} \mathscr{K} = \inf_{T_{\mu,\nu}\in\mathcal{M}} \mathscr{M}.$$

Therefore, the optimal solution to the Kantorovich problem and to the Monge problem coincide for an L^2 cost function. □

Corollary 4.45. *The solution to the Monge problem for an L^2 cost function is unique.*

4.4 Optimal Transport in Higher Dimensions

While we were able to find an explicit expression for the transport map in the one-dimensional case, we will see that this is not possible in higher dimensions. Similarly to the one-dimensional case, we want to find a mapping which minimises

$$\int_{\mathbb{R}^n} \|x - T(x)\|^2 f(x)dx,$$

such that

$$\int_{T^{-1}(\mathcal{A})} f(x)dx = \int_{\mathcal{A}} g(y)dy. \tag{94}$$

for all $\mathcal{A} \in \mathbb{R}^n$ with $n > 1$.

Theorem 4.46. *(Quadratic Wasserstein metric in dimensions > 1) The squared Wasserstein metric is given by*

$$W_2^2(f,g) = \int_X f(x)|x - \nabla u(x)|^2 dx.$$

For the proof, we briefly recall the *change of variables formula.*

Lemma 4.47. *(Change of variables, [Ste23]) Let U be an open set in $\mathbb{R}^n$ and $\phi : U \to \mathbb{R}^n$ an injective, differentiable function with continuous partial derivatives, with non vanishing Jacobian for every $x \in U$. Then, for any real valued, compactly supported, continuous function f, with support contained in $\phi(U)$, it holds*

$$\int_{\phi(U)} f(v)dv = \int_U f(\phi(u))|det(D\phi)(u)|du,$$

where $det(D\phi)(u)$ is the determinant of the Jacobian matrix of partial derivatives of ϕ at u.

Next, we make use of the following well-known theorem by Rockafeller.

Theorem 4.48. *([Roc70], Section 24) A cyclically monotone mapping can be expressed as the gradient of a convex function.*

Proof of Theorem 4.46. By substituting $y = T(x)$ and using Lemma 4.47, we can rewrite equation [94] to

$$\int_{T^{-1}(\mathcal{A})} f(x)dx = \int_{\mathcal{A}} g(T(x))\ det(\nabla T(x))\ dx\ \forall \mathcal{A}.$$

Because of the mass conservation property of the transport mapping, we expect

$$g(T(x))det(\nabla T(x)) = f(x). \tag{95}$$

Analogously to the one-dimensional case, choose $x_1, \dots, x_n \in \mathcal{X}$. Assume $T(x)$ is optimal and let $y_i = T(x_i)$. Further, let ε_i be a ball around x_i such that $\int_{E_i} f(x)dx = \varepsilon$ and define $F_i = T(E_i)$. Therefore, we construct a new mapping $\tilde{T}(x_i)$ which is measure-preserving and for which holds

$$\begin{cases} \tilde{T}(x_i) = y_{i+1} \\ \tilde{T}(E_i) = F_{i+1} \\ \tilde{T}(x) = T(x), \quad \text{if } x \notin \cup E_i. \end{cases}$$

Since we assume that $T(x)$ is optimal, we know that

$$\int_X (x - T(x))^2 f(x)dx \leq \int_X (x - T(x))^2 f(x)dx.$$

As in the one-dimensional case (cf. equation [81]), we obtain

$$\frac{1}{\varepsilon} \sum_{i=1}^{N} \int_{E_i} x(\tilde{T}(x) - T(x))f(x)dx \leq 0. \tag{96}$$

For $\varepsilon \to 0$, we get

$$\sum_{i=1}^{N} x_i \cdot (y_{i+1} - y_i) \leq 0.$$

Therefore, we have cyclical monotonicity. Since we assumed $T(x)$ to be optimal, we can think of it as the gradient of a convex function due to Theorem 4.48. Thus, we write

$$T(x) = \nabla u(x), \tag{97}$$

where u is convex. From equation [95] we know that

$$det(\nabla T(x)) = \frac{f(x)}{g(\nabla u(x))}.$$

Hence, with equation [97] we obtain

$$det(D^2 u(x)) = \frac{f(x)}{g(T(x))}, \tag{98}$$

where $D^2(u(x))$ is the Hessian matrix of $u(x)$. Equation [98] is the Monge-Ampere equation. To compute the Wasserstein metric, we need to compute the optimal map

$$T(x) = \nabla u(x) \tag{99}$$

via the solution of the Monge-Ampere equation together with boundary conditions. In [EF14], the Monge-Ampere equation was equipped with non-homogenous Neumann bound-

ary conditions. By 99, the quadratic Wasserstein metric is then given by

$$W_2^2(f,g) = \int_X f(x)|x - \nabla u(x)|^2 dx.$$

This proves the claim. □

For the Monge-Ampere equation, uniqueness of the optimal map is not guaranteed. In [EF14] and [Yan18], the Monge-Ampere equation was solved by a finite difference scheme. To obtain well-defined solutions, the data must be sufficiently regular. This can be particularly challenging when working with real seismic data, for instance, due to noisy measurements [Yan18]. Furthermore, seismic full waveform inversion involves large-scale data, necessitating strong regularisation. To this end, the Monge-Ampere solver developed in [EF14] was designed to smooth the data sufficiently. However, smoothing the data can lead to a loss of high frequencies [Yan18], which consequently means a loss of information. In [Yan+17b], numerical simulations showed that the Monge-Ampere solver is not very promising in two dimensions. More results on the Monge-Ampere equation in general and on its application in seismic geophysics can be found in [EF14] and [Yan+17b]. In this thesis, we stick to the one-dimensional formulation described in the previous section.

4.5 The Wasserstein Metric for Seismic Signals

In Section 3.4, we illustrated the convexity of the Wasserstein metric with respect to horizontal shifts. Moreover, we discussed Gaussian distribution functions, which have desirable properties due to their positivity and normalisation to volume one. The functions considered in that section differed only by horizontal shifts, with no changes in amplitudes. Hence, from this point we can only conclude that optimal transport works well for functions which are *nice enough* in a certain way. For our setting, it is sufficient if the Wasserstein metric behaves nicely for the main effects that occur in seismic imaging.

Recall that a solution to the wave equation is represented by

$$u(x,t) = u_0(x - mt),$$

where m is our model parameter, the velocity coefficient. We want to address the effects that occur when m is varied. Most common signal distortions in seismic modelling are time shifts and dilations in $u(x,t)$ as well as partial amplitude changes. To demonstrate the occurrence of dilations and shifts, we consider the following example.

Example 4.49. *(One-dimensional constant velocity model [Yan+16]) A one-dimensional constant velocity model is given by*

$$\begin{cases} \frac{\partial^2 u}{\partial t^2} = m^2 \frac{\partial^2 u}{\partial x^2}, & x > 0,\, t > 0 \\ u = 0,\, \frac{\partial u}{\partial t} = 0, & x > 0,\, t = 0, \\ u = u_0(t), & x = 0,\, t > 0. \end{cases}$$

A solution to the above differential equation is given by

$$u(x,t;m) = u_0(t - x/m).$$

This implies that for fixed x, variations in m result in a shift. On the other hand, if we

assume t is fixed, variations in m cause dilations in u_0 when considered as a function of x.

Partial changes in the amplitude of a signal occur due to variations in the reflecting layers.

Example 4.50. *(Piecewise constant velocity model, [Yan+16]) Consider subsurface layers of different materials, which will result in a piecewise constant velocity field, as shown in Figure 21. As we know, the waves' velocity changes when entering a different layer. Consequently, the reflected waves will have different velocities depending on the layer from which they are reflected. An incorrect estimation of the velocity field can lead to either larger or smaller local amplitudes in the resulting wave field.*

Additionally, real seismic data is noisy, another side effect we have do deal with. Therefore, we wish for the Wasserstein metric to be insensitive to noise or at least less sensitive than other norms like the L^2-norm. The effect of noise is addressed in Section 4.5.4. For the time being, let us assume that we have already normalised the signals, such that we deal with probability densities of bounded second moment.

4.5.1 Wasserstein Metric Regarding Time Shifts

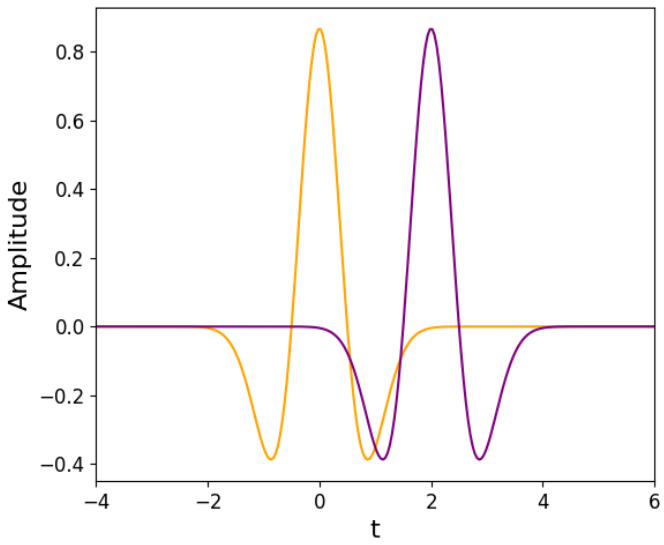

Figure 19: Time-Shifted Ricker Waves

Assume $f(x)$ is a signal, a time-shifted version of $f(x)$ can be described as

$$f(x) = g(x - sv),$$

where the signal g is shifted s units in v direction.

Theorem 4.51. *(Convexity with respect to shift, [Yan+16]) Let $f(x) = g(x - sv)$ for fixed $v \in \mathbb{R}^n$. Then, the quadratic Wasserstein metric $W_2^2(f, g)$ is convex with respect to shift s.*

Proof of Theorem 4.51. By proposition 4.33, the optimal transport mapping T is a constant shift. This is given by

$$T(x) = x - sv.$$

With the definition of the quadratic Wasserstein metric [4.21], we obtain

$$\begin{aligned} W_2^2(f,g) &= \inf_{T_{\mu,\nu}\in\mathcal{M}} \int_{\mathbb{R}^n} |x - T(x)|^2 dx = \int_{\mathbb{R}^n} (x - (x - sv))^2 f(x) dx \\ &= \int_{\mathbb{R}^n} (-sv)^2 f(x) dx = \int_{\mathbb{R}^n} s^2 v^2 f(x) dx \\ &= \int_{\mathbb{R}^n} s^2 |v|^2 f(x) dx \end{aligned}$$

Since we assume $f(x)$ to be normalised to volume one, we have

$$\int_{\mathbb{R}^n} s^2 |v|^2 f(x) dx = s^2 |v|^2 \int_{\mathbb{R}^n} f(x) dx = s^2 |v|^2.$$

Since quadratic functions are always convex, the claim follows. □

Remark 4.52. *Note that we assumed the signals to be positive and have volume one. In practise, the signals have to be normalised beforehand, which can influence the convexity property. We discuss several normalisation methods and their impact on the convexity in Section 4.7.*

4.5.2 Wasserstein Metric Regarding Dilations and Contractions

Before deriving the optimal transportation map in the setting of this section, we briefly recall the formal definition of dilations and contractions (see also [LLM16]).

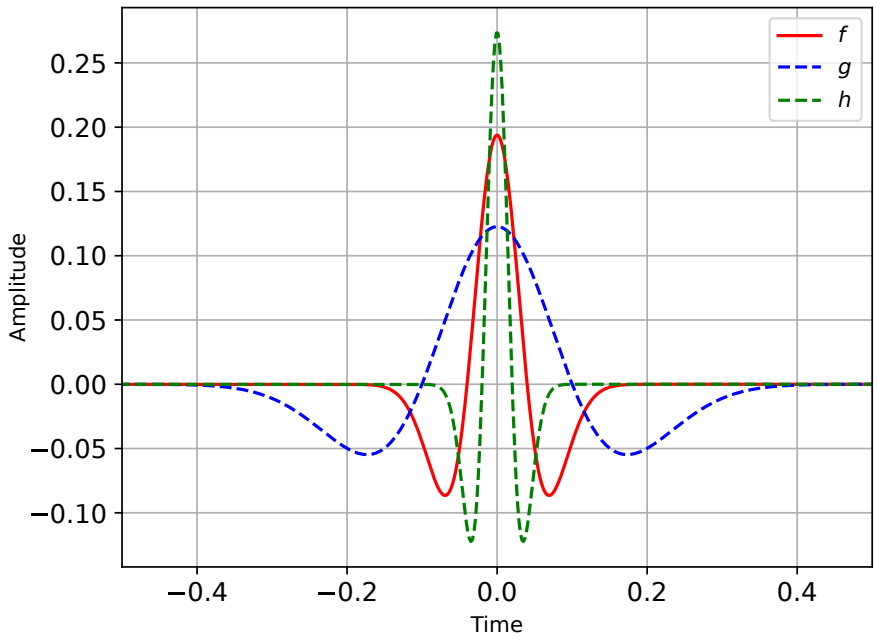

Figure 20: Three Ricker waves; g and h being contractions and dilations of f respectively

Dilations and contractions are special cases of a *scaling* of a function. Clearly, a scaling is a linear transformation. By multiplying a quantity with a scaling factor, we refer to it as dilation, if the scaling factor is larger than 1, while we call it contraction, if the factor is smaller than 1.

In $\mathbb{R}^n$, uniform scaling by a factor $v > 0$ is accomplished by scalar multiplication with v, that is, multiplying each coordinate of each point by v. As a special case of linear transformation, it can be achieved also by multiplying each point (viewed as a column vector) with a diagonal matrix whose entries on the diagonal are all equal to v.

Non-uniform scaling is achieved by multiplication with any symmetric matrix. There, the eigenvalues of the matrix are the scaling factors, and the corresponding eigenvectors represent the axes along which each scale factor applies. In the case of diagonal matrices, the axes of scaling are then the coordinate axes. Hence, the transformation scales along each axis by the factor v_i.

Example 4.53. *The scaling of* $\begin{pmatrix} x \\ y \end{pmatrix}$ *by the factor 2 in* x *direction and by the factor 3 in* y *direction, i.e.*

$$f\begin{pmatrix} x \\ y \end{pmatrix} = \begin{pmatrix} 2x \\ 3y \end{pmatrix},$$

can be written with help of the matrix $A = \begin{pmatrix} 2 & 0 \\ 0 & 3 \end{pmatrix}$*, such that*

$$f\begin{pmatrix} 2x \\ 3y \end{pmatrix} = \begin{pmatrix} 2 & 0 \\ 0 & 3 \end{pmatrix}\begin{pmatrix} x \\ y \end{pmatrix}.$$

Theorem 4.54. *(Convexity with respect to dilation, [Yan+16]) We assume* f *is a dilation of* g*. Thus, we can write*

$$f(x) = g(Ax),$$

where A *is a symmetric, positive definite matrix. Then, the quadratic Wasserstein metric* $W_2^2(f, \frac{g}{\langle g \rangle})$ *is convex with respect to the scaling factors, i.e. eigenvalues* $\lambda_1, \ldots, \lambda_n$ *of the scaling matrix* $A \in \mathbb{R}^{n \times n}$*.*

Remark 4.55. *Note that we want* A *to be positive definite, as the eigenvalues (scaling factors) have to be positive by definition of a scaling.*

To prove the convexity of the Wasserstein metric with respect to the eigenvalues, we first need to make sure we found an optimal mapping.

Proposition 4.56. *The mapping* $T(x) = Ax$ *is optimal [Yan+16].*

Proof of proposition [4.56]. Define $y \coloneqq Ax$. Then we can write

$$\frac{g}{\langle g \rangle} = \frac{f(A^{-1}y)}{\langle f(A^{-1}y) \rangle}.$$

To evaluate the last term's denominator, we use definition 4.47 and obtain

$$\int_{\phi(U)} g(x)dx = \int_U f(A^{-1}y) \cdot |det(DA^{-1}y)|\, dy.$$

Since we assume f to be a probability density function, it has volume 1. A is a constant, linear transformation, hence, the most suitable linear approximation of A^{-1} is A^{-1} itself. Thus,

$$DA(y) = A \quad \forall\, y \in \mathbb{R}^n.$$

In summary, we get

$$\int_{\phi(U)} g(x)dx = |det(A^{-1})|$$

and

$$\frac{g}{\langle g \rangle} = \frac{f(A^{-1}y)}{det(A^{-1})},$$

where we omitted the absolute value function, since A is a positive matrix. Further, the map $T(x)$ is optimal, since it is the gradient of a convex function

$$T(x) = \nabla\left(\frac{1}{2}x^T Ax\right),$$

where A is positive definite. Thus, $T(x)$ is the gradient of a quadratic and thus convex function. □

Proof of Theorem 4.54. Since A is symmetric positive definite, we can find a diagonalisation of A by orthogonal matrices [Fis13]. Let O be an orthogonal matrix and Λ a diagonal matrix which consists of the eigenvalues of A. To find the diagonalised version of A, we decompose

$$A = O\Lambda O^T.$$

For the quadratic Wasserstein metric, we obtain

$$\begin{aligned} W_2^2\left(f, \frac{g}{\langle g\rangle}\right) &= \int_{\mathbb{R}^n} |x - Ax|^2 f(x)dx \\ &= \int_{\mathbb{R}^n} |OI_nO^Tx - O\Lambda O^Tx|^2 f(x)dx \\ &= \int_{\mathbb{R}^n} |x^TOO^Tx - 2x^TO\Lambda O^Tx + x^TO\Lambda^2O^Tx|\, f(x)dx \\ &= \int_{\mathbb{R}^n} |x^TO(I_n - \Lambda)^2O^Tx|\, f(x)dx, \end{aligned}$$

where I_n is the $n \times n$ identity matrix. Let $z \coloneqq O^Tx$. Then

$$\begin{aligned} \int_{\mathbb{R}^n} |x^TO(I_n - \Lambda)^2O^Tx|\, f(x)dx &= \int_{\mathbb{R}^n} z^T(I_n - \Lambda)^2 z f(Oz)dz \\ &= \sum_{i=j}^{n} (\lambda_j - I_n)^2 \int_{\mathbb{R}^n} z_j f(Oz)dz, \end{aligned}$$

since Λ is a diagonal matrix and does not depend on z. Thus, $W_2^2\left(f, \frac{g}{\langle g\rangle}\right)$ is convex in λ for all j. Hence, convexity with respect to the scaling values holds. □

4.5.3 Wasserstein Metric Regarding Partial Amplitude Changes

Decompose Ω into two disjoint domains, such that $\Omega = \Omega_1 \cup \Omega_2$ and $\Omega_1 \cap \Omega_2 = \emptyset$. If we make a wrong guess for m, we get wrong reflection values.

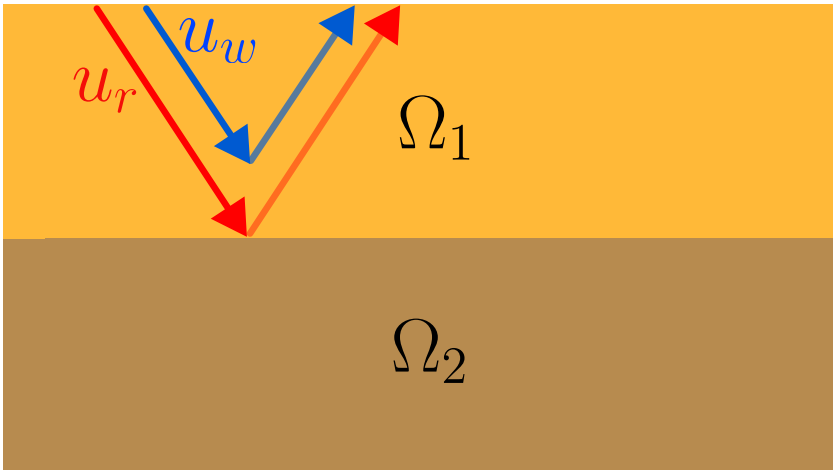

Figure 21: Two layered structure, true coefficient leads to correct reflection point u_r (red), while the wrong coefficient u_w does not.

Without loss of generality, let $\beta \in [0, 1]$ be the parameter for the amplitude loss. Let f_β be the solution to the wave equation for this wrong coefficient m.

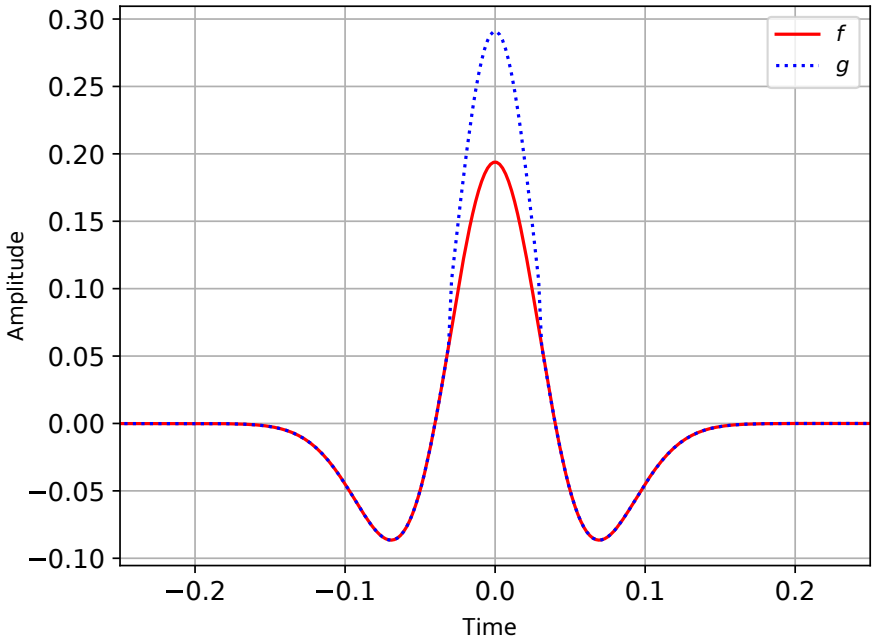

Figure 22: g (blue) equals f (red) except for a local amplitude change

Then,

$$f_\beta(x) = \left\{ \begin{array}{ll} \beta g(x), & \text{for } x \in \Omega_1 \\ g(x), & \text{for } x \in \Omega_2 \end{array} \right\} \qquad [100]$$

is piecewise proportional to g, but with different proportionality constants β. The main goal of this section is to prove the following theorem.

Theorem 4.57. *(Convexity with respect to partial amplitude changes, [Yan+16]) The quadratic Wasserstein metric* $W_2^2\left(\frac{f_\beta}{\langle f_\beta \rangle}, g\right)$ *is convex with respect to* β.

For the proof of the theorem, we introduce another representation of the signal $f_\beta(x)$:

$$h_\alpha(x) = \left\{ \begin{array}{ll} (1+\alpha)g(x), & \text{for } x \in \Omega_1 \\ (1-\gamma_\alpha)g(x), & \text{for } x \in \Omega_2 \end{array} \right\},$$

where

$$\gamma_\alpha = \alpha \frac{\int_{\Omega_1} g}{\int_{\Omega_2} g},$$
$$\alpha = \frac{\beta}{\beta \int_{\Omega_1} g + \int_{\Omega_2} g}.$$

Remark 4.58. *Note that* $h_\alpha(x)$ *is piecewise affine in* α*, while* $f_\beta(x)$ *is not. The affinity will be a useful tool in the proof.*

Remark 4.59. *Since we want* β *to be an amplitude loss, we have to choose* $\alpha \in [-1, 0]$.

As in the following lemma, we see the parameter α as a function of β and show the concavity of α with respect to β.

Lemma 4.60 (Concavity of $\alpha(\beta)$, [Yan+16])**.** *The function* $\alpha(\beta)$ *is concave with respect to* β.

Remark 4.61. *For the proof, recall that a function whose second derivative is negative is concave [Roc70].*

Proof of Lemma 4.60. In order to proof concavity, we differentiate α twice with respect to β. By the chain rule, we obtain

$$\alpha'(\beta) = \frac{\int_{\Omega_1} g}{\left(\beta \int_{\Omega_1} g + \int_{\Omega_2} g\right)^2},$$
$$\alpha''(\beta) = \frac{-2 \int_{\Omega_1} g \int_{\Omega_2}}{\left(\beta \int_{\Omega_1} g + \int_{\Omega_2} g\right)}.$$

Since the second derivative has negative sign, $\alpha(\beta)$ is concave. □

Remark 4.62. *The associated density functions are related by*

$$\hat{f_\beta} = \frac{f_\beta}{\langle f_\beta \rangle} = h_{\alpha(\beta)}.$$

Next, we proof the convexity of W_2^2 with respect to α, and from there we conclude the convexity with respect to β.

Proposition 4.63. *W_2^2 is convex with respect to α [Yan+16].*

Proof. From Lemma 4.30, we know that the quadratic Wasserstein metric itself is convex. We choose ordered $\alpha_1, \alpha_2 \in [-1, 0]$ and scaling factors $s \in [0, 1]$. Since $h_\alpha(x)$ is piecewise affine in parameter α, we get

$$W_2^2(sh_{\alpha_1} + (1-s)h_{\alpha_2}, g) \leq sW_2^2(h_{\alpha_1}, g) + (1-s)W_2^2(h_{\alpha_2}, g).$$

Because of the affinity, we also know that

$$sh_{\alpha_1} + (1-s)h_{\alpha_2} = hs_{\alpha_1} + (1-s)\alpha_2.$$

This implies

$$W_2^2(hs\alpha_1 + (1-s)h_{\alpha_2}, g) \leq sW_2^2(h_{\alpha_1}, g) + (1-s)W_2^2(h_{\alpha_2}, g).$$

Thus, W_2^2 is convex with respect to α. □

Corollary 4.64. *The quadratic Wasserstein metric is decreasing in α [Yan+16].*

Proof. Let $-1 \leq \alpha_1 < \alpha_2 \leq 0$. Choose $s = \frac{\alpha_2}{\alpha_1}$ to make sure $s \in [0, 1]$.

$$\begin{aligned} W_2^2(h_{\alpha_2}, g) &= W_2^2(h_{s\alpha_1 + (1-s)\cdot 0}, g) \\ &\leq sW_2^2(h_{\alpha_1}, g) + (1-s)\underbrace{W_2^2(h_0, g)}_{(\star)} \\ &= sW_2^2(h_{\alpha_1, g}), \end{aligned}$$

where $(\star)$ equals zero by symmetry of the Wasserstein metric, since $h_0 = g$. As $s \leq 1$, it follows that

$$sW_2^2(h_{\alpha_1, g}) \leq W_2^2(h_{\alpha_1, g}).$$

□

Next we translate the result of the previous lemma for α to a convexity result for β.

Theorem 4.65 (Convexity of W_2^2 with respect to β, [Yan+16])**.** *The quadratic Wasserstein metric $W_2^2\left(\frac{f_\beta}{\langle f_\beta \rangle}, g\right)$ is a convex function of β.*

Proof of Theorem 4.65. By the previous results 4.60, 4.63, 4.64, we know that we can relate $\hat{f}_\beta$ to $h_{\alpha(\beta)}$ for a properly chosen α:

$$W_2^2(\hat{f}_{s\beta_1 + (s-1)\beta_2}, g) = W_2^2(h_{\alpha(s\beta_1 + (1-s)\beta_2), g}) \tag{101}$$

As was shown in Lemma 4.60, α is concave with respect to β. That is,

$$\alpha(s\beta_1 + (1-s)\beta_2) \geq s\alpha(\beta_1) + (1-s)\alpha\beta_2.$$

From corollary 4.64 we know that the quadratic Wasserstein distance decreases in α, thus

$$W_2^2(\hat{f}_{s\beta_1 + (s-1)\beta_2}, g) \leq W_2^2(h_{s\alpha(\beta_1) + (1-s)\alpha(\beta_2)}, g).$$

Then, the convexity of W_2^2 with respect to α implies

$$\begin{aligned} W_2^2(\hat{f}_{s\beta_1+(s-1)\beta_2}, g) &\leq sW_2^2(h_{\alpha(\beta_1)}, g) + (1-s)W_2^2(h_{\alpha(\beta_2)}), g \\ &= sW_2^2(\hat{f}_{\beta_1}, g + (1-s)W_2^2(\hat{f}_{\beta_2}), g), \end{aligned}$$

which implies convexity with respect to β. □

4.5.4 Wasserstein Metric and its Insensitivity Regarding Noise

The L^2-norm is widely recognized for its high sensitivity to noise. Given that measurements in practice are often noisy, insensitivity to noise is a desirable characteristic. In this section, we will theoretically outline the Wasserstein metric and its insensitivity to noise. Since we focus on the explicit one-dimensional formulation of the Wasserstein metric, it suffices for this thesis to demonstrate that the Wasserstein distance is insensitive to noise in the one-dimensional case.

Theorem 4.66. *(Insensitivity to noise of the quadratic Wasserstein metric, [Yan+16]) Let $g \geq 0$ be a probability density function on [0,1] and let c be a constant in $(0, \min(g))$. Further define*

$$f_N(x) = g(x) + r^N(x),$$

where $r^N(x)$ is a piecewise constant additive uniform noise on the interval $[-c, c]$. Then it holds

$$\mathbb{E}W_2^2\left(\frac{f_N}{\langle f_N \rangle}, g\right) = \mathcal{O}\left(\frac{1}{N}\right).$$

Proof of Theorem 4.66, [Yan+16]. Without loss of generality, define $g = 1$ on $[0, 1]$. For $x \in \left(\frac{i-1}{N}, \frac{i}{N}\right]$ we define $r^N(x) \cong r_i$, where each r_i is drawn from the uniform distribution $U[-c, c]$. As we increase N up to infinity, $r^N(x)$ approximates the noise function $r(x)$ on $[0, 1]$. Since for each i, we have r_i defined to be a random variable of uniform distribution $U[-c, c]$, we have $\mathbb{E}r_i = 0$ and therefore $\mathbb{E}r = 0$. We furthermore define $h = \frac{1}{N}$ and $x_i = ih$ for $i \in 0, \ldots, N$. The noisy density function f_N is then given by

$$f_N(x) = 1 + r_i, \quad x \in (x_{i-1}, x_i).$$

Next, we calculate the Wasserstein distance between f_N and $g_N = 1 + r^N$ to estimate the effect of the uniform noise. Note that f_N and g^N have equal volume and g_N is constant. To this end, we use the explicit formula of the Wasserstein metric we found in equation 83, namely

$$T(x) = G^{-1}(F(x)).$$

As first step, we derive the cumulative distribution function F_N of f_N. The density $f_N(x)$ is piecewise constant in the intervals $(x_{i-1}, x_i]$, and each interval contributes to the total area described by the cumulative distribution function $F_N(x)$. To calculate the cumulative distribution function at a specific point x, we need to sum the area of all

preceding intervals and then add the contribution of the current interval $(x_{i-1}, x_i]$.

$$F_N(x) = \sum_{j=1}^{i-1} \int_{x_{j-1}}^{x_j} f_N(s)ds + \int_{x_i-1}^{x} f_N(x)ds$$

Since $f_N(s)$ is piecewise constant (i.e. constant on each interval), we obtain

$$\int_{x_{j-1}}^{x_j} f_N(s)ds = (1 + r_j)(x_j - x_{j-1}) = (1 + r_j)h.$$

Thus

$$\begin{aligned} F_N(x) &= \sum_{j=1}^{i-1}(s + r_j)h + \int_{x_{i-1}}^{x} f_N(s)ds \\ \Leftrightarrow &= \sum_{j=1}^{i-1}(s + r_j)h + ((1 + r_i)(x - x_{i-1})) \,. \end{aligned}$$

Since $g_N(x)$ is constant, we obtain the cumulative distribution function by calculating

$$G_N(x) = \int_0^x g_N(s)ds.$$

Recall that $g_N(x) = 1 + r_N$ is constant. Therefore, we obtain

$$G_N(x) = \int_0^x (x + r_N) \int_0^x 1dt = (1 + r_N)x$$

for $x \in [0, 1]$. The inverses of the cumulative distribution functions are given by

$$F_N^{-1}(x) = \frac{(x + ((i - 1)r_i) - \sum_{j=1}^{i-1})h}{1 + r_i}$$

for $x \in \left(\sum_{j=1}^{i-1}(1 + r_j)h,\ \sum_{j=1}^{i}(1 + r_j)h\right]$ and

$$G_N^{-1}(x) = \frac{x}{1 + r^N}$$

for $x \in [0, 1 + r^N]$. □

In [Yan+16], an upper bound for the Wasserstein metric was presented:

$$W_2^2(f_N, g_N) = \left|F_N^{-1}(t) - G_N^{-1}(t)\right|^2 dt \leq \frac{2h^3}{(1 - c)^2} \sum_{i=1}^{N} \left(\sum_{l=1}^{i} r_l - ih \sum_{k=1}^{N} r_k \right)^2 .$$

Since the noise $\{r_i\}_{i=1}^N$ is independent and identically distributed, the following upper bound for the expectation of the Wasserstein metric can be found:

$$\mathbb{E}[W_2^2(f_N, g_N)] \leq C \cdot h^3 \cdot \sum_{i=1}^{N} \mathbb{E}r_1^2 \leq \frac{C_2}{N}.$$

A lower bound was established by

$$C_1 \leq \mathbb{E}[W_2^2(f_N, g_N)] \leq \frac{C_2}{N},$$

where C_1 and C_2 depend on c only [Yan+16].

As last step in this proof, we need to scale the densities to volume one. Following [Vil03], we obtain

$$W_2^2\left(\frac{f_N}{\langle f_N \rangle}, g\right) = \left(\frac{1}{1+r^N}\right)^2 W_2^2(f_N, g_N),$$

where

$$\left(\frac{1}{1+c}\right)^2 \leq \left(\frac{1}{1+r^N}\right)^2 \leq \left(\frac{1}{1-c}\right)^2.$$

From there, we obtain

$$\mathbb{E}W_2^2\left(\frac{f_N}{\langle f_N \rangle}, g\right) = \mathcal{O}\left(\frac{1}{N}\right).$$

Remark 4.67. *For the L^2-norm it holds [Vil03; Yan18]*

$$\mathbb{E}W_2^2\left(\frac{f_N}{\langle f_N \rangle}, g\right) = \mathcal{O}(1).$$

Therefore, the Wasserstein distance is much lesser sensitive to noise than the L^2-norm.

4.6 Optimal Transport for Full Waveform Inversion

In Section 4.3, we found an explicit formulation for the optimal transport mapping in the one-dimensional case, while we have seen in Section 4.4 that this is not possible for higher dimensions. Since we focus on the one-dimensional case in this thesis, we stick to the explicit formulation of the transport mapping. Recall that it is given by

$$T(x) = G^{-1}(F(x))$$

as in equation [83]. Also recall that the FWI scheme consists of three main steps (cf. Section 3.1):

1. Solve the forward problem.
2. Compare the solutions of forward modelling and observed data.
3. Update the velocity coefficient and go back to the first step.

We have already explained the first step in Sections 2.1 and 2.2. Clearly, for the second step, we chose the quadratic Wasserstein metric, which is given by

$$W_2^2(f, g) = \int_0^1 |t - G^{-1}(F(t))|^2 f(t) dt. \qquad [102]$$

For updating the velocity coefficient in the third step, we choose standard gradient descent as optimisation method. As we have seen in equation 48, the corresponding scheme is given by

$$m^{k+1} = m^k - \alpha \frac{\partial J}{\partial m}[m^k], \tag{103}$$

where $J(m)$ is the distance between the synthetic and the observed data. Due to the adjoint state method (see Section 3.3), we have found a formal representation of $\frac{\partial J}{\partial m}$:

$$\frac{\partial J}{\partial m} = -\int_0^T \frac{d^2u(x,t)}{dt^2} v(x,t),$$

where v is the solution to the adjoint wave equation. In equation [62], we stated the adjoint wave equation when using the L^2-norm as misfit function:

$$\begin{cases} m(x)\frac{\partial^2 q(x,t)}{\partial t^2} - \Delta q(x,t) = \frac{\partial J}{\partial u}, \\ q(x,T) = 0, \\ \frac{\partial q_t}{\partial t}(x,T) = 0. \end{cases}$$

When one changes the misfit function, the adjoint wave equation remains the same except for the source term $\frac{\partial J}{\partial u}$ (cf. Section 3.3 and [FBI06]). Thus, to apply the Wasserstein metric to the FWI scheme, we need to calculate $\frac{\partial J}{\partial u}$ for

$$J(m) \coloneqq W_2^2(f,g) = \int_0^1 |t - G^{-1}(F(t))|^2 f(t) dt.$$

The dependency on u is implicitly given via f.

We assume that $f(t)$ and $g(t)$ are normalised to volume one and scaled to be positive, continuous density functions on the time interval $[0, T_1]$, where T_1 is the last time point at the first receiver. To calculate the derivative of J with respect to u, we vary f by a small amount δf [Yan+17b]:

$$W_2^2(f,g) + \delta W(f,g) = \int_0^{T_1} |t - G^{-1}(F(t) + \delta F(t))|^2 \ (f(t) + \delta f(t)) \ dt \tag{104}$$

$$= \int_0^{T_1} |t - G^{-1}(F(t) + \delta F(t))|^2 f(t) dt \tag{105}$$

$$+ \int_0^{T_1} |t - G^{-1}(F(t))|^2 \delta f(t) dt + \mathcal{O}((\delta f)^2). \tag{106}$$

Next, we approximate $G^{-1}(F(t) + \delta F(t))$ by Taylor expansion:

$$G^{-1}(F(t) + \delta F(t)) = G^{-1}(F(t) + \frac{dG^{-1}(y)}{dy})\Big|_{y=F(t)} \delta F(t) + \mathcal{O}((\delta f)^2). \tag{107}$$

To obtain the first variation $\delta W(f,g)$, we put [107] back into [105]:

$$\delta W(f,g) = \int_0^{T_1} \left(\int_t^{T_1} -2\left(s - G^{-1}(F(s)\right) \frac{dG^{-1}(y)}{dy}\bigg|_{y=F(s)} f(s)ds \right) \delta f(t)dt \qquad [108]$$

$$+ \int_0^{T_0} |t - G^{-1}(F(t))^2 \delta f(t)dt, \qquad [109]$$

where $t \in [0, T_1]$ and $s \in [t, T_1]$. In term [108], we have plugged [107] in [105] and therefore applied the derivative of the squared norm [105]. In summary, we obtain

$$\delta W(f,g) = \left(\int_t^{T_1} -2\left(s - G^{-1}(F(s)\right) \frac{dG^{-1}(y)}{dy}\bigg|_{y=F(s)} f(s)ds \right) + \int_0^{T_0} |t - G^{-1}(F(t))^2 dt \qquad [110]$$

and thus have found the corresponding source term for the adjoint wave equation.

4.6.1 Trace–By–Trace Technique

So far we have developed a scheme for a one-dimensional reconstruction algorithm. To achieve results in two dimensions with the one-dimensional formulation, we divide the domain into its traces. Recall from Section 1.2, that a seismic trace is the time history measured at one single receiver. Thus, we divide the domain into one-dimensional sections defined by the receiver's measurements over time [Yan+16]. In these sections, we consider one receiver for a single source at a given time. In other words, we iterate through all receivers for each source. When comparing the data trace by trace, we solve a bunch of one-dimensional optimal transportation problems and eventually compute the sum over all traces r. Therefore the final misfit becomes

$$\mathcal{K}(m) \coloneqq \sum_{r=1}^{R} W_2^2(f(x_r, t; m), g(x_r, t)). \qquad [111]$$

We summarise our steps for FWI with the trace-by-trace technique in the following corollary.

Corollary 4.68. *(Full waveform inversion with trace–by–trace technique)*

1. *Solve the forward problem by using finite differences (see Section 2.2)*
2. *Compare solutions of forward modelling and observed data with the Wasserstein distance* [102] *for each receiver.*
3. *Add up the results as in equation* [111].
4. *Update the velocity coefficient by gradient descent 103 and go back to the first step.*

4.7 Data Normalisation

To apply optimal transport to seismic signals within the framework of full waveform inversion, it is essential that both the synthetic and observed data meet specific criteria: they must be positive and have a total volume of one each. Consequently, we need to implement appropriate normalisation techniques to transform the signals accordingly. In the following subsections, we present various data normalisation methods and evaluate their suitability for use in FWI.

We wish for a proper scaling method to be suitable for both the adjoint state method and the gradient update in FWI. This means that the normalisation techniques should not only ensure the required properties of the data (positivity and volume of one) but also maintain consistency and stability in both procedures. In summary, the normalisation should be designed to fulfil:

1. Positivity and volume preservation: The transformed data must be positive and the volume of the normalised values must be equal to one to ensure optimal transport can be applied.

2. Differentiability: The normalisation functions should be differentiable to enable the calculation of gradients within the FWI framework. This is crucial for the application of the adjoint state method.

3. Stability: The methods should be numerically stable to avoid unwanted artifacts during computations. This is important when applied to large datasets, where small errors can propagate and lead to inaccurate inversion results.

4. Efficiency: The normalisation should be efficiently implementable to minimise computation time during inversion. This is important since FWI is an iterative procedure, which implies multiple passes over the data.

In the following subsections, we summarise normalisation methods discussed in literature [EF14; Yan+17a; Yan+17b; Yan+19]. We define $\langle f \rangle \coloneqq \int_{-\infty}^{\infty} f(t)\, dt$.

4.7.1 Linear Scaling

Definition 4.69. *(Linear Scaling, [Yan+19]) We scale f and g by adding constant c,*

$$\tilde{f} = \frac{f(t) + c}{\langle f + c \rangle}, \quad \tilde{g} = \frac{g(t) + c}{\langle g + c \rangle},$$

such that $c = \min_t(f(t), g(t))$.

The linear scaling provides a bijection between the original and the normalised data, such that no phase information is lost. However, it does not necessarily guarantee convexity as will be discussed in Section 4.8. Nevertheless, in the numerical examples in Section 5, the linear scaling tends to have at least fewer local minima compared to the L^2-norm.

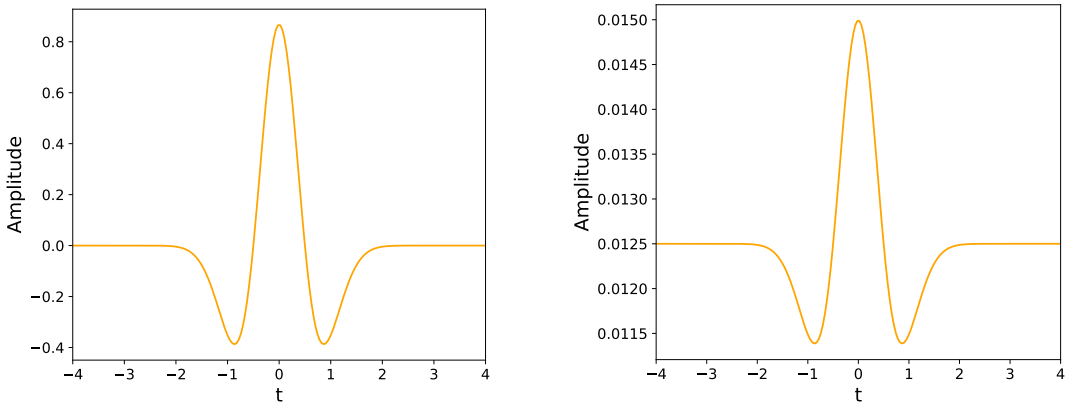

(a) Two Ricker waves

(b) Ricker waves from Figure 23a normalised by the linear scaling

Figure 23: Two Ricker waves: non normalised (left), normalised (right)

4.7.2 Partial Scaling

Definition 4.70. *(Partial Scaling, [EF14; Yan18]) We divide f and g by their positive and negative parts, such that $f^+ = \max f, 0$ and $f^- = \max -f, 0$. Therefore, the scaled partial signals are given by*

$$\tilde{f} = \frac{f^+}{\langle f^+ \rangle}, \; \tilde{g} = \frac{g^+}{\langle g^+ \rangle}$$

and analogously for the negative sign:

$$\tilde{f} = \frac{f^-}{\langle f^- \rangle}, \; \tilde{g} = \frac{g^-}{\langle g^- \rangle}.$$

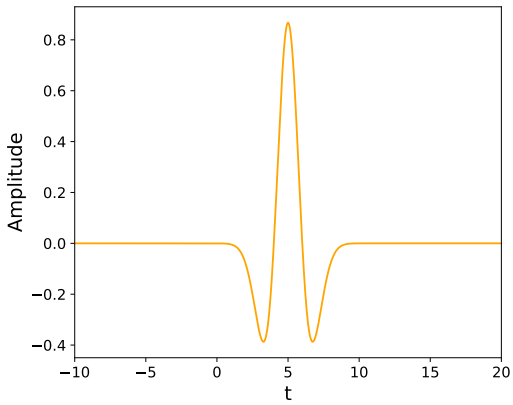

(a) A Ricker wave

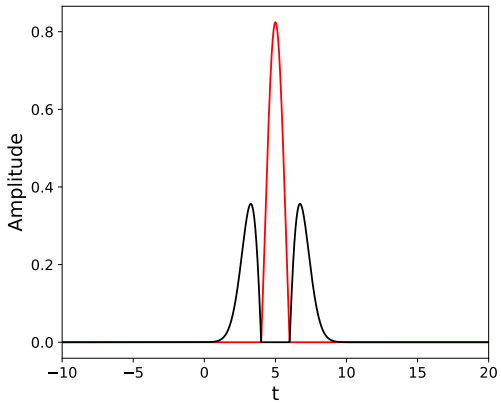

(b) Positive parts of the Ricker wave in Figure 24a normalised (red), negative parts of 24a normalised (black)

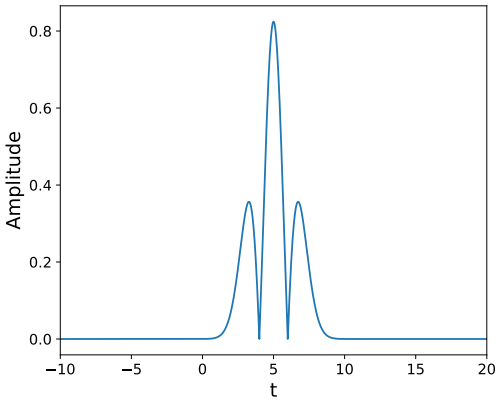

(c) Sum of positive and negative normalised parts

Figure 24: A Ricker wave normalised by partial scaling

With partial scaling, the quadratic Wasserstein metric is given by the sum of both the scaling of the positive and negative parts:

$$W_2^2\left(\frac{f^+}{\langle f^+\rangle}, \frac{g^+}{\langle g^+\rangle}\right) + W_2^2\left(\frac{f^-}{\langle f^-\rangle}, \frac{g^-}{\langle g^-\rangle}\right).$$

In [EF13] and [Yan+16], the concept of positive part scaling was further studied. While this approach successfully preserved convexity with respect to shifts, its application to FWI with realistic datasets such as the Marmousi model was outlined to be challenging.

4.7.3 Absolute Value Scaling

Definition 4.71. *(Absolute Value Scaling, [Yan+19]) We scale f and g by composition with the absolute value function:*

$$\tilde{f} = \frac{|f(t)|}{\langle \max(g(t))\rangle}, \quad \tilde{g} = \frac{|g(t)|}{\langle \max(g(t))\rangle}.$$

Due to the non–differentiability of the absolute value function at zero, it is not suitable for the adjoint state method, which relies on the computation of the gradient $\frac{\partial J}{\partial f}$.

While we could add a very small $\varepsilon > 0$ to make the function differentiable, this would distort the data any further. Additionally, like the squared scaling, absolute value scaling does not preserve a bijection to the non-normalised data points.

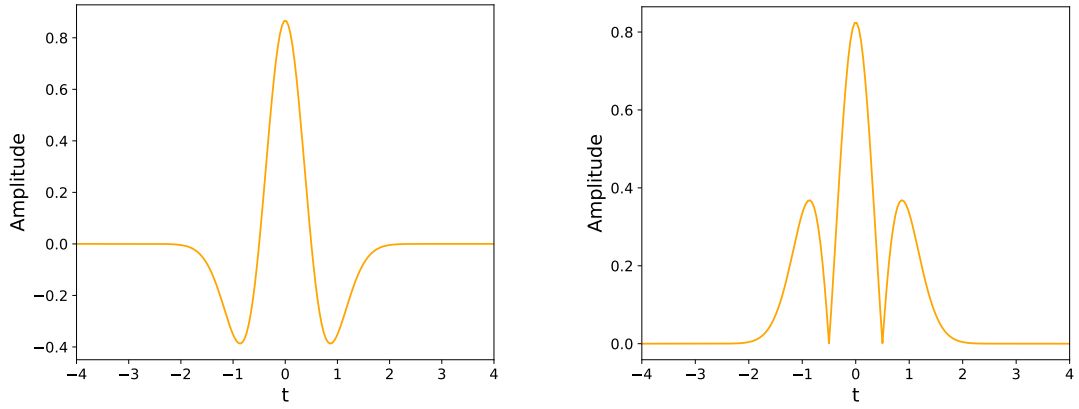

(a) A Ricker wave

(b) Normalisation of 25a by the absolute value scaling

Figure 25: Two Ricker waves: non normalised (left), normalised by the absolute value scaling (right)

4.7.4 Squared Scaling

Different to the absolute value scaling, the squared scaling works well with the adjoint state method due to its differentiability.

Definition 4.72. *(Squared Scaling, [Yan18]) We scale f and g by squaring and afterwards normalising them to ensure volume balance:*

$$\tilde{f} = \frac{f^2}{\langle g^2 \rangle}, \quad \tilde{g} = \frac{g^2}{\langle g^2 \rangle}.$$

Unfortunately, this method can introduce high frequencies and therefore phase information my be lost. This can be problematic especially for large-scale inversions. Unlike the linear scaling, the quadratic scaling does not maintain a bijection to the non-normalised data points.

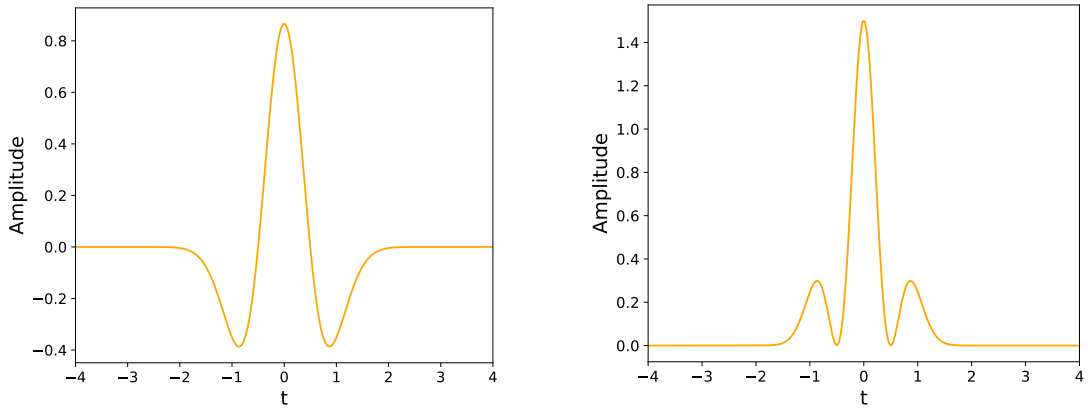

(a) A Ricker wave

(b) Normalised by the squaring scaling

Figure 26: Two Ricker waves: non-normalised (left), normalised by the squaring scaling (right)

4.7.5 Exponential Scaling

Definition 4.73. *(Exponential scaling, [Yan18; EF13])*

$$\tilde{f}(t) = \begin{cases} \frac{f(t)+\frac{1}{c}}{\langle f(t)+\frac{1}{c}\rangle}, & f(t) \geq 0, \\ \frac{\frac{1}{c}\exp(cf(t))}{\langle \frac{1}{c}\exp(cf(t))\rangle}, & f(t) < 0 \end{cases}$$

for $c \in \mathbb{R}_{>0}$. The choice of parameter c depends on the data set [Yan18]. For the numerical simulations in Section 5, we will define the parameter c as

$$c = \min(f, g) \cdot \tau,$$

where $\tau \in (0, 1]$ and f, g are the synthetic and observed data respectively. In Figure 27b the parameter is c is chosen as above for different values of τ.

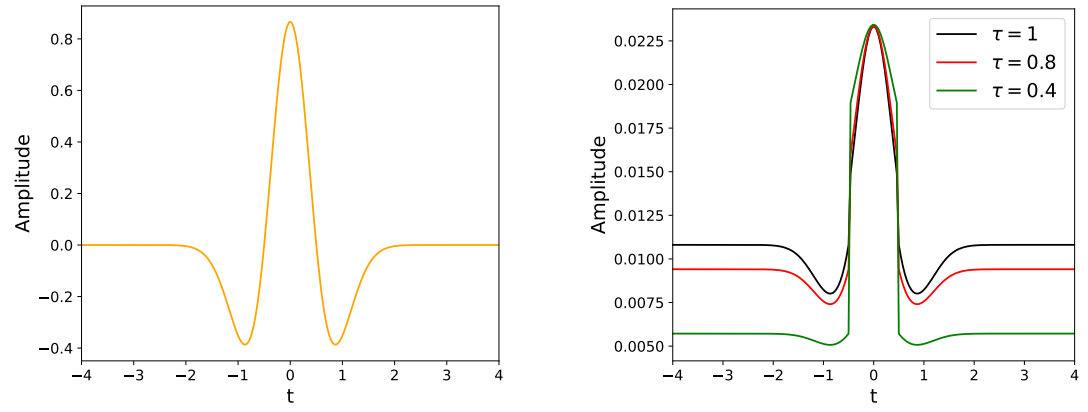

(a) A Ricker wave

(b) Normalisation by the exponential scaling for different values of τ

Figure 27: Two Ricker waves: non-normalised (left), normalised by the exponential scaling (right)

We can relate exponential scaling in relation to linear scaling and partial scaling. This can be seen by a Taylor expansion of the exponential part in definition [4.73]. Define $h \coloneqq \frac{1}{c}\exp(cf(t))$. Since for all $x \in \mathbb{R}$ it holds $\frac{d}{dx}\exp(x) = \exp(x)$, the Taylor expansion T of h is given by

$$\begin{aligned} Th(x;0) = \sum_{n=0}^{\infty} \frac{(cf(t))^n}{n!} &\approx \frac{1}{c} \cdot \left[1 + \frac{cf(t)}{1!} + \frac{(cf(t))^2}{2!} + \frac{(cf(t))^3}{3!} + \dots\right] \\ &= \frac{1}{c} + f(t) + \frac{cf(t)^2}{2} + \frac{c^2 f(t)^3}{3!} + \dots . \end{aligned}$$

Corollary 4.74. *For small values of c, especially for $0 < c < 1$, the scaling does not affect the shape of the signal except for a shift of $\frac{1}{c}$. Therefore it is similar to the linear scaling.*

Corollary 4.75. *For large values of c, h and therefore also $\tilde{f}$, converges to $f^+ = \max\{f, 0\}$.*

The exponential scaling method can be seen as a compromise between the positive part scaling – which maintains convexity – and the linear scaling, which, despite not preserving convexity, was found yielding satisfactory results with realistic datasets in [Yan18]. With the exponential scaling, $\tilde{f}$ is suitable for optimisation problems, which follows directly by the next lemma.

Lemma 4.76. *Assuming $f(t)$ is a smooth signal, then $\tilde{f}$ is a C^1 function.*

Proof of Lemma 4.76. To prove that $\tilde{f}$ is a C^1 function, we need to show smoothness of $\tilde{f}$ and its once smooth differentiability at the transition point, which is $f(t) = 0$. First, note that the normalisation factor $\langle\cdot\rangle$ in both cases of $\tilde{f}$ equals $\frac{1}{c}$ at $f(t) = 0$. The condition for smoothness is

$$\lim_{f(t)\to 0^+} \tilde{f}(t) = \lim_{f(t)\to 0^-} \tilde{f}(t).$$

For $f(t) \geq 0$ it holds

$$\lim_{f(t)\to 0^+} \tilde{f}(t) = \frac{\frac{1}{c}}{\langle\cdot\rangle}$$

and for $f(t) < 0$ it holds

$$\lim_{f(t)\to 0^-} \tilde{f}(t) = \frac{\frac{1}{c}\exp(cf(t))}{\langle\cdot\rangle} = \frac{\frac{1}{c}\exp(0)}{\langle\cdot\rangle} = \frac{\frac{1}{c}}{\langle\cdot\rangle}.$$

Therefore, $\tilde{f}$ is smooth. Next we show differentiability. For $f(t) \geq 0$ it holds

$$\lim_{f(t)\to 0^+} \frac{d\tilde{f}(t)}{dt} = \frac{\frac{df(t)}{dt}}{\langle\cdot\rangle}.$$

For $f(t) < 0$ it holds

$$\lim_{f(t)\to 0^-} \frac{d\tilde{f}(t)}{dt} = \frac{\frac{1}{c}c\frac{df(t)}{dt}exp(cf(t))}{\langle\cdot\rangle} = \frac{\frac{df(t)}{dt}}{\langle\cdot\rangle}.$$

Therefore, $\tilde{f}$ is continuously differentiable. □

4.8 The Influence of Data Normalisation on the Behaviour of the Wasserstein Metric

In this section we discuss the influence of the data normalisation process on the behaviour of the Wasserstein metric. When applied to two Ricker waves that are identical except for a horizontal shift, all normalisation methods proposed in the prior Subsections 4.7.2 - 4.73 (absolute value scaling, partial scaling, squared scaling, exponential scaling) except for the linear scaling lead to a strictly convex Wasserstein metric with respect to horizontal shifts.

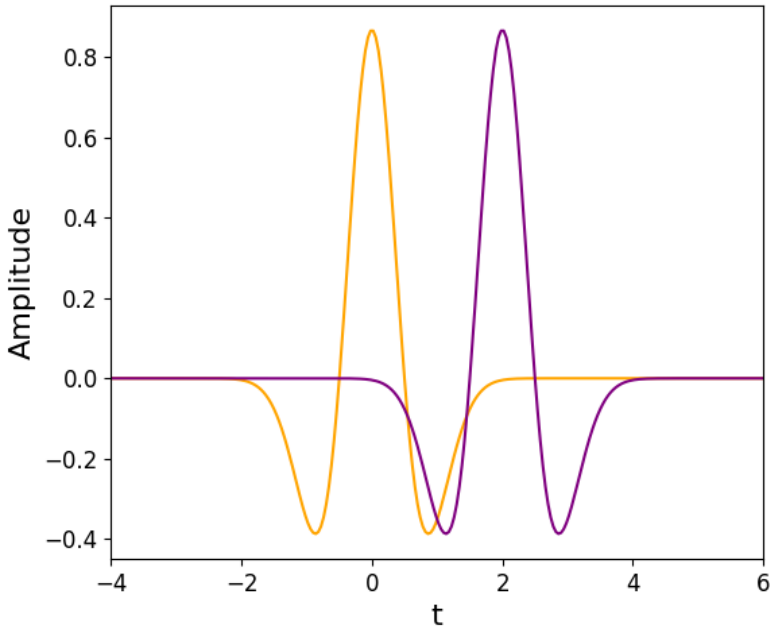

Figure 28: Two time-shifted Ricker waves

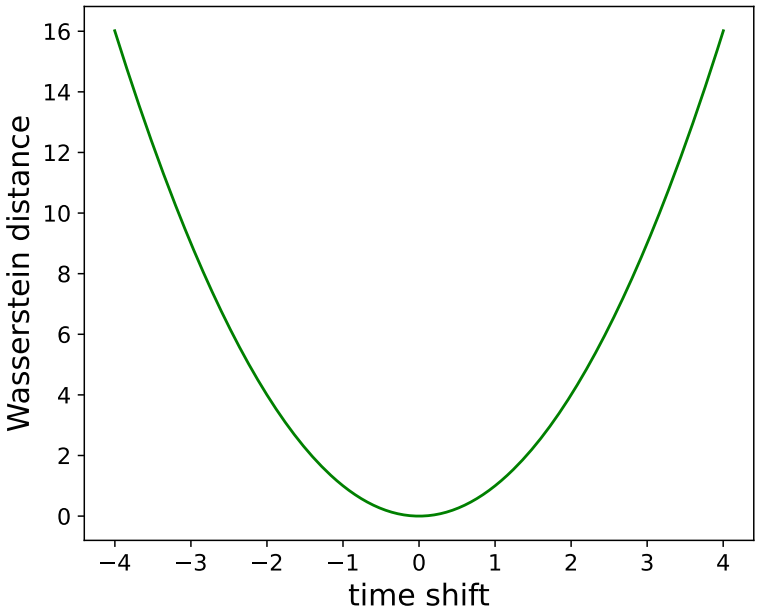

Figure 29: Wasserstein metric between shifted Ricker waves from Figure 28, which were normalised by the methods proposed in 4.7.2 - 4.7.5.

In case of linear scaling, the Wasserstein metric is not convex as can be seen in Figure 30. Nevertheless, it yields slightly better results than the L^2-norm (see Figure 15 in Section 3.4), since the result is void of local minima.

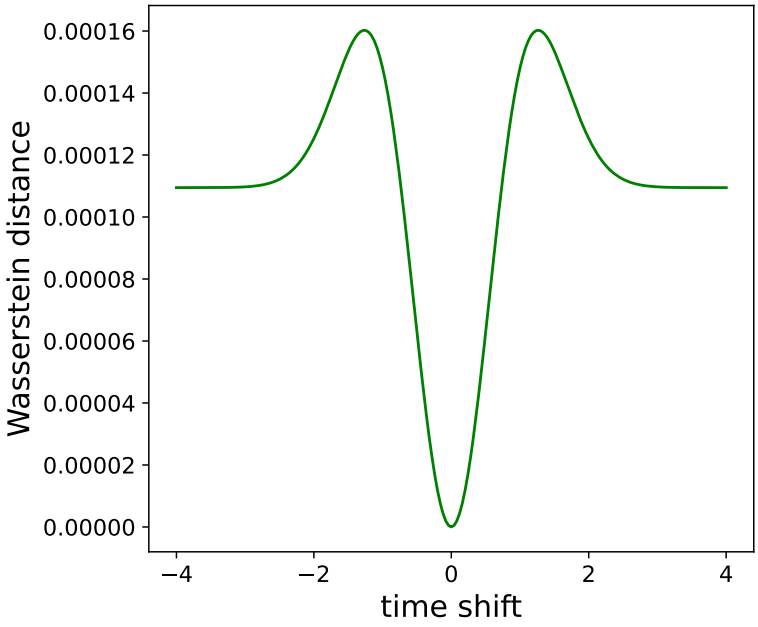

Figure 30: Wasserstein distance with respect to the shift values between the linearly scaled Ricker waves from Figure 23b.

The lack of convexity as seen in the numerical results does not contradict Theorem 4.51. This is because the divisor of the linear scaling

$$\tilde{f} = \frac{f(t) + c}{\langle f + c \rangle}$$

causes the weights of the integrals not to be equal. In Theorem 4.51, the second signal f_s is defined as a shifted version of the first signal f. However, in the context of FWI, we compare synthetic and observed data, which are independent of each other. To this end, assume that d^{obs} is identical to d^{syn} except for a time shift, meaning the signals exist in different domains. Consequently, when integrating each signal separately, their values will differ. As a result, the scaled signals are no longer shifts of each other and Theorem 4.51 does not apply.

Moreover, following the findings in [Yan18], linear scaling can mitigate the absence of zero frequencies in d^{syn} and d^{obs}. This can cause the transport to be local instead of global [Yan18]. Global transport is a transportation process in which mass is shifted within the same phase (i.e., positive values are transported to positive values and negative values to negative values). For an illustration of local and global transport, see Figure 31. In essence, these results in [Yan18] can be explained as follows:

1. Signals without zero frequencies exhibit Fourier transforms that lack oscillations.
2. In the absence of oscillations, phase differences cannot be distinguished.
3. Consequently, the transport may appear to be local rather than global.

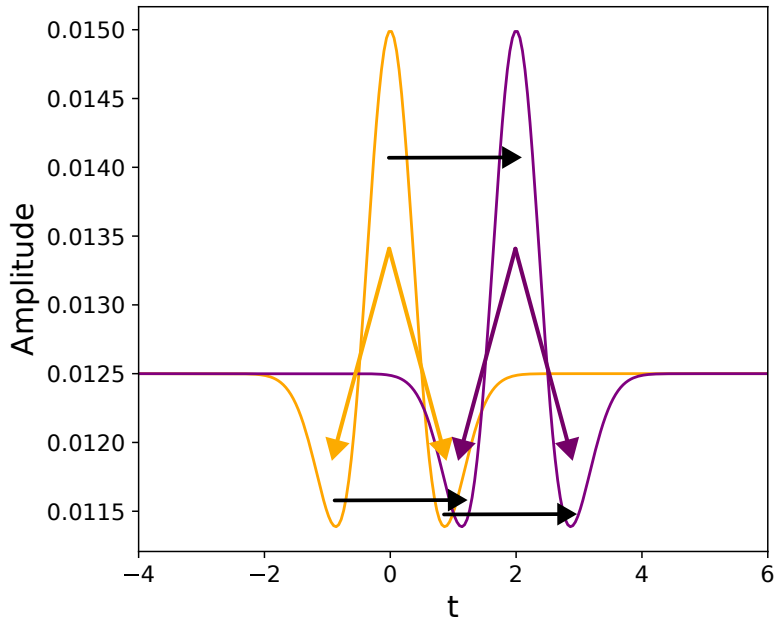

Figure 31: Global transport (black arrows) and local transport (orange and purple arrows)

To explain the first point, recall the definition of a Fourier transform [AW08]:

$$\hat{f}(\omega) = \int_{-\infty}^{\infty} f(t) e^{-i\omega t}\, dt, \qquad [112]$$

where $f(t)$ is the time-domain signal and $\hat{f}(\omega)$ is its Fourier transform in the frequency domain. Now, consider the case where the frequency $\omega = 0$. Substituting $\omega = 0$ into the definition, we get

$$\hat{f}(0) = \int_{-\infty}^{\infty} f(t) e^{0}\, dt = \int_{-\infty}^{\infty} f(t)\, dt. \qquad [113]$$

Here, the exponential term becomes 1, resulting in a constant value that corresponds to the integral of $f(t)$. This shows that when zero frequencies are present, the Fourier transform represents the overall amplitude of the signal without oscillations. As a result, signals lacking zero frequencies fail to produce this constant term, which contributes to the absence of oscillations and impairs the ability to distinguish phase differences. Consequently, mass from the same phase of one signal is not transported back into the corresponding phase of the other signal. Instead, the transport may occur locally. Thus, $W_2^2(d^{\text{syn}}, d^{\text{obs}})$ is not convex [Yan18].

4.9 Pseudocode for FWI

Now that we have discussed all the steps necessary for the FWI process, we summarise the algorithm in the following pseudocode.

Algorithm 1: Full Waveform Inversion (FWI)

Input: num_receivers, num_shots, fwi_iterations, true_model m, initial_model m_0, source_coordinates, receiver_coordinates, observed data g

Output: misfit values and gradient

Initialize parameters;
Compute synthetic data f with forward operator using Finite differences;
for $k = 0$ **to** *num_shots - 1* **do**
    Compute forward wave field with Finite differences;
    Initialize Wasserstein sum to 0;
    for *rec = 0* **to** *num_receivers - 1* **do**
        Normalise f and g;
        Compute Wasserstein distance $W_2^2(f, g)$;
        Update misfit function: $\sum_{r=1}^{num\_receivers} W_2^2(f, g)$;
        Update adjoint source term $\partial W_2^2(f, g)$;
    Define step length α for gradient descent;
    Run gradient descent with adjoint source term $\partial W_2^2(f, g)$:
    $m^{k+1} = m^k - \alpha \frac{\partial W_2^2}{\partial m}[m^k]$;
Initialize history array for misfit values;
for *iteration = 0* **to** *fwi_iterations - 1* **do**
    Compute misfit and adjoint source term;
    Update model estimate using gradient descent;

5 Numerical Simulations

To discretise the scheme we employ Finite Differences as explained in Section 2.2. The source term of the adjoint wave equation can be discretised using the following approach:

$$\delta W[f,g] = \left(U \cdot diag\left(\frac{-2f[t]dt}{g(G^{-1} \circ F[t])}\right)\right) \cdot (t - G^{-1} \circ F[t])\Delta t + |t - G^{-1} \circ F[t]|^2 \Delta t, \tag{114}$$

where Δt is the time domain spacing.

In the following subsections, we describe the experimental design we chose for the simulations. Of course, the results of the experiments depend not only on the choice of the misfit function and the gradient based optimisation method we discussed in the previous sections. The results also depend on the parameters chosen during the experimental design, as there are many possibilities for the sources and receivers to be placed. To further optimise the latter parameters was not part of this thesis and the results serve more as a proof of concept for using the Wasserstein metric in FWI.
The following simulations were done using Python with Devito (see [Lou+19; Lup+20]). The corresponding code can be found in the appendix.

5.0.1 Camembert model I

The Camembert model is a synthetic velocity model. This model is a circular inclusion in a homogeneous medium and was proposed in [GVT86]. The experiment is designed as follows: We set the circle with radius $0.1\,km$ located in the center of the rectangular velocity model. The velocity is $3\,km/s$ inside the circle and $2.5\,km/s$ outside the circle in the homogenous medium (see Figure 32a). For the initial velocity model we choose a smooth velocity of $2.5\,km/s$ (see Figure 32b).

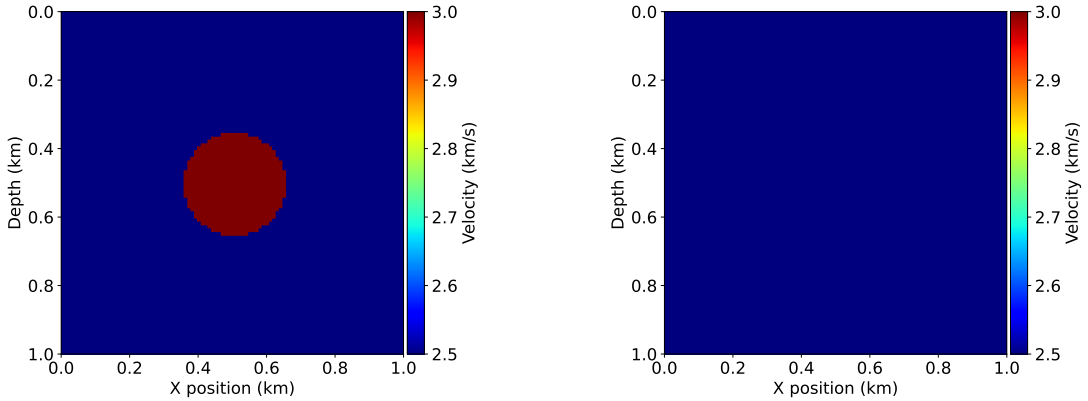

(a) True velocity

(b) Initial velocity

Figure 32: True and initial velocities of the Camembert model

Nine equally spaced sources are placed along a vertical line extending from the surface to a depth of $1\,km$. In addition, 101 receivers are placed at a horizontal distance of $1\,km$ from the origin, aligned vertically. The nine sources are represented by the dots on the left of Figure 33a, while the receivers on the right are illustrated by a vertical line due to

their larger quantity. The linear scaling is applied for normalising the seismic data when using the Wasserstein metric as misfit function.

The FWI algorithm starts with the initial velocity. After 15 iterations of FWI with the Wasserstein metric, the algorithm is able to roughly reconstruct the circular structure with a radius of 0.1 km, see Figure 33a.

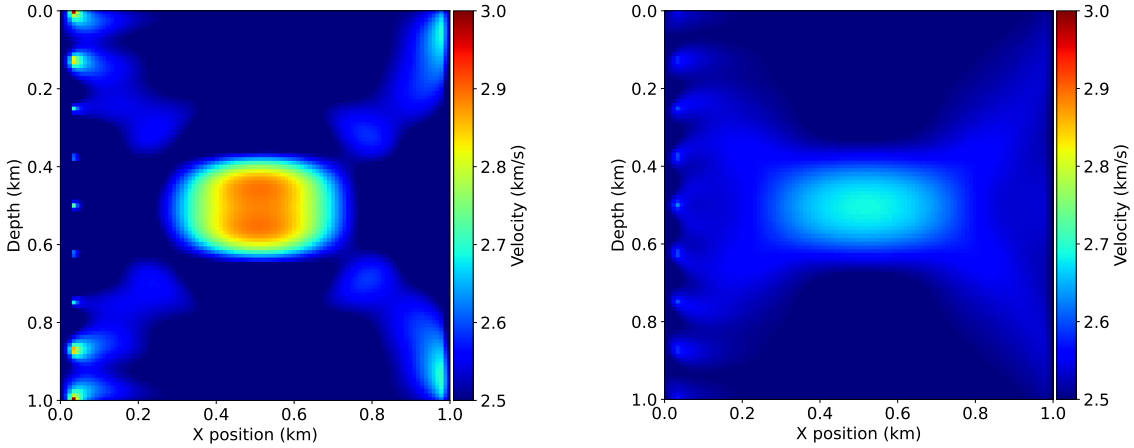

(a) $W_2^2(d^{syn}, d^{obs})$ (b) $L_2^2(d^{syn}, d^{obs})$

Figure 33: After 15 iterations of FWI with 9 shots and 101 receivers

In the upper and lower third of this circular structure, a velocity of 2.90 km/s was reconstructed. In the middle third, a speed of 2.85 km/s was calculated. In comparison, the algorithm which uses the L^2 distance as misfit function determined a more oval-shaped structure after 15 iterations. The maximum velocity in the L^2 based algorithm was reconstructed to be 2.67 km/s after 15 iterations, see Figure 33b.

5.0.2 Camembert model II

The experiment is designed as described in Section 5.0.1, except for the true velocity, which is set to 6 km/s.

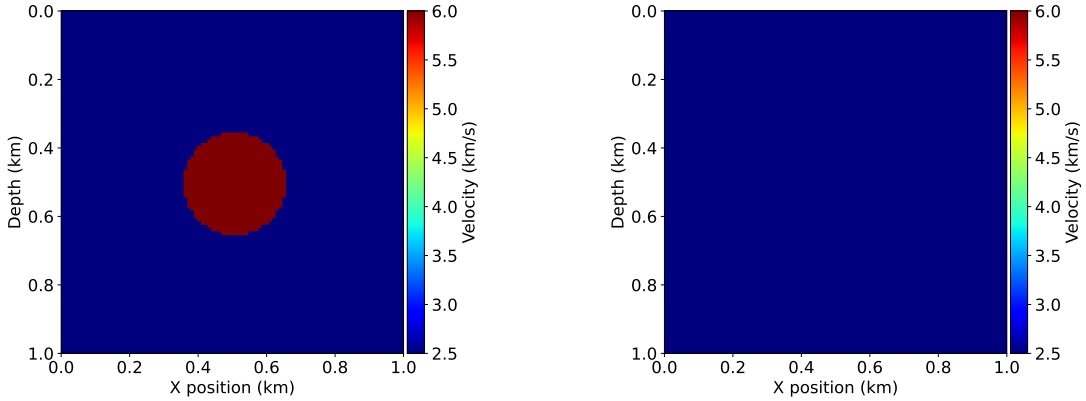

(a) True velocity (b) Initial velocity

Figure 34: True and initial velocities of Camembert model

In this section, we present the results obtained with the FWI algorithm when applying linear and exponential scaling. We specifically compare the effect of different parameter values for the exponential scaling.

As described in Section 4.73, the exponential scaling is defined as

$$\tilde{f}(t) = \begin{cases} \frac{f(t)+\frac{1}{c}}{\langle f(t)+\frac{1}{c}\rangle}, & f(t) \geq 0, \\ \frac{\frac{1}{c}\exp(cf(t))}{\langle \frac{1}{c}\exp(cf(t))\rangle}, & f(t) < 0 \end{cases}$$

for $c \in \mathbb{R}_{>0}$. Following [Yan18], the parameter must be selected based on the specific seismic data set. In this thesis, the parameter c was chosen similarly to the parameter used in linear scaling but with a damping factor $\tau \in (0, 1]$:

$$c = \min(d^{obs}, d^{syn}) \cdot \tau.$$

As seen in Section 4.73, exponential scaling is similar to linear scaling for small values $0 < c << 1$.

We run the FWI algorithm for $c = 0.1$, $c = 0.01$ and $c = 1$ and compare the results. Additionally, we evaluate the algorithm using the L^2-norm as misfit function.

With linear scaling (see Figure 5.0.2), a maximum velocity of $4.04\,km/s$ was reconstructed after 30 iterations of FWI. After 100 iterations, the maximum velocity reached $6.0\,km/s$ and the reconstructed shape was quite circular.

When applying exponential scaling, the results for $c = 0.01$ and $c = 0.1$ are similar to those obtained with linear scaling. However, for $c = 1$, the structure becomes more oval-shaped, and the velocity in the inner region is $5.85\,km/s$. Furthermore, the misfit values decrease consistently when using exponential scaling (see Figures 37a - 37c).

Using the L^2-norm, a maximum velocity of $3.96\,km/s$ was reconstructed after 100 iterations of FWI. However, the inner structure is quite circular. Comparing the results obtained with the L^2-norm and the Wasserstein metric, we find that the Wasserstein distance provides a promising misfit function. Specifically, the misfit value using the L^2-norm did not lead to significant improvements in the reconstruction results, developing from maximum velocity of $3.35\,km/s$ after 30 iterations (see Figure 35e) to $3.96\,km/s$ after 100 iterations (see Figure 36e).

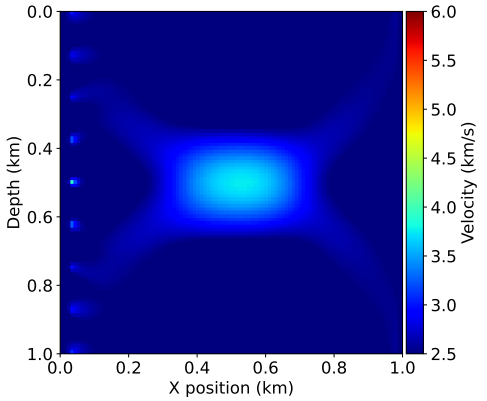

(a) $W_2^2(d^{syn}, d^{obs})$ with exponential scaling and $\tau = 1$

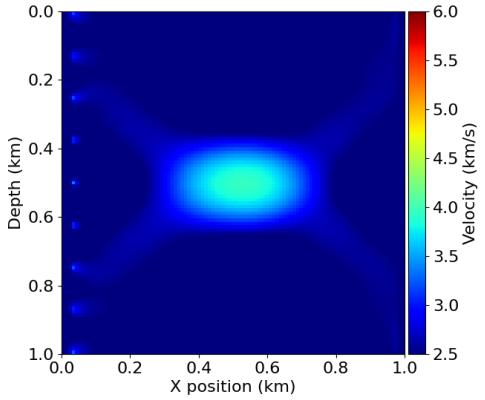

(b) $W_2^2(d^{syn}, d^{obs})$ with exponential scaling and $\tau = 0.1$

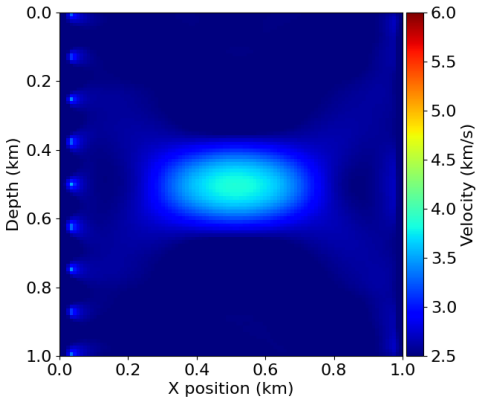

(c) $W_2^2(d^{syn}, d^{obs})$ with exponential scaling and $\tau = 0.01$

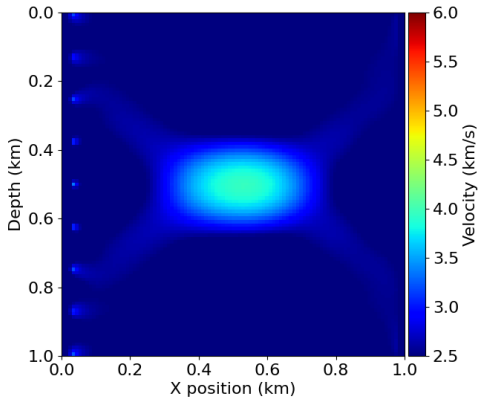

(d) $W_2^2(d^{syn}, d^{obs})$ with linear scaling

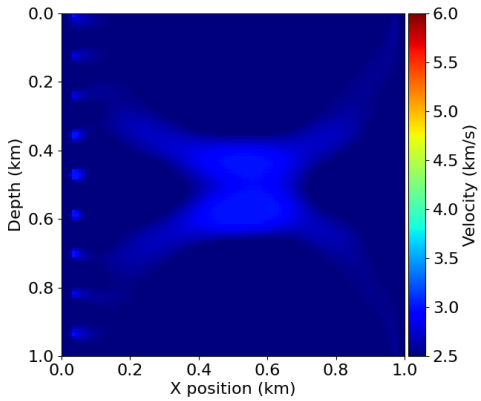

(e) $L_2^2(d^{syn}, d^{obs})$

Figure 35: After 30 iterations of FWI with 9 shots and 101 receivers

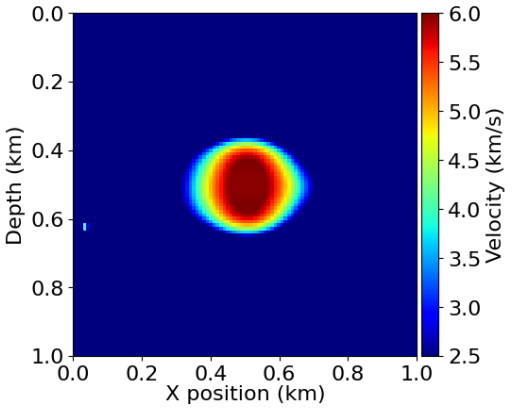

(a) $W_2^2(d^{syn}, d^{obs})$ with exponential scaling and $\tau = 1$

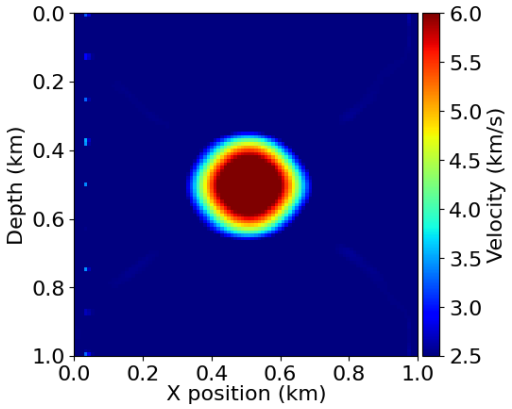

(b) $W_2^2(d^{syn}, d^{obs})$ with exponential scaling and $\tau = 0.1$

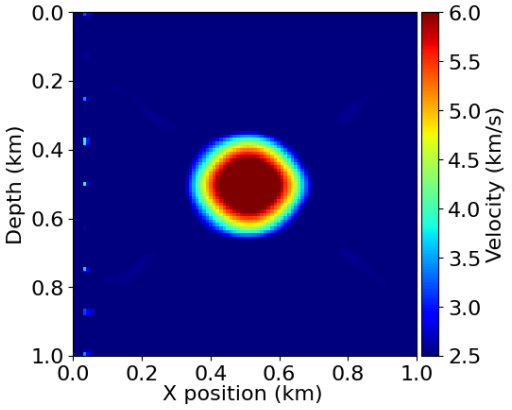

(c) $W_2^2(d^{syn}, d^{obs})$ with exponential scaling and $\tau = 0.01$

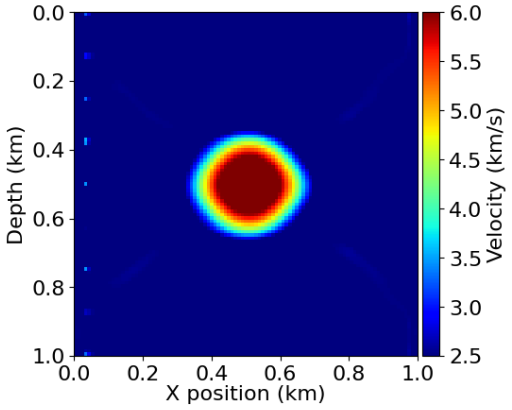

(d) $W_2^2(d^{syn}, d^{obs})$ with the linear scaling

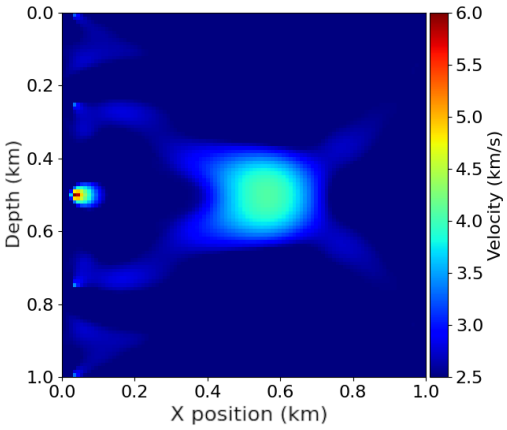

(e) $L_2^2(d^{syn}, d^{obs})$

Figure 36: After 100 iterations of FWI with 9 shots and 101 receivers

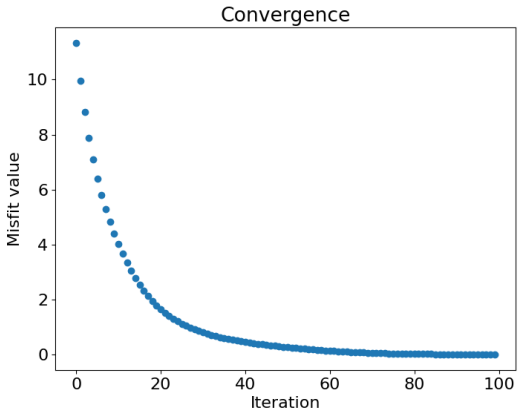

(a) $W_2^2(d^{syn}, d^{obs})$ with exponential scaling and $\tau = 0.1$

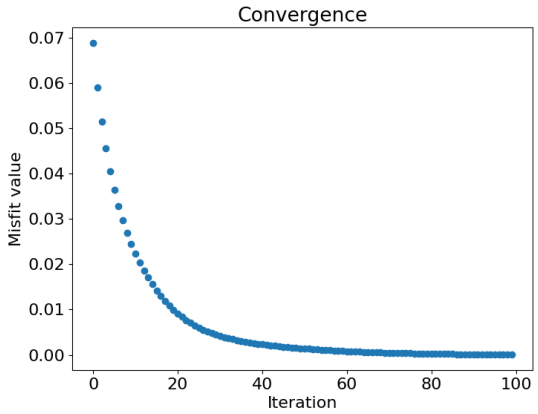

(b) $W_2^2(d^{syn}, d^{obs})$ with exponential scaling and $\tau = 0.01$

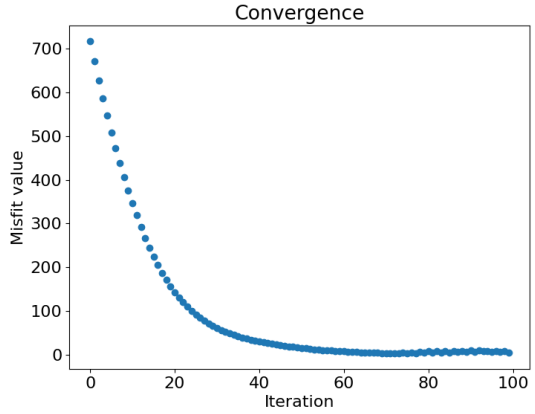

(c) $W_2^2(d^{syn}, d^{obs})$ with exponential scaling and $\tau = 1$

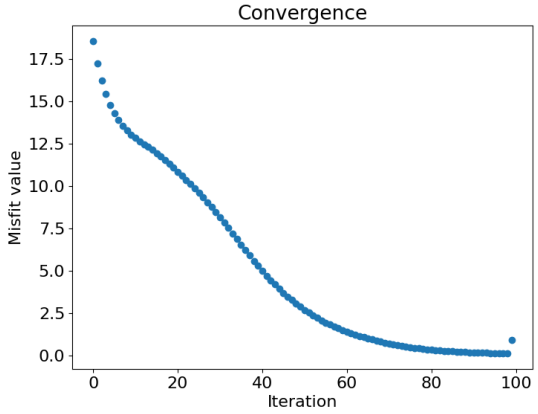

(d) $W_2^2(d^{syn}, d^{obs})$ with linear scaling

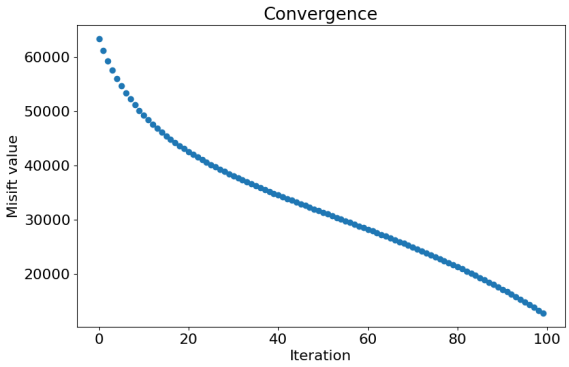

(e) $L_2^2(d^{syn}, d^{obs})$

Figure 37: After 100 iterations of FWI with 9 shots and 101 receivers

6 Conclusion

The results of the numerical simulations in Section 5.0.1 align well with the theoretical considerations outlined earlier. The full waveform inversion process utilising the Wasserstein distance as the misfit function demonstrated a more accurate model update compared to the L^2-based approach. This was also evident in Section 5.0.2, where the initial model was further away from the true model. However, additional enhancements are necessary to improve the algorithm's efficiency.

A critical aspect to consider is the choice of the optimisation method. In this thesis, we used the gradient descent method with which we were able to show the expected difference between the Wasserstein metric and the L^2-norm as misfit functions respectively. Using alternative gradient-based techniques, such as Gauss-Newton iterations or quasi-Newton methods like LM-BFGS, could yield more accurate results more quickly. In [Yan18], conjugated gradient descent was successfully used in context of seismic FWI. Additionally, global optimisation methods, such as swarm-based optimisation, have seen recent advancements [LTZ24a] and may also be beneficial, especially to avoid getting stuck in local minima. This leads to the second key point, data normalisation.

While the Wasserstein metric exhibits strict convexity with respect to horizontal shifts for various normalisation methods applied to Ricker waves, this property does not generally hold for real seismic data. Achieving (strict) convexity with respect to horizontal shifts is desirable, as horizontal shifts are a primary characteristic of seismic waves' behaviour. Although the linear scaling does not guarantee convexity, it has shown promising results, as was also demonstrated in [Yan18]. To enhance the efficiency of the FWI process, it is essential to minimise the occurrence of local minima and optimise the gradient update step accordingly.

Moreover, the wave equation as a model for the propagation of seismic waves is quite approximative. For a more realistic modelling operator, the elastic wave equation would be a more suitable choice. Linear elasticity was recently studied in the context of FWI in [NMR24]. It would be interesting to apply the elastic wave equation together with the Wasserstein metric in the FWI framework. For that, it would be necessary to revisit the calculation of the adjoint equation and the derivative of the source term of the adjoint equation (compare to Sections 3.2 and 3.3) regarding the new model equation.

A Python code for FWI algorithm

```
import math
import multiprocessing
import matplotlib.pyplot as plt
import numpy as np
from devito import configuration, Eq, Operator, Function, Min, Max, mmax
from examples.seismic import AcquisitionGeometry, Receiver, demo_model, plot_velocity
from examples.seismic.acoustic import AcousticWaveSolver
from scipy.integrate import trapezoid, cumulative_trapezoid
from scipy.ndimage import gaussian_filter

# Setting options for logging
configuration['log-level'] = 'WARNING'
np.set_printoptions(linewidth=200)

# Number of receivers
num_receivers = 101
# Number of source positions
num_shots = 9

shape = (101, 101)  # Number of grid point (nx, nz)
spacing = (10., 10.)  # Grid spacing in m. The domain size is now 1km by 1km
origin = (0., 0.)  # Need origin to define relative source and receiver locations

# Setting model options for Marmousi and Camembert model respectively

# Marmousi model
# Synthetic data
# model = demo_model('marmousi2d-isotropic', data_path='data-master/', origin =
↪  origin, shape=shape,
# spacing=spacing, nbl=20)
# Observed data (obtained by a Gaussian filter, determined by sigma)
# model0 = demo_model('marmousi2d-isotropic', data_path='data-master/',
↪  origin=origin, shape=shape, spacing=spacing,
# grid=model.grid, nbl=20)
# sigma = 30
# model0.vp.data[:] = gaussian_filter(model0.vp.data, sigma=sigma)
# Set time interval for measurements
# t0 = 0
# tn = 3500
# Frequency for model equation's source (Ricker wavelet)
# f0 = 0.025

# Camembert model
# Synthetic data
model = demo_model('circle-isotropic', vp_circle=6, vp_background=2.5, nbl=40)
# Observed data
model0 = demo_model('circle-isotropic', vp_circle=2.5, vp_background=2.5, nbl=40,
↪  grid=model.grid)
# Set time interval for measurements
t0 = 0
tn = 1000
# Frequency for model equation's source (Ricker wavelet)
f0 = 0.01
```

```
# The source is placed horizontally in the center, vertically on the left, in 20m depth
src_coordinates = np.empty((1, 2))
src_coordinates[0, :] = np.array(model.domain_size) * .5
src_coordinates[0, 0] = 20.

# The receivers are equidistantly positioned in depth at 980m distance to the origin
rec_coordinates = np.empty((num_receivers, 2))
rec_coordinates[:, 1] = np.linspace(0, model.domain_size[1], num_receivers)
rec_coordinates[:, 0] = 980.

# Geometric setting to obtain observed data
geometry = AcquisitionGeometry(model, rec_coordinates, src_coordinates, t0, tn, f0=f0, src_type='Ricker')
# Compute synthetic data with forward operator with finite differences
solver = AcousticWaveSolver(model, geometry)
solver.forward(vp=model.vp)
# Compute initial synthetic data with forward operator
solver.forward(vp=model0.vp)

# Prepare the varying source locations' sources
source_locations = np.empty((num_shots, 2))
source_locations[:, 0] = 30.
source_locations[:, 1] = np.linspace(0., 1000, num_shots)

# Plot the observed and initial synthetic data
# plot_velocity(model, source=source_locations)
# plot_velocity(model0, source=source_locations)


# Computations to obtain the quadratic Wasserstein metric between synthetic and observed data
# with the explicit formula in 1D
def wasserstein_distance(f: np.ndarray, g: np.ndarray, t: np.ndarray):
        s = f.size
        dt = t[1] - t[0]

        # Cumulative distribution functions for synthetic data f and observed data g with values taken exactly inbetween the
        # measurement times of f and g respectively
        F_tmp = cumulative_trapezoid(f, t)  # type: np.ndarray
        G_tmp = cumulative_trapezoid(g, t)  # type: np.ndarray

        # Corrected cumulative distribution functions with same time points as f and g
        F = np.array([0] + [F_tmp[i]/2 + F_tmp[i+1]/2 for i in range(F_tmp.size - 1)] + [F_tmp[-1]])
        G = np.array([0] + [G_tmp[i]/2 + G_tmp[i+1]/2 for i in range(G_tmp.size - 1)] + [G_tmp[-1]])

        # G^{-1}(F(t)) - assigns the time b to each time a, for which G(b) = F(a) holds
        G_i = np.ones(s) * t[-1]
        # fill G_i for every time point
        for i in range(F.size):
                # search for the fitting value in G
                for j in range(G_i.size - 1):
```

```
                        if F[i] < G[j+1]:
                                #Time point lies between j and j + 1, therefore
↪  interpolate
                                G_i[i] = t[j] + (F[i] - G[j]) / (G[j + 1] - G[j]) *
↪  dt
                                break

        tGF = (t - G_i)
        w = trapezoid(tGF ** 2 * f, t)

        #Computation of adjoint source term corresponding to the Wasserstein distance
        g_G_i = np.zeros(s) + g[-1]
        # Assigns to each time value from G^{-1} (for each time point of t) the value
↪  from g
        for k in range(s):
                index = int(math.floor(G_i[k] / dt))
                frac = G_i[k] / dt - index
                if index < s - 1:
                        g_G_i[k] = g[index] + frac * (g[index + 1] - g[index])

        a = -2 * tGF / g_G_i * f
        adj = [float((trapezoid(a[timepoint:], t[timepoint:]) + tGF[timepoint] ** 2)
↪  * dt) for timepoint in range(f.size)]

        return float(w), list(adj)


def linear_norm(f: np.ndarray, g: np.ndarray, t: np.ndarray):
        c = np.min(np.concat((f, g))) * -1.1
        f_norm = f + c
        g_norm = g + c
        f_norm /= trapezoid(g_norm, t)
        g_norm /= trapezoid(g_norm, t)

        return f_norm, g_norm, t

def exp_norm(f: np.ndarray, g: np.ndarray, t: np.ndarray):
        c = np.min(f + g) * -0.1
        exp_norm = np.vectorize(lambda f_x: f_x + 1 / c if f_x >= 0 else 1 / c *
↪  np.exp(c * f_x))
        f_norm = exp_norm(f)
        g_norm = exp_norm(g)
        f_norm /= trapezoid(g_norm, t)
        g_norm /= trapezoid(g_norm, t)

        return f_norm, g_norm, t

# Template for L²-norm
def l2norm(f: np.ndarray, g: np.ndarray, residual):
        l2 = 0.5 * (f - g) ** 2
        residual.data[:] = f.data[:] - g.data[:]
        return l2, residual

def calc_receiver(args):
        return wasserstein_distance(*linear_norm(*args))
```

```
# Create gradient function for FWI
def fwi_gradient(vp_in):
        # Create symbols to hold the gradient
        grad = Function(name="grad", grid=model.grid)

        # Create placeholders for the data and the data residual
        residual = Receiver(name='residual', grid=model.grid,
↪  time_range=geometry.time_axis,
                                                coordinates=geometry.rec_positions)
        d_obs = Receiver(name='d_obs', grid=model.grid,
↪  time_range=geometry.time_axis, coordinates=geometry.rec_positions)
        d_syn = Receiver(name='d_syn', grid=model.grid,
↪  time_range=geometry.time_axis, coordinates=geometry.rec_positions)

        t = residual.time_values[:]
        objective = 0.

        for k in range(num_shots):
                # Update source location
                geometry.src_positions[0, :] = source_locations[k, :]

                # Generate synthetic data from true model
                solver.forward(vp=model.vp, rec=d_obs)

                # Compute smooth data and full forward wave field u0
                _, u0, _ = solver.forward(vp=vp_in, save=True, rec=d_syn)

                # Create pool for parallelisation
                pool = multiprocessing.Pool()
                results = pool.map(calc_receiver, [(list(d_syn.data[:, rec]),
↪  list(d_obs.data[:, rec]), t) for rec in range(num_receivers)])

                # Captures the results, sums the distances and saves the residual
                objective += sum([r[0] for r in results])
                residual.data[:] = np.array([r[1] for r in results]).transpose()

                solver.gradient(rec=residual, u=u0, vp=vp_in, grad=grad)

        objective /= num_shots * num_receivers

        return objective, grad


# Run FWI with gradient descent
fwi_iterations = 30
history = np.zeros(fwi_iterations)
for iteration in range(fwi_iterations):

        # Compute the functional value and gradient for the current model estimate
        obj, direction = fwi_gradient(model0.vp)

        # Plot the FWI gradient
        # plot_image(-direction.data, vmin=-1000, vmax=1000, cmap="jet")

        # Plot the difference between the true and initial model.
        # plot_image(model0.vp.data - model.vp.data, vmin=-0.1, vmax=0.1, cmap="jet")
```

```
        # Store the history of the functional values
        history[iteration] = obj

        # Artificial step length for gradient descent; for smaller step size for
↪  smaller objective values choose first alpha
        # alpha = .5 / mmax(direction) * obj**2 / 4
        alpha = .05 / mmax(direction)
        # Update the model estimate and enforce minimum/maximum values
        update = model0.vp + alpha * direction
        update_eq = Eq(model0.vp, Max(Min(update, 6), 2.5))
        Operator(update_eq)()
        # plot_velocity(model0)
        # plot_velocity(model0)
        # Log the progress made
        print('Objective value is %f at iteration %d' % (obj, iteration + 1))


plot_velocity(model0)
# Plot values of Wasserstein distance in the different iterations (before the update
↪  step)
plt.figure()
plt.scatter(range(fwi_iterations), history)
plt.xlabel('Iteration')
plt.ylabel('Misfit value')
plt.title('Convergence')
plt.show()
```

References

[ACB17] Martin Arjovsky, Soumith Chintala, and Léon Bottou. *Wasserstein GAN*. arXiv:1701.07875. Dec. 2017. DOI: 10.48550/arXiv.1701.07875.

[Alp10] Ethem Alpaydin. *Introduction to machine learning*. 2nd ed. Adaptive computation and machine learning. OCLC: ocn317698631. Cambridge, Mass: MIT Press, 2010. ISBN: 9780262012430.

[Alt12] Hans Wilhelm Alt. *Lineare Funktionalanalysis: Eine anwendungsorientierte Einführung*. de. Berlin, Heidelberg: Springer Berlin Heidelberg, 2012. ISBN: 9783642222603 9783642222610. DOI: 10.1007/978-3-642-22261-0. URL: https://link.springer.com/10.1007/978-3-642-22261-0.

[AW08] George B. Arfken and Hans J. Weber. *Mathematical Methods for Physicists*. Cambridge University Press, 2008. ISBN: 9780521389914.

[BM21] Marco Bohnhoff and Peter Malin. "Borehole Seismic Networks and Arrays". en. In: *Encyclopedia of Solid Earth Geophysics*. Ed. by Harsh K. Gupta. Cham: Springer International Publishing, 2021, pp. 44–52. ISBN: 9783030586300 9783030586317. DOI: 10.1007/978-3-030-58631-7_268.

[BOV09] Romain Brossier, Stéphane Operto, and Jean Virieux. "Seismic imaging of complex onshore structures by 2D elastic frequency-domain full-waveform inversion". en. In: *GEOPHYSICS* 74.6 (Nov. 2009), WCC105–WCC118. ISSN: 0016-8033, 1942-2156. DOI: 10.1190/1.3215771.

[Bre91] Yann Brenier. "Polar factorization and monotone rearrangement of vector-valued functions". en. In: *Communications on Pure and Applied Mathematics* 44.4 (June 1991), pp. 375–417. ISSN: 0010-3640, 1097-0312. DOI: 10.1002/cpa.3160440402.

[BT08] Dimitri P. Bertsekas and John N. Tsitsiklis. *Introduction to probability*. eng. 2nd ed. Optimization and computation series. Belmont: Athena scientific, 2008. ISBN: 9781886529236.

[BTT11] Ebru Bozdağ, Jeannot Trampert, and Jeroen Tromp. "Misfit functions for full waveform inversion based on instantaneous phase and envelope measurements: Misfit functions for full waveform inversion". en. In: *Geophysical Journal International* 185.2 (May 2011), pp. 845–870. ISSN: 0956540X. DOI: 10.1111/j.1365-246X.2011.04970.x. URL: https://academic.oup.com/gji/article-lookup/doi/10.1111/j.1365-246X.2011.04970.x.

[Bun+95] Carey Bunks et al. "Multiscale seismic waveform inversion". en. In: *GEOPHYSICS* 60.5 (Sept. 1995), pp. 1457–1473. ISSN: 0016-8033, 1942-2156. DOI: 10.1190/1.1443880. URL: https://library.seg.org/doi/10.1190/1.1443880.

[But16] J. C. Butcher. *Numerical Methods for Ordinary Differential Equations*. en. 1st ed. Wiley, July 2016. ISBN: 9781119121503 9781119121534. DOI: 10.1002/9781119121534.

[Cao+03] Yang Cao et al. "Adjoint Sensitivity Analysis for Differential-Algebraic Equations: The Adjoint DAE System and Its Numerical Solution". en. In: *SIAM Journal on Scientific Computing* 24.3 (Jan. 2003), pp. 1076–1089. ISSN: 1064-8275, 1095-7197. DOI: 10.1137/S1064827501380630. URL: http://epubs.siam.org/doi/10.1137/S1064827501380630.

[Cla71] Jon F. Claerbout. "Toward a unified theory of reflector mapping". In: *Geophysics* 36.3 (1971), pp. 467–481.

[Dem16] Laurent Demanet. *Waves and imaging class notes — 18.325*. 2016.

[EF13] Bjorn Engquist and Brittany D. Froese. *Application of the Wasserstein metric to seismic signals*. arXiv:1311.4581. Nov. 2013. DOI: 10.48550/arXiv.1311.4581.

[EF14] Bjorn Engquist and Brittany D. Froese. "Application of the Wasserstein metric to seismic signals". en. In: *Communications in Mathematical Sciences* 12.5 (2014), pp. 979–988. ISSN: 15396746, 19450796. DOI: 10.4310/CMS.2014.v12.n5.a7. URL: https://link.intlpress.com/JDetail/1806264603271188481.

[FBI06] A. Fichtner, H.-P. Bunge, and H. Igel. "The adjoint method in seismology—". en. In: *Physics of the Earth and Planetary Interiors* 157.1-2 (Aug. 2006), pp. 105–123. ISSN: 00319201. DOI: 10.1016/j.pepi.2006.03.018. URL: https://linkinghub.elsevier.com/retrieve/pii/S0031920106001038.

[Fis13] G. Fischer. *Lineare Algebra*. Springer, 2013.

[FN24] Willi Freeden and Helga Nutz. "Potential data and basic mathematical modeling". en. In: Cham: Springer Nature Switzerland, 2024. ISBN: 9783031544118 9783031544125. DOI: 10.1007/978-3-031-54412-5_3.

[GKnd] Afshin Gholamy and Vladik Kreinovich. *Why Ricker wavelets are successful in processing seismic data: Towards a theoretical explanation*. 500 W. University El Paso Texas 79968 USA, n.d.

[GS01] I. M. Gelfand and Mark Saul. *Trigonometry*. en. Boston, MA: Birkhäuser Boston, 2001. ISBN: 9780817639143 9781461201496. DOI: 10.1007/978-1-4612-0149-6. URL: http://link.springer.com/10.1007/978-1-4612-0149-6.

[GVT86] Odile Gauthier, Jean Virieux, and Albert Tarantola. "Twodimensional nonlinear inversion of seismic waveforms". en. In: *GEOPHYSICS* 7 (July 1986), pp. 1387–1403. DOI: 10.1190/1.1442188.

[Her24] Russell Herman. *Introduction to Partial Differential Equations*. 2024.

[HH80] J. A. Hudson and J. R. Heritage. "The use of the Born approximation in seismic scattering problems". In: *Geophys. J. R. astr. Soc.* 66 (1980), pp. 221–240.

[Hub64] Peter J. Huber. "Robust Estimation of a Location Parameter". en. In: *The Annals of Mathematical Statistics* 35.1 (Mar. 1964), pp. 73–101. ISSN: 0003-4851. DOI: 10.1214/aoms/1177703732. URL: http://projecteuclid.org/euclid.aoms/1177703732.

[Joh21] Stephen G. Johnson. *Notes on Adjoint Methods for 18.335*. 2021.

[Kan06] L. V. Kantorovich. “On the Translocation of Masses”. en. In: *Journal of Mathematical Sciences* 133.4 (Mar. 2006), pp. 1381–1382. ISSN: 1072-3374, 1573-8795. DOI: 10.1007/s10958-006-0049-2.

[Kel76] J. B. Keller. “Inverse problems”. In: *Amer. Math. Monthly* 83.2 (1976), pp. 107–118.

[Kut20] N. Kutz. *Advanced Differential Equations: Asymptotics & Perturbations*. 2020.

[LLM16] David C. Lay, Steven R. Lay, and Judith McDonald. *Linear algebra and its applications*. Fifth edition. Boston: Pearson, 2016. ISBN: 9780321982384.

[Lou+19] M. Louboutin et al. “Devito (v3.1.0): an embedded domain-specific language for finite differences and geophysical exploration”. In: *Geoscientific Model Development* 12.3 (2019), pp. 1165–1187. DOI: 10.5194/gmd-12-1165-2019. URL: https://www.geosci-model-dev.net/12/1165/2019/.

[LTZ24a] Jingcheng Lu, Eitan Tadmor, and Anil Zenginoglu. *Swarm-Based Gradient Descent Method for Non-Convex Optimization*. arXiv:2211.17157. Apr. 2024. DOI: 10.48550/arXiv.2211.17157.

[LTZ24b] Jingcheng Lu, Eitan Tadmor, and Anil Zenginoğlu. “Swarm-based gradient descent method for non-convex optimization”. en. In: *Communications of the American Mathematical Society* 4.17 (Dec. 2024), pp. 787–822. ISSN: 2692-3688. DOI: 10.1090/cams/42. URL: https://www.ams.org/cams/2024-04-17/S2692-3688-2024-00042-1/ (visited on 01/30/2025).

[Lup+20] Fabio Luporini et al. “Architecture and Performance of Devito, a System for Automated Stencil Computation”. In: *ACM Trans. Math. Softw.* 46.1 (2020). ISSN: 0098-3500. DOI: 10.1145/3374916. URL: https://doi.org/10.1145/3374916.

[NMR24] Vahid Negahdari, Seyed Reza Moghadasi, and Mohammad Reza Razvan. *Integrating Physics of the Problem into Data-Driven Methods to Enhance Elastic Full-Waveform Inversion with Uncertainty Quantification*. arXiv:2406.05153. Nov. 2024. DOI: 10.48550/arXiv.2406.05153.

[PC19] Gabriel Peyre and Marco Cuturi. “Computational Optimal Transport”. In: *Foundations and Trends in Machine Learning* 11.5-6 (2019), pp. 355–607.

[Ple06] R.-E. Plessix. “A review of the adjoint-state method for computing the gradient of a functional with geophysical applications”. In: *Geophysical Journal International* 167.2 (2006), pp. 495–503.

[Ric15] Mathias Richter. *Inverse Probleme: Grundlagen, Theorie und Anwendungsbeispiele*. ger. Mathematik im Fokus. Berlin [u.a.]: Springer Spektrum, 2015. ISBN: 9783662458112.

[Ric20] Mathias Richter. *Inverse Problems: Basics, Theory and Applications in Geophysics*. Lecture Notes in Geosystems Mathematics and Computing. Birkhäuser, 2020.

[Rob10] Etienne Robein. *Seismic Imaging: A Review of the Techniques, their Principles, Merits and Limitations*. Houten: EAGE Publications, 2010.

[Roc70] Ralph Tyrell Rockafellar. *Convex Analysis:* Princeton University Press, Dec. 1970. ISBN: 9781400873173. DOI: 10.1515/9781400873173. URL: https://www.degruyter.com/document/doi/10.1515/9781400873173/html.

[Rud13] Walter Rudin. *Real and complex analysis*. eng. 3. ed., internat. ed., [Nachdr.] McGraw-Hill international editions Mathematics series. New York, NY: McGraw-Hill, 2013. ISBN: 9780070542341 9780071002769.

[San15] Filippo Santambrogio. *Optimal Transport for Applied Mathematicians: Calculus of Variations, PDEs, and Modeling*. 1st ed. 2015. Progress in Nonlinear Differential Equations and Their Applications 87. Cham: Springer International Publishing : Imprint: Birkhaeuser, 2015. ISBN: 9783319208282.

[SJV22] Malcolm Sambridge, Andrew Jackson, and Andrew P Valentine. "Geophysical inversion and optimal transport". en. In: *Geophysical Journal International* 231.1 (June 2022), pp. 172–198. ISSN: 0956-540X, 1365-246X. DOI: 10.1093/gji/ggac151.

[SSBD14] Shai Shalev-Shwartz and Shai Ben-David. *Understanding machine learning: from theory to algorithms*. New York, NY, USA: Cambridge University Press, 2014. ISBN: 9781107057135.

[Ste23] N. Steinmetz. *Analysis*. Springer, 2023.

[Stu10] A. M. Stuart. "Inverse Problems: A Bayesian Perspective". In: *Acta Numerica* 19 (2010), pp. 451–559.

[Tar05] Albert Tarantola. *Inverse Problem Theory and Methods for Model Parameter Estimation*. en. Society for Industrial and Applied Mathematics, Jan. 2005. ISBN: 9780898715729 9780898717921. DOI: 10.1137/1.9780898717921.

[Tho18] Matthew Thorpe. "Introduction to Optimal Transport, University of Cambridge 2017-2018, 2018-2019, Part III. Notes. Problem Sheets 1, 2, 3 and 4". In: (2018). Accessed: 2024-12-03. URL: https://www.matthewthorpe.co.uk/teaching.

[TW98] A. Tveito and R. Winther. *Introduction to Partial Differential Equations*. Springer, 1998.

[Vil03] Cedric Villani. *Topics in Optimal Transportation*. Vol. 58. Graduate Studies in Mathematics. Providence, RI: American Mathematical Society, 2003.

[VO09] J. Virieux and S. Operto. "An overview of full-waveform inversion in exploration geophysics". en. In: *GEOPHYSICS* 74.6 (Nov. 2009), WCC1–WCC26. ISSN: 0016-8033, 1942-2156. DOI: 10.1190/1.3238367. URL: https://library.seg.org/doi/10.1190/1.3238367.

[Yan+16] Yunan Yang et al. "Optimal transport for seismic full waveform inversion". In: *Communications in Mathematical Sciences* 14.8 (2016), pp. 2309–2330.

[Yan+17a] Yunan Yang et al. "Analysis of optimal transport related misfit functions in seismic imaging". In: *International Conference on Geometric Science of Information*. Springer, 2017, pp. 109–116.

[Yan+17b] Yunan Yang et al. "Application of optimal transport and the quadratic Wasserstein metric to full waveform inversion". In: *Geophysics* 83.1 (2017), pp. 1–103.

[Yan18] Yunan Yang. “Optimal transport for seismic inverse problems”. PhD thesis. The University of Texas at Austin, Texas Scholar Works, University of Texas Libraries, 2018.

[Yan+19] Yunan Yang et al. “Seismic inversion and the data normalization for optimal transport”. In: *Methods and Applications of Analysis* 26.2 (2019), pp. 133–148.

Julius-Maximilians-
UNIVERSITÄT
WÜRZBURG

Versicherung zur selbständigen Leistungserbringung

Titel der Masterarbeit:

On Optimal Transport for Seismic Inverse Problems

Thema bereitgestellt von (Titel, Vorname, Nachname, Lehrstuhl):

Professor Dr. Christian Klingenberg,
Mathematische Strömungsmechanik

Eingereicht durch (Vorname, Nachname, Matrikel):

Melissa Lange, 2840826

Ich versichere, dass ich die vorstehende schriftliche Arbeit selbständig verfasst und keine anderen als die angegebenen Quellen und Hilfsmittel benutzt habe. Die benutzte Literatur sowie sonstige Hilfsquellen sind vollständig angegeben. Wörtlich oder dem Sinne nach dem Schrifttum oder dem Internet entnommene Stellen sind unter Angabe der Quelle kenntlich gemacht.

Weitere Personen waren an der geistigen Leistung der vorliegenden Arbeit nicht beteiligt. Insbesondere habe ich nicht die Hilfe eines Ghostwriters oder einer Ghostwriting-Agentur in Anspruch genommen. Dritte haben von mir weder unmittelbar noch mittelbar Geld oder geldwerte Leistungen für Arbeiten erhalten, die im Zusammenhang mit dem Inhalt der vorgelegten Arbeit stehen.

☐ Mit dem Prüfungsleiter bzw. der Prüfungsleiterin wurde abgestimmt, dass für die Erstellung der vorgelegten schriftlichen Arbeit Chatbots (insbesondere ChatGPT) bzw. allgemein solche Programme, die anstelle meiner Person die Aufgabenstellung der Prüfung bzw. Teile derselben bearbeiten könnten, entsprechend den Vorgaben der Prüfungsleiterin bzw. des Prüfungsleiters eingesetzt wurden. Die mittels Chatbots erstellten Passagen sind als solche gekennzeichnet.

Der Durchführung einer elektronischen Plagiatsprüfung stimme ich hiermit zu. Die eingereichte elektronische Fassung der Arbeit ist vollständig. Mir ist bewusst, dass nachträgliche Ergänzungen ausgeschlossen sind.

Die Arbeit wurde bisher keiner anderen Prüfungsbehörde vorgelegt und auch nicht veröffentlicht. Ich bin mir bewusst, dass eine unwahre Erklärung zur Versicherung der selbstständigen Leistungserbringung rechtliche Folgen haben kann.

Würzburg, 4.2.2025 Melissa Lange

Ort, Datum, Unterschrift